Discovery of Bile Acid-Associated Molecular Changes in the Murine Gastrointestinal Tract During *Clostridioides difficile* Infection

By

Emma Ryan Guiberson

Dissertation

Submitted to the Faculty of the

Graduate School of Vanderbilt University

in partial fulfillment of the requirements

For the degree of

DOCTOR OF PHILOSOPHY

in

Chemistry

August 31, 2022

Nashville, Tennessee

Approved:

Richard Caprioli, Ph.D.

Jeffrey Spraggins, Ph.D.

Eric Skaar, Ph.D.

Renã Robinson, Ph.D.

Kevin Schey, Ph.D.

To my family.

In a special way, to my grandparents who are no longer with us, Richard Krumholz and Lilly Ryan.

ACKNOWLEDGEMENTS

I am incredibly fortunate to have so many people to thank that have supported me throughout this process. First, a massive thanks to my advisors and mentors. **Richard**, you made me a better writer and encouraged me to always think about the broader human impact of my work. Thank you for giving me the freedom to uniquely shape this project and for supporting that endeavor, even if that meant leaving the mass spectrometry world sometimes. **Jeff**, you've been an incredible mentor both in science and life and it has been an honor working with you. I know your future students will also be incredibly lucky to have you as a mentor, and I will always remember and try to emulate your dedication to family in a difficult industry for work-life balance. Thank you for guiding me and for serving as one of my strongest advocates. **Eric**, thank you for genuinely welcoming me into your lab even if it wasn't the project you had envisioned. Thank you for supporting me as I branched out of my comfort zone, and for advocating so strongly for my success. I truly wouldn't be where I am, and as happy about it, without the three of you and I am so thankful for such a supportive mentoring team for my graduate work. As part of that team, I also want to thank my other committee members, **Kevin** and **Renã**. Your insightful questions in meetings, as well as your support and conversations one on one, have helped me grow as a scientist, and made my work that much stronger. I also had an incredible mentor in Angela Kruse, who was always there with kind words and patient teaching. **Angela**, you are so supportive and encouraging, and despite taking on an incredible amount of work you were always there to help me whether it was science-related, help navigating my postdoc search, or just a great chat and laugh. I'm incredibly grateful for all the time and help you've given me over the years, and that I can call you a friend. Finally, I want to thank my first chemistry teacher **Erica** Gearhart, for instilling a love of chemistry early on that led me here.

Next, I have to thank those who were with me every day, my lab mates. From the lab that I joined in 2019, to the blended lab here today, grad school would have been a lot less joyful without all of you. From traveling the world with **Josiah**, road trips and Costco trips and endless conversations with **Kate**, parties and deep chats at **Emilio**'s, wiki-races and Google sleuthing with **Chris**, and general lab shenanigans and Chipotle runs with everyone in lab, you've all made coming to work a joy. You've been there for me through a lot of life changes, with a level of support uncharacteristic of normal coworkers, and with a lot more laughs. Thank you all for everything, and I will miss you immensely.

My friends, especially those who came in my cohort, have at times been my one tether to sanity and for that I am so thankful. I can't think of a greater group to complain about science with, get sunburned on lazy pool days, drink borderline problematic amounts of coffee, and eat through the entire Nashville brunch scene. They say to make friends outside of science, but the friends I've made in science have been the ones that truly understand this unique pressure cooker and know just what to say to help you keep working through this marathon degree. I'm so thankful to all of you for your friendship, and for helping me finally get to the finish line in one piece.

Last, but certainly not least, I wouldn't be here without my family. It has been hard going through this process without you all nearby, but I have felt your immense love and support every day. Through the tearful phone calls when my experiments failed, to the excited ramblings when celebrating a win only academics would care about, you all have been my rock. **Dad**, you taught me the value of education and faith which has fundamentally shaped my worldview and my dreams of the future. **Mom**, you were always there to listen and celebrate even the most mundane of occasions, and helped me to keep everything in perspective when it all felt too overwhelming. To my sisters, **Lucy, Molly** and **Kate**: you are my best friends. You were always there for a facetime discussion of some terrible tv show or childhood memories, and these mean more to me than you'll ever know. I'm so incredibly proud of the women you've become, and I'm so thankful to have you all as part of my life. I wouldn't be the person I am today without my family, and I'm so thankful for all of your support in getting me to this milestone.

TABLE OF CONTENTS

LIST OF TABLES

LIST OF FIGURES

LIST OF ABBREVIATIONS

9-AA	9-aminoacridine
ACN	acetonitrile
AF	ammonium formate
ASBT	apical sodium-dependent bile acid transporter
BA	bile acid
bMCA	β-muricholate
BMP-2	bone morphogenic protein
BSEP	bile salt export pump
BSH	bile salt hydrolase
CA	cholic acid
cAMP	cyclic adenosine monophosphate
CASI	continuous accumulation of selected ions
CDCA	chenodeoxycholic acid
CDI	*C. difficile* infection
CF	cystic fibrosis
CFU	colony forming units
CID	collision-induced dissociation
CMC	carboxymethyl cellulose
DAN	1,5-diaminonapthalene
DCA	deoxycholic acid
DHA	2′,6′-Dihydroxyacetophenone
dpi	days post infection
DSS	dextran sulfate sodium
DTT	Dithiothreitol
EDTA	ethylenediaminetetraacetic acid
ESI	electrospray ionization
EtOH	ethanol
FFA	free fatty acid
FT-ICR	fourier transform ion cyclotron resonance
FTU	functional tissue unit
FXR	farnesoid X receptor
GCA	glycocholic acid
GCDCA	glycochenodeoxycholic acid
GDCA	glycodeoxycholic acid
GI	gastrointestinal
GUDCA	glycoursodeoxycholic acid
H&E	hematoxylin and eosin
HNF4a	hepatic nuclear factor 4a
IAA	iodoacetamide
I-BABP	intestinal bile acid-binding protein

IBD	inflammatory bowel disease
IHC	immunohistochemistry
IMS	imaging mass spectrometry
IPC	cer phosphoinositol
ITO	indium tin oxide
LA-ICP	laser ablation inductively-coupled plasma
LC-MS/MS	liquid chromatography tandem mass spectrometry
LRH-1	liver receptor homolog-1
m/z	mass-to-charge ratio
MALDI	matrix-assisted laser desorption/ionzation
MAPK	mitogen activated protein kinases
MCA	muricholate
NTCP	sodium/bile acid cotransporter
OST	organic solute transporter
PBS	phosphate buffered saline
PBST	phosphate buffered saline with 0.5% Tween
PE	phosphatidylethanolamine
qRT PCR	quantitative real-time polymerase chain reaction
RNA	ribonucleic acid
SDS	sodium dodecyl sulphate
SHP	small heterodimer partner
SORI	sustained off-resonance irradiation
TbMCA	tauro-β-muricholate
TCA	taurocholic acid
TCCFA	taurocholate cycloserine cefoxitin fructose agar
TCDCA	taurochenodeoxycholic acid
TFA	trifluoroacetic acid

CHAPTER 1

Bile Acids and Mass Spectrometry in the Context of *C. difficile* Infection

1.1. OVERVIEW

Clostridioides difficile is a gram-positive, nosocomial, sporulating pathogen with a large impact on the healthcare community.[1] *C. difficile* thrives as an endospore which enters the body through the oral-fecal route and, in the presence of chemical markers such as bile acids, germinates into vegetative bacteria.[2] These bacteria are then able to produce toxins that attack the gut epithelium, causing inflammation and diarrhea.[3] *C. difficile* and the host both use chemical signals to communicate, resulting in a rich molecular environment to be studied. By better understanding these signals, and how they can be manipulated, it is possible to discover novel therapeutics and diagnostic markers for this disease. One powerful method for detecting and visualizing these chemical markers is mass spectrometry, especially the combination of imaging mass spectrometry and quantitative small molecule analysis.[4] Paired together, these technologies offer incredible insight into the molecular landscape of the gastrointestinal tract in the context of infection. Of particular interest are the host-produced signaling molecules bile acids that induce germination in *C. difficile*.[5] Bile acids are produced in the liver by the host, reabsorbed in the ileum, and recirculated.[6] They aid in the digestion of fats from food by serving as emulsification agents for lipid droplets.[7] As these bile acid pools are controlled by the host, yet serve a crucial role in the germination and colonization of *C. difficile*, further investigation into the relationship between *C. difficile* and bile acids utilizing mass spectrometry approaches offers a plethora of molecular and mechanistic information that can aid the healthcare community in understanding, diagnosing, and treating CDI.

1.2. *CLOSTRIDIOIDES DIFFICILE* IS AN URGENT THREAT TO THE HEALTHCARE COMMUNITY

Clostridioides difficile (formerly known as *Clostridium difficile*) is a prominent gastrointestinal pathogen with a substantial impact on human health.[8] *C. difficile* is the leading cause of hospital-acquired infections and is considered an urgent threat by the Centers for Disease Control.[9,10] This gram-positive bacterial pathogen is transmitted primarily through feces, where metabolically inactive spores are transmitted and ingested through the oral-fecal route.[2]

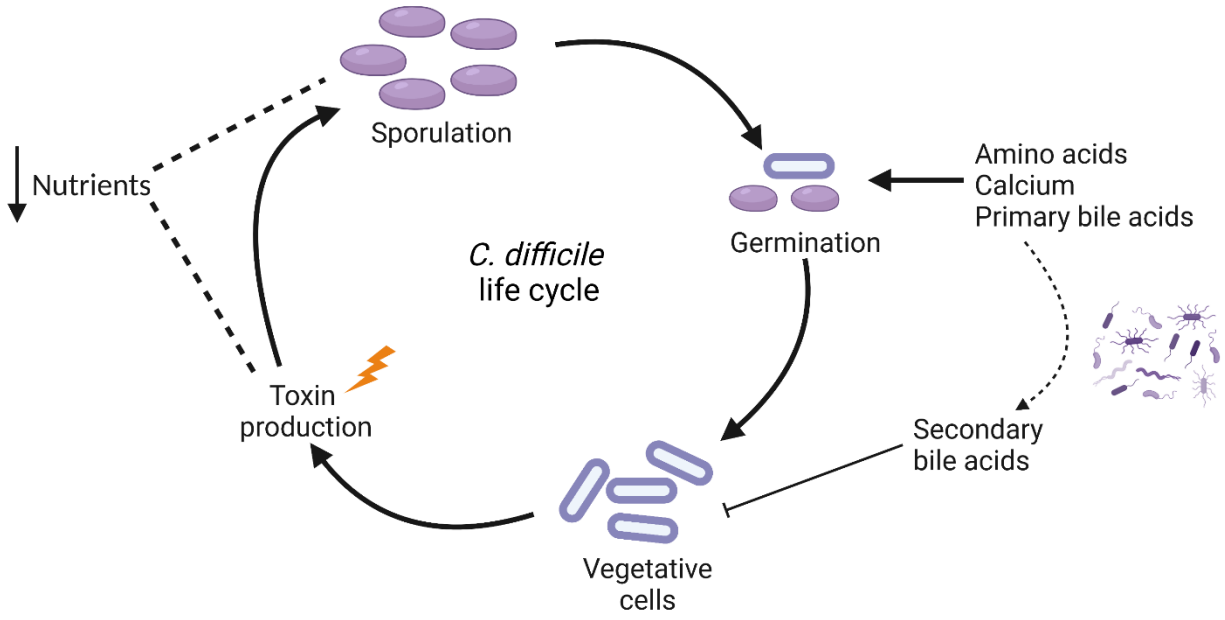

Figure 1.1. Representation of the *C. difficile* life cycle from spores to vegetative cells in the presence of germination factors. Figure adapted from "Targeting the Metabolic Basis of *C. difficile*'s Life Cycle" by Madeline Barron.

While the bacterium itself is rod-shaped, *C. difficile*'s excellent survival is due to its ability to produce metabolically-inactive spores.[11] These spores are resistant to heat and a plethora of cleaning products, and can exist in an oxygen-rich environment.[12–14] The vegetative cell form of *C. difficile*, however, is an obligate anaerobe that is easily out-competed by commensals in the gut microbiome of a healthy individual.[15] When vegetative *C. difficile* is in an environment where it cannot properly grow or proliferate, it releases these spores until chemical signals initiate their conversion back to vegetative cells.[2]

The pathogenesis of *C. difficile* begins when a compromised host ingests spores which are able to travel through the digestive tract.[16] Once these spores reach the small intestine of a host, they convert into vegetative cells where they are then able to compete with healthy gut microbiota for resources (Figure 1.1).[17] These cells then produce cytotoxins (mainly TcdA and TcdB) which attack the gut epithelium of the intestine, most prominently in the large intestine.[18] While strains of *C. difficile* exist that do not produce both types of toxins, or even produce others such as TcdD, the toxins produced by *C. difficile* serve as the major virulence factors of *C. difficile* infection (CDI).[19,20] The impact of these toxins results in characteristic CDI symptomology, such as diarrhea and colitis or inflammation of the colon.[21]

Due to the strong survival skills of *C. difficile* spores, they are easily spread in healthcare settings. This leads to a huge burden on the healthcare community, with over half a million patients infected annually with *C. difficile* in the United States alone, and an attributable healthcare cost of over a billion dollars.[1] This problem is confounded by two facts. First, *C. difficile* can only successfully colonize hosts with microbial dysbiosis in the gut microbiome community.[15] In its vegetative cell form, *C. difficile* is a poor competitor for nutrients compared with the robust gut microbiome, making it difficult for *C. difficile* to create a niche for pathogenesis.[22] While this benefits healthy individuals, greatly reducing any risk of becoming infected with *C. difficile*, it also means that those most commonly afflicted with CDI are already vulnerable populations. In particular, *C. difficile* infects hosts that are being treated with antibiotics, as well as patients undergoing chemotherapy. Antibiotics are heavily prescribed in hospital settings, and while they are effective at eliminating most pathogenic bacteria such as *Staphylococcus aureus*, they also severely damage commensal bacterial populations.[23] This leads to a large population of hospitalized patients that are susceptible to *C. difficile* infection, who are already infected with other bacterial infections. This can make a CDI extremely dangerous for hospitalized patients, and results in over 29,000 deaths annually in the United States alone.[24] Second, CDIs have a high rate of recurrence. Approximately 20% of patients that are diagnosed with *C. difficile* infection will be diagnosed with *C. difficile* again within 2-8 weeks of initial treatment.[25] Patients that experience one cycle of recurrence are even more likely (60%) to be diagnosed with *C. difficile* a third time and so on.[25] This leads to a continuous cycle of infection that can be devastating for both the patient and the healthcare system continuously trying to cure the same disease.

A major component of these high recurrence rates is due to the existing treatment methods for *C. difficile*. The most common treatments for CDI are the antibiotics vancomycin or metronidazole.[26] While these antibiotics are effective in 80% of cases, the risk of recurrence is further compounded by this treatment method. Since antibiotic treatment is a major risk factor for CDI, if treatment is unable to completely clear the infection then the gut continues to exist in a perturbed state due to continued antibiotic use. Additionally, patients that experience recurrent CDI will most likely undergo the same treatment method in most cases, which leads to further recurrence in patients that are again unable to clear the infection. In severe cases, a fecal microbiome transplant has shown high success in restoring the gut microbiome.[27] This treatment, however, only exists as a last result due to the need for a donor that matches their lifestyle, and the expense of the treatment. While antibiotic-resistant *C. difficile* is uncommon, it has been reported.[28] Antibiotic resistance is a major concern for treatment of a wide variety of bacterial pathogens, and *C. difficile* is no exception. As treatment for CDI is heavily reliant on antibiotic

use, any bacterial resistance to vancomycin could prove debilitating for the treatment of CDI using current therapeutics. For this reason, it is crucial to develop new targets and therapeutics for the treatment of CDI, to reduce recurrence and limit the potential for antibiotic resistance.

While the diagnosis of *C. difficile* is ordinarily straightforward, certain populations can be difficult to diagnose. Patients with underlying gastrointestinal diseases such as inflammatory bowel disease (IBD), which includes ulcerative colitis and Crohn's disease, can be extremely difficult to diagnose due to similar symptomology to CDI.[29] There is a considerable overlap in symptomology between an IBD flare up and CDI, which can make diagnosis complicated, and may result in patients that are not properly treated for CDI.[10] A CDI diagnosis can sometimes be made through the detection of toxins in the stool,[30] but this is not routinely performed without a reason to suspect CDI. Additionally, many of these assays and tests for CDI diagnosis are developed, designed and optimized for use on adult patients.[31] Many pediatric patients with these same underlying conditions will experience frequent *C. difficile* infections over their life, in part due to susceptibility to CDI from gut dysbiosis and in part due to regular visits to hospitals.[32] These difficulties are further confounded by the fact that many pediatric patients will be asymptomatic for CDI.[32,33] Despite comparable toxin and bacterial burdens, many of these patients will never show traditional symptomology and therefore will not be properly diagnosed and treated for CDI.[33] When considering these difficulties in diagnostics, in tandem with treatment efficiency concerns, it becomes clear that novel therapeutics and diagnostic markers are crucial for continued protection against *C. difficile.*

1.3. MASS SPECTROMETRY APPROACHES CAN FURTHER ELUCIDATE CHANGES IN THE *C. DIFFICILE* MOLECULAR ENVIRONMENT

Bacterial pathogens such as *C. difficile* interact with the host during infection by sensing chemical signals and secreting their own.[34] This relationship offers a wealth of molecular information that can be harnessed for understanding pathogenesis and developing novel therapeutics. Matrix-assisted laser desorption/ionization imaging mass spectrometry (MALDI IMS) is an underutilized technology for molecular discovery.[35] MALDI IMS combines the robust molecular information offered by mass spectrometry with the spatial information of microscopy.[36] Importantly, this technology is usually untargeted which makes it an incredible resource as a discovery tool. The results of MALDI IMS experiments show a variety of molecules detected from

a tissue, their localization within the tissue, as well as relative abundance of these molecules across different regions.[4]

MALDI IMS works through the application of a small organic molecule, known as a matrix, to a thin section of tissue mounted onto a glass slide.[37,38] After matrix application, a laser is fired onto the tissue to ionize molecules within the sample, which are then transported to the detector (Figure 1.2).[38] The matrix absorbs the majority of the energy, allowing the analytes of interest to travel intact to the detector where they are measured in units of mass-to-charge ratios.[38] A full spectrum is generated each time the laser fires, which then correlates to a pixel in the final image.[4] This allows for the mapping of thousands of analytes onto one tissue, as well as the ability to see the same *m/z* intensity values across a single sample.[35] Since these data can be acquired with minimal information about the sample, they offer an untargeted dataset of all the ionized molecules present within a sample. This discovery-based approach can elucidate interesting localization and intensity differences for further investigation that may have been overlooked with targeted methods. When applied to a condition such as infection, this technology can show molecular changes that occur during infection and give rich insight into changes in the molecular landscape that the bacteria encounters and alters.[39–41]

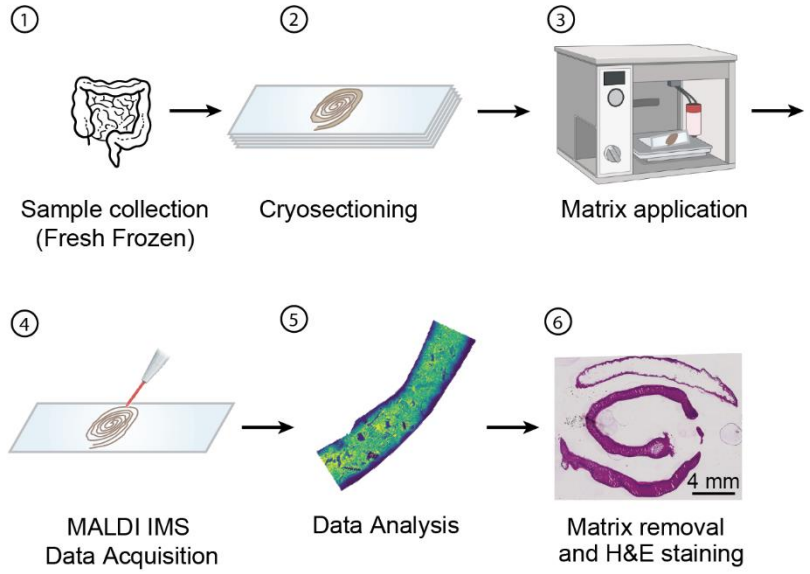

Figure 1.2. Workflow for MALDI IMS analysis of tissue.

While MALDI IMS can be quantitative with the inclusion of standards,[42] liquid chromatography tandem mass spectrometry (LC-MS/MS) can also be applied in parallel to further deepen the molecular information from a sample.[43] LC-MS/MS includes an additional level of separation, and therefore information, by separating analytes by retention time prior to MS analysis.[44] MALDI IMS can be utilized to identify molecules of spatial interest, and LC-MS/MS can work in tandem to both 1) identify these molecules more concretely and 2) determine abundances of these molecules in various samples using standards and calibration curves. Together, these

two MS-based technologies can be incredibly powerful for the discovery of novel therapeutics and biomarkers by elucidating the already-changing molecules during infection, which can offer further information on how the molecular landscape may change in the presence of bacteria such as *C. difficile.*

Imaging mass spectrometry has previously been applied to the gastrointestinal tract for a variety of applications.[45–51] The majority of these images, however, only utilized cross-sections of tissue, limiting the broader localization information throughout the intestines. A variety of biological questions have been asked with this method, but most of these investigations merely used intestinal tissue as a model to highlight improvements in technological and sample preparation methods. For instance, in 2013 Hong, *et. al*. applied a novel matrix to jejunal tissue to better detect absorptive bioactive small peptides.[45] Absorption of various molecular classes, including pharmaceuticals, occurs within the GI tract making it a major focus for these types of applications.[52] This group utilized the jejunum, cut traditionally along the mesenteric border, to highlight the advances their novel matrix enables. As with many of these intestinal investigations, the analysis focused exclusively on cross sections of tissue without including luminal content. A similar investigation by Garate *et. al*. in 2015 highlights another novel matrix combination to improve imaging resolution, and utilized a human colon tissue for their sample.[49] This study illustrated unique lipid distributions throughout the layers of the human GI tract. Kaya *et. al*. applied a dual polarity IMS method, where both positive and negative mode MS can be acquired from the same tissue, using a jejunal mucosal region of the small intestine.[46] This investigation focused on lipid homeostasis, and was able to detect two taurine-conjugated bile acids in the tissue as well (taurocholic acid and taurodeoxycholic acid). One notable exception to the cross section approach is Carter *et. al.,* who used a traditional swiss roll preparation to study nonhuman primate jejunal samples after acute radiation.[53] This investigation showed significant lipidomic alterations in the intestine that could impact function, and emphasized how important a broad view of the intestine can be for drawing large-scale conclusions.

Many of the other GI investigations with MALDI IMS in the past few years focused on the absorption of drugs into the intestine. These offer great insight into how the GI environment can change with the introduction of exogenous material, as well as polyphenols as studied by Nguyen *et. al*.[54] Huizing *et. al*. quantitatively visualized intestinal drug distribution in the ileum as well as the colon, once again utilizing cross sections of tissue.[50] They were able to show that there was a large amount of drug in the lumen, despite thoroughly flushing the area, as well as some passage of drugs across the intestinal wall. Strindberg *et. al.* conducted a similar investigation of

prodrug absorption in the rat duodenum and jejunum.[51] They determined that the prodrug was actually hydrolyzed prior to reaching its target in the small intestine. This study also detected taurocholic acid in the lumen of the samples. These investigations highlight the complex dynamic of the gastrointestinal tract, and the depth of information that can be acquired with IMS. The exclusive utilization of cross sections of tissue without luminal content, however, leave a large gap in our current imaging approaches to the intestine.

MALDI IMS can also be a powerful tool to investigate molecular changes in the context of infection. A multitude of investigations into *Staphylococcus aureus* have shown unique spatial distributions of molecules in the abscess formed by *S. aureus*,[39,40,55,56] but *C. difficile* has been an underexplored infection model in the context of IMS. *C. difficile* infections raise additional considerations for imaging of the GI tract, because the spores localize to the lumen and luminal content, which was not studied in the investigations previously discussed. This motivated the examining of the gastrointestinal tract with the retention of luminal content, and the development of preparation strategies to retain both tissue types as discussed in Chapter Two. There have, however, been a few IMS investigations of tissue from mice infected with CDI. The first utilized a different ionization method, laser ablation inductively-coupled plasma (LA-ICP IMS) to measure elemental abundances in the colon. Zackular *et. al*. in 2016 showed that zinc levels in colon tissue are elevated during infection with *C. difficile*.[41] They also showed that calprotectin, a metal-binding protein associated with inflammation, can be detected in the cecum during infection while undetected in the control tissue. This example emphasizes the complex molecular dynamic occurring during CDI infection, which can be more effectively harnessed to understand the disease at a molecular level. Knippel *et. al*. also applied MALDI IMS in 2018 to study CDI in the cecum.[55] This investigation targeted hemoglobin, specifically hemoglobin subunit alpha, which they showed accumulated during infection. This spatially-targeted molecular approach can elucidate a wide variety of interesting potential biomarkers, especially when applied to the gastrointestinal tract in its full complexity.

These various applications of MALDI IMS to both the gastrointestinal tract and the pathogen *C. difficile* highlight the potential for discovering novel molecular changes that can be targeted through deepening our understanding of CDI. MALDI IMS is a powerful tool that allows us to see the molecular environment that *C. difficile* encounters during infection, as well as how CDI can change and manipulate this environment. Chemical signaling plays a crucial role in the host-pathogen interface, which imaging can further elucidate. Additionally, the GI tract includes both the epithelium and the luminal content. Both of these regions have robust molecular

compositions that differ significantly from each other. Especially in the context of CDI, as *C. difficile* spores localize to the luminal content, studying how these regions respond differently to infection further strengthens our understanding.

The pathogenesis of *C. difficile* relies heavily on chemical signaling through the process of germination.[57] As mentioned previously, *C. difficile* enters a host as a endospore and then converts into a vegetative cell while in the intestines. These vegetative cells then initiate toxin production, the underlying cause of much of CDI symptomology.[58] The process of converting from a spore into a vegetative cell is known as germination. *C. difficile* only initiates this process when it senses certain chemical signals in the environment as a way to map the safety of the location for survival of the anaerobic vegetative cell.[2,57] This chemical trail includes bile acids, amino acids and nutritional calcium.[59] These molecules and metals have the ability to change how the spores respond to the gut environment, by indicating that germination would be beneficial to the pathogen. Interestingly, these are host-produced chemical signals, suggesting a rich interplay in signaling between the host and pathogen. The chemical interplay in the gut during CDI needs to be further explored to better understand how *C. difficile* can impact the host, and how therapeutics can exploit this relationship for novel treatments.

While a variety of molecular classes can initiate this germination protocol, this study focuses exclusively on the molecular class of bile acids. This was initiated by preliminary MALDI IMS investigations, which further highlight the strength of the technology as a discovery-based tool. Initial images of the CDI small intestine show dramatically increased abundance of taurocholate (a bile acid) as compared to mock-infected intestine.[60] As a host-produced molecule that positively impacts *C. difficile* germination efficiency,[59] this molecular class warranted further investigation in the context of infection.

1.4. BILE ACIDS ARE HOST-PRODUCED AND RECYCLED MOLECULES WITH A DIRECT ROLE IN *C. DIFFICILE* INFECTION

Bile acids are a class of small molecules produced and recycled by the host. They are derived from cholesterol in the liver and shuttled between the liver and the intestine through a highly conserved process known as enterohepatic circulation.[61] In the context of the gastrointestinal tract these molecules are of great interest because they can be host-derived or microbe-derived, and are acted upon by the gut microbiome.[62] Additionally, growing evidence

suggests a variety of roles for bile acids as signaling molecules for the host in addition to their studied role in digestion.[63–66]

Historically, bile acids have been studied primarily in the context of lipid digestion. These amphipathic molecules are optimal for transporting highly hydrophobic lipid droplets through the hydrophilic environment of the gastrointestinal tract.[7] These lipid droplets undergo emulsification and form emulsion droplets, which consist of lipid droplets surrounded by bile acids.[7,67] The hydrophobic side of these bile acids surround the lipids, while the hydrophilic side allows the emulsion droplet to continue traveling through the intestine for the digestion process (Figure 1.3). Pancreatic lipase is then secreted from the pancreas to further break down these droplets into free fatty acids (FFAs) through hydrolysis.[68] With the smaller free fatty acids, the bile acids can then completely surround the FFAs and form micelles similar to a lipid bilayer. In this micellar form, the lipids are then able to be absorbed by enterocytes and circulated appropriately through the host where they can be broken down even further.[68] Once the FFAs are absorbed into the enterocyte, the bile acids are recycled and continue through the intestine (Figure 1.3). While most of the lipid absorption occurs in the jejunum, the middle and longest section of the small intestine, bile acids continue to the ileum, the distalmost region of the small intestine, where they are then absorbed into enterocytes and recycled.[6,67]

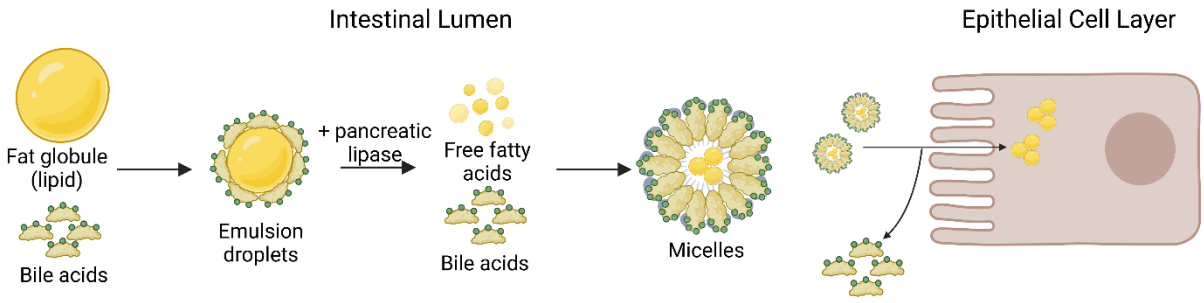

Figure 1.3. Schematic of bile acid assisted lipid digestion and absorption in the intestines.

While more and more bile acids are being discovered yearly, all can be classified into four main categories.[6] Bile acids are referred to based on whether they are host or microbe-produced, as well as their conjugation status. As previously mentioned, most bile acids are produced by the liver from cholesterol.[69] This is why medications for high cholesterol commonly target bile acid levels to initiate further conversion of cholesterol into bile acids.[70] The bile acids produced in the liver are referred to as primary bile acids, or host-produced, and are the majority of bile acids present in the body (Figure 1.4).[62] In humans, the main primary bile acids are cholic acid (CA)

and chenodeoxycholic acid (CDCA). In murine models, CDCA is rapidly converted into muricholic acid.[71] All three of these base bile acids can then be conjugated with either a taurine or a glycine group. These groups replace the carboxylic acid on the end of the other primary bile acids, and change the properties of the bile acids in a variety of functions including germination. Most bile acids are conjugated when they leave the liver, and conjugation patterns are also species-dependent.[63] In humans, approximately 35% of primary bile acids are conjugated with taurine, with the other 65% conjugated with glycine.[72] In mice, however, taurine is strongly preferred and ~95% of bile acids are conjugated with taurine in murine systems. Bile acids that are produced in the liver and conjugated are referred to as conjugated primary bile acids (e.g. taurocholic acid), while CA, MCA and CDCA are unconjugated bile acids (Table 1.1).[72]

Ordinarily bile acids are highly conserved, with 95% reabsorbed in the ileum and returned to the liver.[68] Approximately 5% of bile acids, however, continue through to the large intestine. The large intestine or colon houses trillions of gut microbes, some of which act upon these bile acids through bile salt hydrolases (BSH).[62,73] These enzymes first cleave off conjugation groups

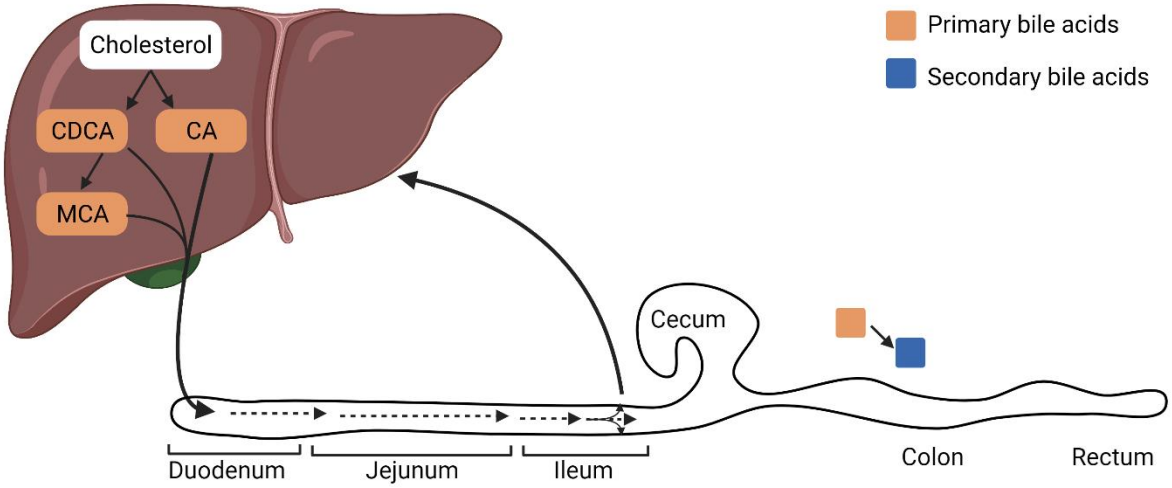

Figure 1.4. Representation of the enterohepatic circulation of bile acids. Adapted from figure by Dr. Aaron Wexler.

from conjugated bile acids, which allows for more complex chemistry by the microbiota.[62] These unconjugated primary bile acids can then be converted into new bile acids, known as secondary or microbe-produced bile acids (Figure 1.4).[73] These secondary bile acids can also be reabsorbed in the colon and returned to the liver where they can be conjugated with taurine and glycine as well, producing secondary bile acids.[73] There is a plethora of secondary bile acids still being discovered, and they have unique roles as antimicrobials in the context of CDI. This further

emphasizes the importance of understanding the bile acid chemical landscape during infection, as the same class of molecules can both stimulate germination of *C. difficile* and inhibit growth of vegetative cells.

Recently, the discovery of a variety of bile acid receptors have suggested additional roles for bile acids as hormones. The primary bile acid receptor, Farnesoid X receptor (FXR) will be discussed in further detail in the following section. In addition to FXR, there is a G-protein-coupled bile acid receptor (GPCR) specific to bile acids. TGR5 is expressed in almost every tissue or cell type.[74] When activated by conjugated or unconjugated bile acids, TGR5 couples to Gαs proteins to activate a pathway increasing the amount of cAMPs present.[75] Additionally, TGR5 can also activate MAPK signaling which communicates signals from cell surface receptors to DNA.[76] Bile acids can activate a variety of receptor types, including nuclear receptors (e.g. FXR) and cell surface receptors (e.g. TGR5).[77,78] While much of this activation is used for bile acid homeostasis within the system, they also have interesting applications to other functions in the cell. For instance, tauroursodeoxycholic acid (TUDCA) can promote the differentiation of osteoblasts from mesenchymal stem cells though cell surface reporters and an integrin-mediated pathway.[65] It does so by stimulating Integrin 5, which is associated with the activation of the ERK1/2 pathway. Due to this effect, TUDCA is a potential substitute for BMP-2 (bone morphogenetic protein) in assisting with bone tissue regeneration.[65] Through muscarinic receptors, secondary bile acids can also promote the growth of cancer cells by stimulating epidermal growth factor receptors.[66] These studies suggest that bile acids may play a much larger role than currently realized in human health, in particular through signaling to invaders such as pathogenic bacteria.

Table 1.2. Examples of various bile acids investigated by category.

Primary Unconjugated	**Primary Conjugated**	**Secondary Unconjugated**	**Secondary Conjugated**
Cholic acid (CA)	Taurocholic acid (TCA)	Deoxycholic acid (DCA)	Glycodeoxycholic acid (GDCA)
Chenodeoxycholic acid (CDCA)	Glycocholic acid (GCA)	Lithocholic acid (LCA)	Glycoursodeoxycholic acid (GUDCA)
β-Muricholic acid (bMCA)	Glycochenodeoxycholic acid (GCDCA)	Ursodeoxycholic acid (UDCA)	
	Tauro- β-muricholic acid (TbMCA)		

In addition to studying levels of bile acids, it is important to understand their circulation and production, with a particular focus in this study on primary bile acids. We have seen that increased bile acid levels may be necessary for successful colonization and germination of *C. difficile*, which opens the possibility that *C. difficile* may directly impact bile acid homeostasis to promote its colonization.[60] The biosynthesis of primary bile acids from cholesterol in the liver occurs via an 18-step synthesis for the classical pathway.[79] The enzyme Cytochrome P450 7a1 (CYP7A1) initiates this classical pathway, as well as serving as the rate limiting step. CYP7A1 converts cholesterol into 7a-hydroxycholesterol through the addition of a hydroxyl group.[71] This enzyme is directly controlled by receptors as a way to regulate bile acid levels, where lower activity results in less bile acid production.[64] Approximately 90% of bile acids are produced via this classical pathway.[61] Bile acid synthesis can also occur through alternative pathways, which makes up the remaining 10% of bile acids.[80] One of these pathways is the acidic pathway initiated by CYP27A1, which is a prominent enzyme towards the end of the classic pathway as well.[81] The acidic pathway uses oxysterol intermediates to reach the final bile acid products.[81]

While CYP7A1 controls the quantity of primary bile acids present through the classic pathway, the makeup of bile acid pools is also important for bile acid production. CA and CDCA, and their conjugated counterparts, have different binding efficiencies for receptors, and their relative abundances can result in changes in signaling.[82] While all primary bile acids initiate from the same molecule, their synthesis branches and occurs in parallel early on. The enzyme CYP8B1 determines bile acid pool makeup through the addition of an extra hydroxyl group to form cholic acid.[83] Increased CYP8B1 activity leads to higher ratios of cholic acid derivatives compared to chenodeoxycholic acid, while decreased activity increases the ratio of CDCA.[83] Cholate derivatives are also potent germination factors for CDI, so increasing the abundance of these bile acids could benefit the colonization of *C. difficile.*[59] In mice, CDCA is rapidly converted into muricholic acid (MCA).[84] This conversion is completed by the murine-specific enzyme CYP2C70, which adds another hydroxyl group.[84] This group can be added in two orientations leading to both α-muricholate and β-muricholate, where βMCA is more common. The presence of MCA in the context of mass spectrometry, however, complicates analysis using MALDI IMS as MCA and CA are isomeric. For this reason, LC-MS/MS methods are usually employed for bile acid analyses. Finally, conjugation in the liver of both primary and secondary bile acids occurs through the enzymes BACS and BAAT. BAAT removes the CoA group on the bile acids and replaces it with either a taurine or glycine group.[85] After this process, bile acids are sent to the gall bladder for storage. Once the host ingests a meal, the gall bladder then secretes the bile acids into the small intestine, along with pancreatic lipase from the pancreas, to aid in lipid breakdown.[61]

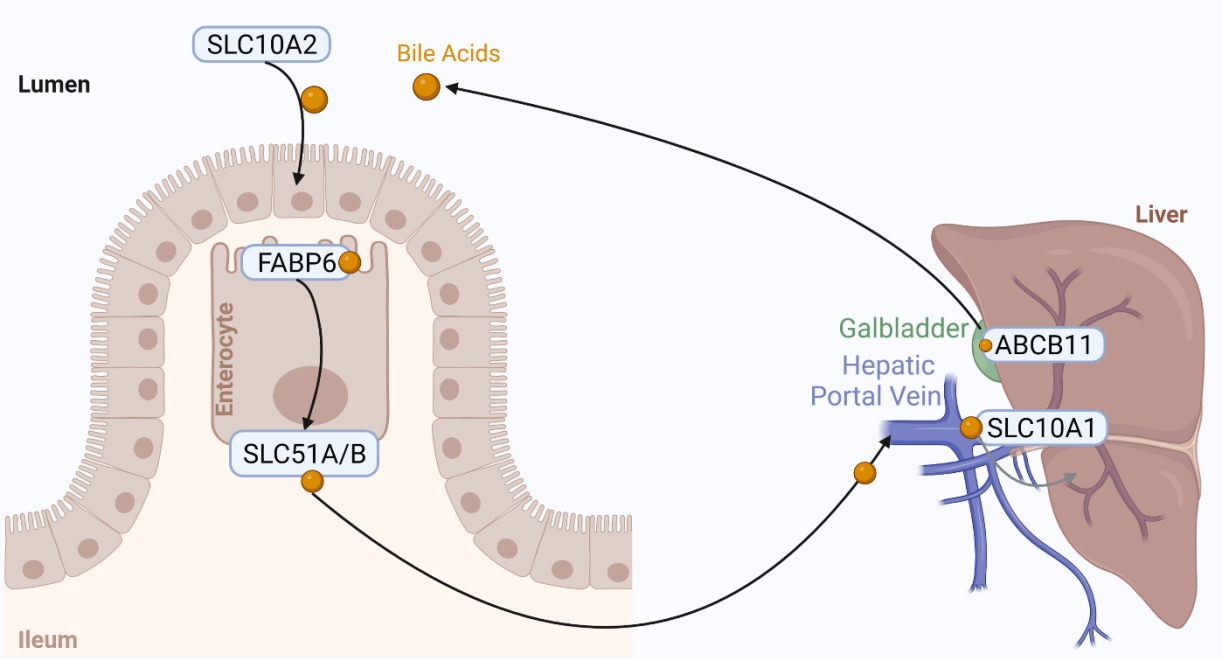

Figure 1.5. Schematic of bile acid recycling from the ileum to the liver. Light blue ovals represent the genes that encode for the enzymes at each location of the transport of bile acids.

Bile acids are also efficiently recycled through absorption.[68] As mentioned above, approximately 95% of bile acids are reabsorbed in the ileum.[86] This process occurs through a highly conserved network of proteins, many of which are transporters and channels, shown in Figure 1.5. In the liver, the enzyme ABCB11 (also known as bile salt export pump or BSEP) is responsible for pushing bile acids stored in the gall bladder into the small intestine.[87] Once bile acids make it to the ileal lumen, the sodium-dependent transporter SLC10A2 (also known as apical sodium-dependent bile acid transporter, ASBT) brings these bile acids from the lumen into the intestine enterocytes.[6] Once the bile acids reach the enterocyte, FABP6 (also known as intestinal bile acid-binding protein, I-BABP or gastrotropin) transports them to the basolateral membrane.[7] At this membrane, the heterodimer SLC51A/B (also known as the organic solute transporters α and β, OSTα/β) pushes the bile acids out of the enterocyte into blood vessels where they will be transported back to the liver via the hepatic portal vein.[6] Finally, upon return to the liver, another sodium-dependent transporter SLC10A1 (also known as sodium/bile acid cotransporter, NTCP) transports the bile acids back into the liver where they may be conjugated or returned to the gall bladder to continue the cycle.[71]

Research over the past decade has elucidated the major role that FXR plays in this circulatory pathway in both the liver and the intestine. FXR is an intracellular ligand-activated

nuclear receptor commonly associated with bile acids and enterohepatic circulation.[64] Many illnesses associated with abnormal bile acid metabolism, which are discussed below, have been directly linked to FXR. For instance, FXR has a known role in the prevention of bacterial translocation in the GI tract, as well as in regulating liver inflammation.[77] As bile acids are continuously circulated from the liver to the ileum and then returned back to the liver, FXR activation in one of these regions leads to changes in the overall pathway. Bile acids are potent ligands for FXR activation, and enterohepatic circulation is largely controlled through negative feedback loops based on the concentration of bile acids in the liver and small intestine.[88] In addition to other regions of the body, FXR is found within hepatocytes and enterocytes where it interacts with conjugated and unconjugated bile acids.[64]

In the liver, bile acids that have been produced or recycled bind to FXR as ligands (Figure 1.6). This activation causes an FXR-mediated upregulation of the small heterodimer partner (SHP).[89] SHP is then able to inhibit activity of both hepatic nuclear factor 4α (HNF4α) and liver receptor homolog-1 (LRH-1).[89] Through the inhibition of HNF4α and LRH-1 activity, the bile acid response element is effectively turned off by preventing binding to this region in both *Cyp7a1* and *Cyp8b1*. A similar process occurs to generate a negative feedback loop for the expression of *Slc10a2.* Bile acids are able to decrease the expression of *Slc10a2,* which in turn leads to FXR-mediated SHP production, resulting in repression of LRH-1 for *Slc10a2*.[89] This relationship between FXR and *Slc10a2* was shown using mice with either an overexpression of FXR, or a knockout of FXR. After feeding control mice with bile acids, *Slc10a2* expression decreased due to increased bile acids being introduced to the system. When mice had an overexpression of FXR, there was no longer a down-regulation of *Slc10a2* after bile acid feeding. Interestingly, in mice without FXR, the expression of *Slc10a2* was unresponsive to feeding with bile acids, suggesting a complex role for FXR in regulating the uptake of bile acids.[89]

Bile acid ligand-binding to FXR also impacts bile acid transport in the ileum (Figure 1.6). FXR in enterocytes is activated through bile acid binding, which increases expression of *Fabp6* and *Slc51a/b*.[90] FABP6 transports bile acids from the apical to basolateral membrane within the enterocyte, where OSTA/B then transports them from the basolateral membrane to the portal vessels.[91] This response is interestingly two-fold, where FXR activation in the enterocyte leads to limited uptake of bile acids via SLC10A2, while also promoting basolateral bile acid secretion.

Overall, this leads to decreased intracellular levels of bile acids within the enterocyte, resulting in the removal out of bile acids from the cell and restricted uptake of bile acids into the cell.

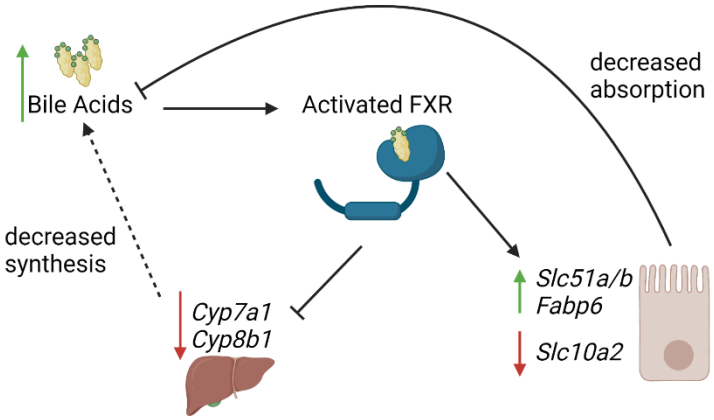

Figure 1.6. Schematic of FXR signaling pathways in the liver and enterocytes after activation by bile acids. Downstream changes in gene expression in the liver and enterocytes controlled via FXR activation by bile acids. FXR activation leads to decreased hepatic synthesis, decreased ileal absorption, and increased removal of bile acids from enterocytes.

Bile acid pool sizes are tightly controlled, and this is due in part due to the toxicity of bile acids at certain concentrations. Indeed, when bile acid dysregulation occurs it has major implications for metabolism and liver health. Ordinarily, bile acids maintain liver metabolite homeostasis, and have anti-inflammatory properties.[61] An accumulation of bile acids, however, can cause cholestasis which results in liver inflammation and injury.[92] In the intestines, bile acids also control the microbiome by preventing gut bacterial overgrowth.[93] These implications, as well as many more that will not be discussed in detail, highlight the crucial regulation of bile acids and the importance of gut-liver signaling and cross-talk.[94] Bile acids are implicated in various metabolic disorders, such as diabetes.[82] For instance, insulin has been shown to directly increase *Cyp7a1* expression within human hepatocytes, a direct correlation between metabolic disorder and bile acid regulation.[95] *Cyp7a1* expression is also implicated in "high-fat high-cholesterol diet-induced metabolic disorders", where *Cyp7a1*$^{-/-}$ mice are protected from these disorders even on such diets.[96]

Bile acids are also commonly associated with, and implicated in, liver health. The maintenance of bile acid homeostasis has been shown to be crucial for protecting against liver injury.[61] FXR signaling activation by bile acids has also been shown to be beneficial for reducing liver inflammation.[77] When bile acid levels increase, NF-κB cytokine production increases as well

to cause liver inflammation.[61] In severe cases, the buildup of these bile acids is toxic to the bile duct and can damage the epithelium, or even elevate biliary pressure to the point of rupturing the bile duct.[97] This causes an accumulation in the liver as well, resulting in hepatocyte cell death.[92] FXR manipulation by bile acids can help ameliorate some of these metabolic concerns, and antagonistic bile acids such as UDCA have been previously used to successfully treat metabolic diseases.[78,98] In addition to many other health implications, the tight regulation of bile acids is crucial for preventing metabolic disorders such as cholestatic liver diseases, diabetes and obesity, making the rapid influx of bile acids seen during CDI additionally concerning for metabolic processes.[97]

As mentioned previously, bile acids play unique roles in the context of *C. difficile* infection. Although these molecules are host-produced, they contribute significantly to the life cycle of the pathogen. As highlighted in Figure 1.1, primary bile acids serve as germination factors for *C. difficile* spores through recognition by the CspC receptor.[57] Cholate derivatives, including TCA, GCA and TCA, act as co-germinants with amino acids in the presence of spores.[59] Chenodeoxycholate derivates, despite being primary bile acids, may actually inhibit germination, further complicating the relationship between bile acids and CDI.[63] Secondary bile acids such as deoxycholate, however, both induce germination of *C. difficile* spores while simultaneously preventing the growth of the vegetative bacteria.[59] One potential contributor to antibiotics causing susceptibility to CDI is that antibiotics remove members of the microbiota with bile salt hydrolase activity that can produce secondary bile acids to inhibit *C. difficile* vegetative cells. Without microbiota that can produce bile salt hydrolases, primary bile acids quickly become the majority of the bile acid pool which further supports the survival of *C. difficile* spores and colonization.[99]

A difficulty in treating CDI is the high level of recurrence in patients diagnosed with infection. An investigation led by Allegretti, *et. al* probed bile acid levels in 60 patients with CDI, including patients with recurrent infection.[25] They showed that primary bile acids were significantly elevated in patients with recurrent CDI compared to both control populations and patients experiencing their first CDI. They also showed that secondary bile acids were higher abundance in control groups compared to patients with CDI. Since secondary bile acids can protect against *C. difficile*, this offers a potential part of the mechanism for susceptibility to CDI after antibiotic use. While the relationship between bile acids and germination during CDI is well understood, not enough work has been done to understand how *C. difficile* may in turn manipulate bile acid levels to improve its own survival in the intestine. This thesis demonstrates the dramatic changes to bile acid levels and pools in the context of infection and shows how these changes may come about

in response to pathogenic activity during CDI, utilizing mass spectrometry approaches and novel sample preparation techniques.

1.5. RESEARCH OBJECTIVES AND SUMMARY

Clostridioides difficile is an urgent health threat that needs novel diagnostic and therapeutic developments for effective treatment. This research ultimately aims to further understand the role of a specific molecular class, bile acids, in how the host impacts and is impacted by CDI. Therefore, a multi-omic approach was used, including imaging mass spectrometry, quantitative small molecule LC-MS/MS, immunohistochemistry, proteomics, and transcriptional analysis, to elucidate the role of bile acids in shaping the gut during CDI, and how *C. difficile* may initiate these changes.

The motivation for this research began due to preliminary observations using IMS to investigate rolled intestinal tissue and luminal content to study the intestine. This was a novel sample preparation method that required optimization and alterations to better study the intestine in its entirety. Thus, the first objective of this work was to develop sample preparation strategies to study the gastrointestinal tract with retained luminal content. The results of this method are detailed in Chapter Two. This method allowed us to perform multimodal imaging of the small intestine with intact luminal content, which highlighted the unique molecular makeup of both tissue and luminal content. In particular, this approach highlighted a previously unknown accumulation of primary bile acids in the ileum during infection, which has major ramifications for the host as well as *C. difficile* sporulation.

After this discovery, we harnessed both IMS and quantitative LC-MS/MS to better understand exactly how primary bile acid pools changed during infection. The second objective of this investigation, therefore, was to determine how bile acid pool abundance and makeup changed over the first three days of infection in the liver and intestine. Additionally, we aimed to understand how the trends we saw impacted the fitness of *C. difficile* sporulation and germination, and whether this phenotype was reliant on toxins or inflammation. These results, which show a 100x increase in conjugated primary bile acids in the ileal content during CDI, raised a variety of questions about how and why these changes come about. In addition, with the discovery that without access to the influx of bile acids *C. difficile* germination and colonization were greatly delayed, the motivation for the increased production of bile acids by the host was convoluted.

In light of these trends, as well as additional data from human pediatric patients, further mechanistic questions were needed to understand why these bile acid levels were changing. As transcriptional changes would be the first to occur in an infection setting, this research primarily focused on the transcript abundances of genes involved in enterohepatic circulation in the context of *C. difficile*. Thus, the goal for this section was to determine if transcript levels for enterohepatic circulation genes changed during CDI, and whether these changes contribute to the rising levels of bile acids during infection. These results show that enterohepatic circulation does in fact change during infection at the transcript level, even without the presence of bile acids, in a way that would result in higher levels of bile acids in the ileum at 1 day post infection (dpi). Genes that encode for proteins involved in the synthesis of bile acids are initially upregulated during infection, while genes for proteins involved in ileal absorption are initially downregulated, although these changes are gone by 3 dpi in both processes. These data suggest that *C. difficile* is somehow manipulating this pathway, although protein abundances show that these changes are not translated to the proteomic level, raising questions to how these changes are actually impacting bile acid levels.

Ultimately, this thesis attempts to understand the complex dynamic between CDI and the host through the lens of bile acids. The results highlight this interplay and suggest that the host and pathogen are in a competition to control bile acid levels at the transcriptional level, and the outcome leads to improved germination and colonization of *C. difficile* in the presence of an abundance of bile acids in the intestine. Additional questions about the role of antibiotics in this process, as well as the specific mechanism in light of minimal changes in protein expression levels, would further deepen our understanding of this process and potential avenues for improved treatment and diagnosis.

CHAPTER 2

Development of sample preparation protocols for small intestinal tissue with retained luminal content for analysis by imaging mass spectrometry

A version of the following chapter was previously published and has been adapted from Guiberson et al., *JASMS,* Copyright 2022 by American Chemical Society[100]

2.1 OVERVIEW

Digestive diseases impact over 60 million people a year in the U.S. alone, and yet existing imaging investigations into the gastrointestinal tract are incomplete. Current approaches remove luminal content from the intestines, and images focus on small regions of tissue at a time. Here we demonstrate the use of a novel sample preparation method that expands the amount of tissue imaged on one slide and retains luminal content. To ensure tissue and luminal content retention, we utilized a poly-l-lysine coating onto ITO slides for retention during various washing protocols. This approach has shown unique molecular profiles between tissue and luminal content using multimodal imaging modalities including protein, lipid and elemental imaging. We then demonstrate a case study comparing intestinal tissue infected with *C. difficile* against control tissue that showed clear lipid abundance differences during infection, including the primary bile acid taurocholate. Various matrices were then compared on bile acid-spiked tissue homogenates to determine optimal matrix methods for the imaging of bile acids in intestinal sample. Overall, these studies highlight the potential for this intestinal sample preparation approach to detect unique biological markers and signs of infection in the gut using MALDI IMS.

2.2 INTRODUCTION

The human gastrointestinal (GI) tract is the largest interface between the gut microbiota, host, and environmental factors within the body.[101] Within the United States alone, over 62 million people are diagnosed with a digestive disease annually, and the prevalence of these diseases increase with patient age.[102] Despite impacting such a large population and playing such a major role in human health, imaging studies of the GI tract frequently limit the available information from tissue models. Imaging mass spectrometry (IMS) entails ionization of thousands of analytes directly from the tissue surface in an untargeted manner, offering extensive molecular information from tissue samples.[4] Current imaging protocols, both for mass spectrometry and histological studies, flush out the luminal content within the GI tract, removing a key component of information. This luminal content contains bacteria from the gut microbiota, dietary molecules such as ingested

fats, as well as pathogenic bacteria in infected tissues such as spores during *Clostridioides difficile* infection.[18,103] Additionally, by removing luminal content components the host tissue and mucus layer are disrupted or removed entirely, greatly reducing the wealth of information we can gain from studying the GI tract. By retaining luminal content, we increase both the molecular information and spatial integrity of the tissue as a whole, a necessary step in preparing samples for imaging modalities and differentiating between fecal and host molecules of interest.

Luminal content, however, has a high fat and water content.[104,105] This leads to difficulties with retention throughout the IMS sample preparation workflow. In particular, tissue washing protocols utilized for lipid and protein imaging experiments significantly disrupt the spatial integrity of the luminal content and its surrounding tissue with routine preparation methods. Optimal parameters have not been previously determined for the gastrointestinal tract with intact luminal content. Herein we report that the addition of a poly-l-lysine coating onto slides prior to sample mounting allows for retention of both tissue and luminal content spatial integrity through a variety of imaging modalities. Additionally, the inclusion of luminal content showed stark differences in intensity between control and *C. difficile*-infected lumen bile acid levels, the investigation of which was then optimized for MALDI IMS.

In addition to the removal of luminal content, previous IMS experiments have lessened spatial information by only imaging small sections of the GI tract, thereby reducing the comparative power between various regions.[46,106] The GI tract consists of the small intestine and large intestine, with the small intestine consisting of the duodenum, jejunum and ileum. All of these regions have unique functions and molecular characteristics, owning in part to the dramatically different bacterial burden in proximal and distal regions of the intestine,[107] yet existing studies focus on only one region at a time due to slide size limitations. Histological studies of the intestine have thus harnessed the “Swiss roll” conformation, which entails rolling the intestinal tissue in a circular pattern.[108,109] This approach allows for much larger sections of the intestine (~16 mm) to be imaged in the same sample, and therefore allow for comparisons between the different regions of the GI tract. Traditional “Swiss roll” protocols, however, still remove luminal content.[53,110] Thus, we present an approach that allows for simultaneous analysis of luminal content and tissue along large sections of the GI tract using a modified Swiss roll approach, reintroducing the full complexity of the gut for IMS analysis.

2.3 RESULTS AND DISCUSSION

2.3.1 A modified Swiss roll conformation allows for simultaneous analysis of proximal and distal tissue regions with intact luminal content.

Proximal and distal regions of the gastrointestinal tract can have dramatically different molecular makeup, due in part to the higher microbial burden in the distal intestine.[107] The microbiota contribute greatly to the molecular diversity within the GI tract, including producing their own unique metabolites and interactions with dietary fats. The length of the GI tract, however, is a limiting factor for analysis of the entire system simultaneously. The small intestine of a mouse is around 33 mm long, greatly surpassing the space on a traditional glass slide.[111] The Swiss roll conformation allows for ~16 mm of this organ to be imaged at once with only one section (Figure 2.1). While this has previously been achieved with histological tools, the compact size has been at the cost of luminal content. The sections produced using our method are still able to retain this region and information without sacrificing the breadth of the GI tract available to be imaged.

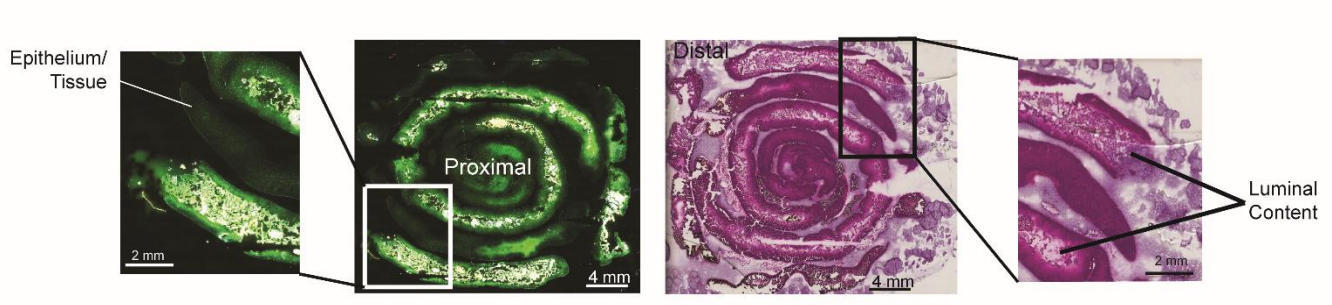

Figure 2.1. Autofluorescence and hematoxylin & eosin stains of adapted Swiss roll conformation. Microscopy images of a proximal intestine sample with intact luminal content in a Swiss roll conformation.

The inclusion of luminal content, however, adds additional sample preparation considerations for routine imaging analysis. In particular, we saw loss of luminal content or tissue retention on glass and ITO-coated slides with various washing protocols (Figure 2.2). To address this sample loss, we applied a poly-l-lysine coating to ITO slides. Poly-l-lysine is a highly polar lysine homopolymer that promotes attachment and adhesion of tissue by increasing the electrostatic attraction between the surface and the sample.[112] Due to its high molecular weight (>150 kDa) poly-l-lysine does not appear in routine MALDI IMS analysis, making it an ideal adhesive for IMS. We compared poly-l-lysine coated, non-coated ITO, and glass microscope slides for tissue and luminal content retention through two different common washing protocols (Figure 2.2). For imaging of lipids, we tested retention after an ammonium formate (AF) and water

wash to remove salt adducts (Figure 2.2.A).[113] For imaging of proteins, we tested a Carnoy Wash, which consists of graded ethanol washes and Carnoy's fluid to remove lipids (Figure 2.2.B). The tissue on a purely glass slide lost all tissue integrity and luminal content with an AF wash, and lost some luminal content with a Carnoy wash as well. An ITO slide was insufficient for luminal content retention in both washes. While some luminal content was lost with a poly-l-lysine coating and a Carnoy wash, initial retention was improved prior to washing and post-washing retention was comparable ITO slides. Overall, poly-l-lysine improved tissue and luminal content retention with an ammonium formate wash and to a lesser scale with a Carnoy wash.

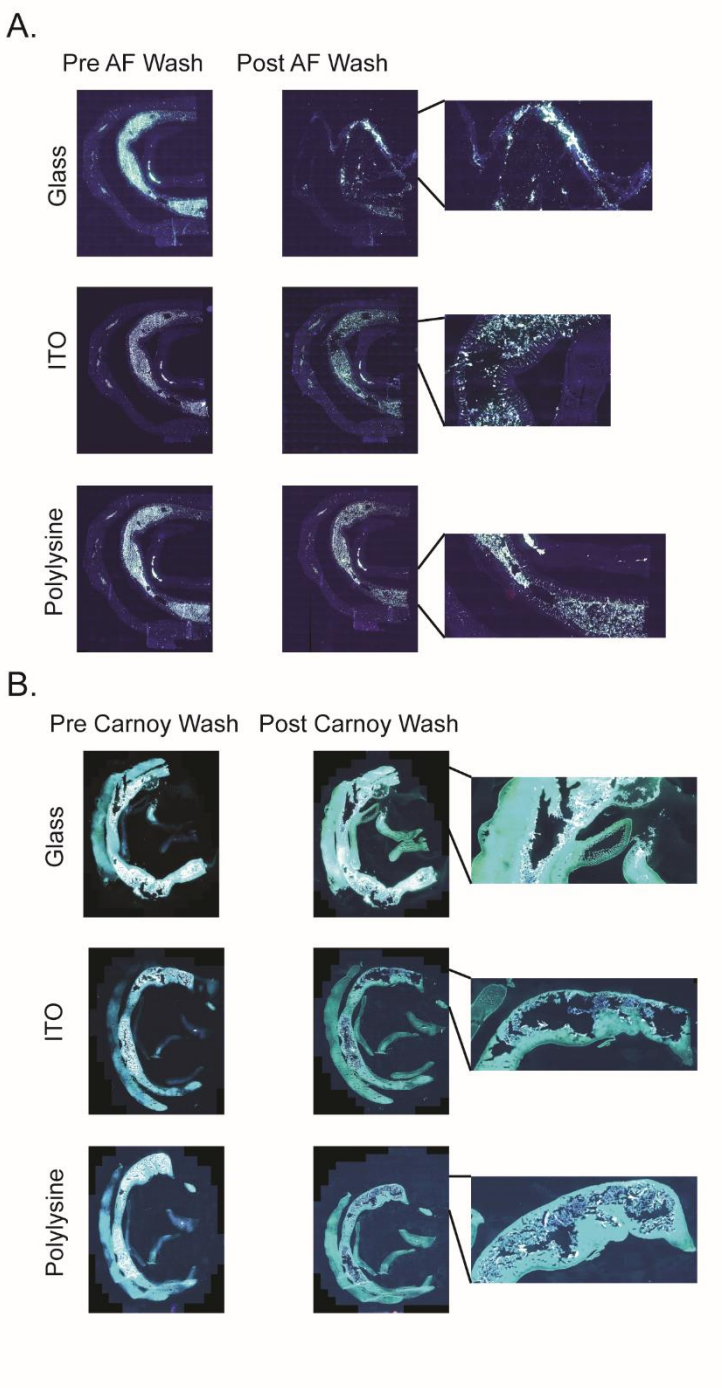

Figure 2.2. Poly-l-lysine coating improves luminal content retention for various washing methods. (**A**) Pre- and post-washing autofluorescence images on glass, ITO, and polylysine-coated ITO slides using an ammonium formate wash. (**B**) Pre- and post-washing autofluorescence images on glass, ITO, and polylysine-coated ITO slides using a Carnoy wash.

2.3.2 Tissue and luminal content in the gastrointestinal tract show unique molecular profiles in various imaging modalities.

To fully elucidate the molecular differences between gut tissue and luminal content, we applied a variety of IMS modalities to proximal intestine tissues. Using the poly-l-lysine coating, and respective washing methodologies (Figure 2.4), we saw unique molecular distributions in protein, elemental, and lipid images of the proximal intestine. Figure 2.3.A shows proteins that localize either exclusively to the tissue (left) or to luminal content (right), highlighting the unique molecular profile of the luminal content. Figure 2.3.B shows various phosphocholines with distinct localization patterns despite being from the same lipid class. The same trend is seen in Figure 2.3.C showing elemental imaging using laser ablation inductively-coupled plasma MS, contrasting dietary metals in the feces (calcium) against those within the tissue (phosphorus). These various imaging modalities highlight the reproducibility of poly-l-lysine coating for tissue retention, as well as the value in studying luminal content alongside intestinal tissue as a unique microenvironment. The addition of this region offers a deeper profile of the intestinal tract, which can potentially be applied to study digestive disease and biomarkers within the fecal content. These data highlight the importance of comparing tissue and luminal content for a representative understanding of the gastrointestinal tract, and how it changes molecularly as a result of various conditions such as diet and disease.

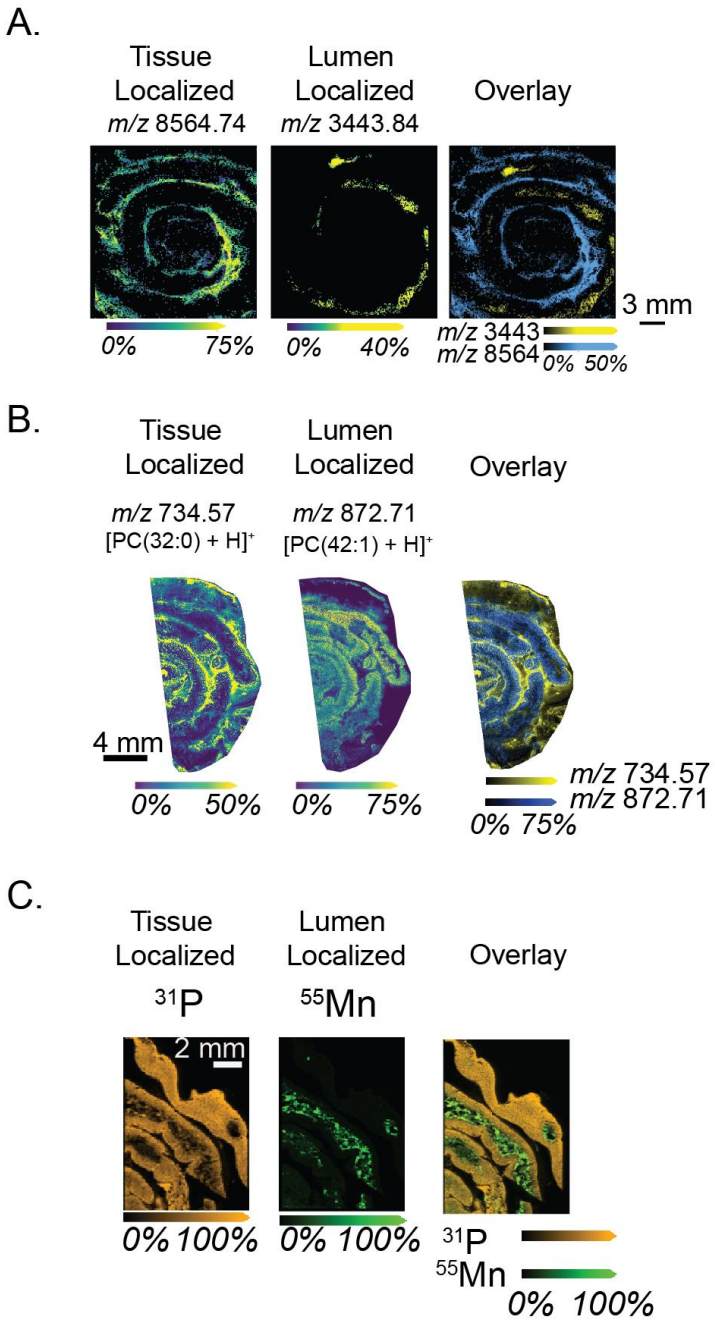

Figure 2.3: Multimodal IMS shows unique molecular profiles between tissue and luminal content regions. A) Imaging of proteins shows tissue-specific localized proteins (left) and luminal content-specific proteins (right) and overlaid proteins. B) Lipid imaging showing tissue-specific localization (left) or lumen-specific localization (right) and overlaid lipids. C) Elemental imaging using LA-ICP IMS shows unique elemental distributions between tissue-specific (P), or lumen-specific (Mn) and overlaid images.

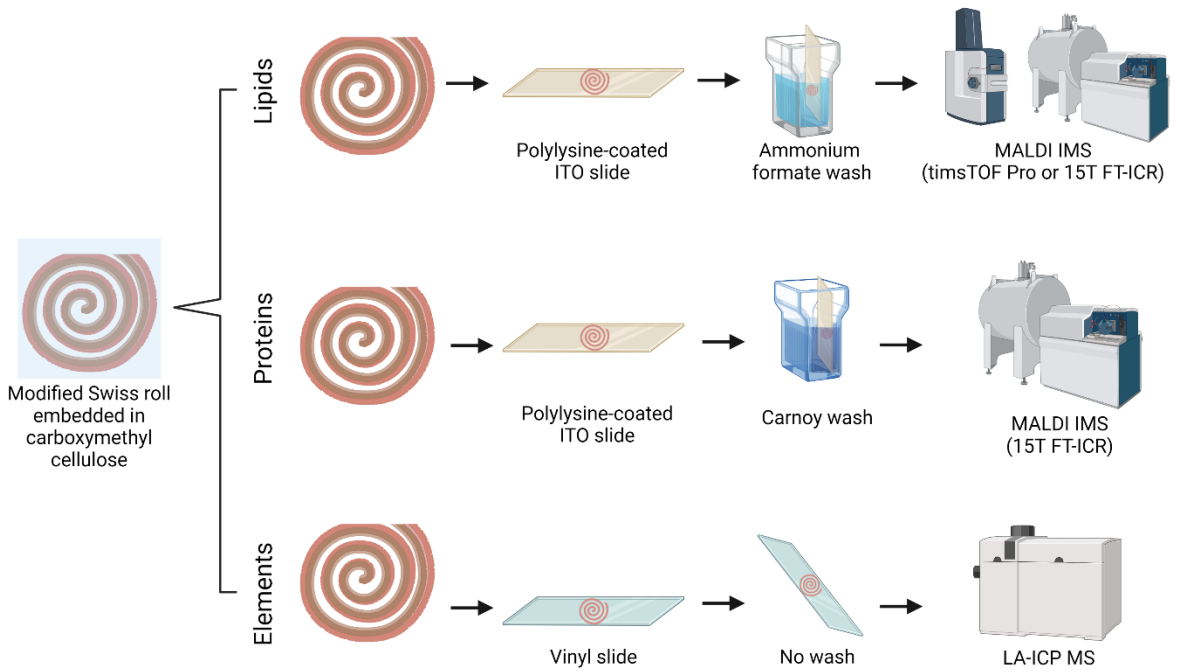

Figure 2.4: Sample preparation workflows for multimodal IMS of modified Swiss roll gastrointestinal tissue samples. Created with Biorender.com.

2.3.3 Fecal lipids and bile acids differ in a *C. difficile* infection model.

To further emphasize the dynamic nature of luminal content, and its potential for detecting novel molecular differences in the gut, we contrasted lipid abundances between *Clostridioides difficile*-infected and control proximal intestine tissue. *C. difficile* produces toxins that attack intestinal tissue, causing inflammation, and is introduced into the GI tract as spores that localize to luminal content.[18] Due to the impact of *C. difficile* on the host, and its localization patterns, this was an ideal infection model for a preliminary case study. Indeed, our preliminary data shows clear differences in multiple lipid classes (phosphatidylethanolamine, PE, and Cer phosphoinositol, IPC) between the luminal content of infected and control tissue. Figure 2.5.A demonstrates two lipids (identified with MS/MS, Figure 2.6) with luminal localization in control tissue that are no longer detected in infected tissue. Due to their localization, it is likely that these lipids are diet-derived, despite both mice being on identical diets, suggesting a more profound impact of *C. difficile* on lipid absorption. Additionally, lipid images of CDI tissue, and mock-infected tissue show a dramatic increase in *m/z* 514.29 (Figure 2.5.B). Based on its exact mass from a high resolution 15T FTICR mass spectrometer, we tentatively identified this ion as the bile acid taurocholate (TCA). To confirm the identity of *m/z* 514.29 as being TCA, we subjected a TCA standard and CDI intestinal tissue homogenate to liquid chromatography tandem mass spectrometry (LC-MS/MS) analysis. We observed both the parent ion at *m/z* 514.3 and a fragment peak corresponding to the taurine moiety at *m/z* 124.0 in both the standard and the sample (Figure 2.7). As bile acids play a critical role in *C. difficile* spore germination, further investigations were done to optimize future imaging of bile acids from intestinal tissue. This difference in abundance between control and infected intestinal tissue would have likely gone undetected without retained luminal content. This case study demonstrates the potential applications of this approach for biomarker analysis from fecal content, as shown by the clear molecular changes in luminal content as a result of gastrointestinal disease.

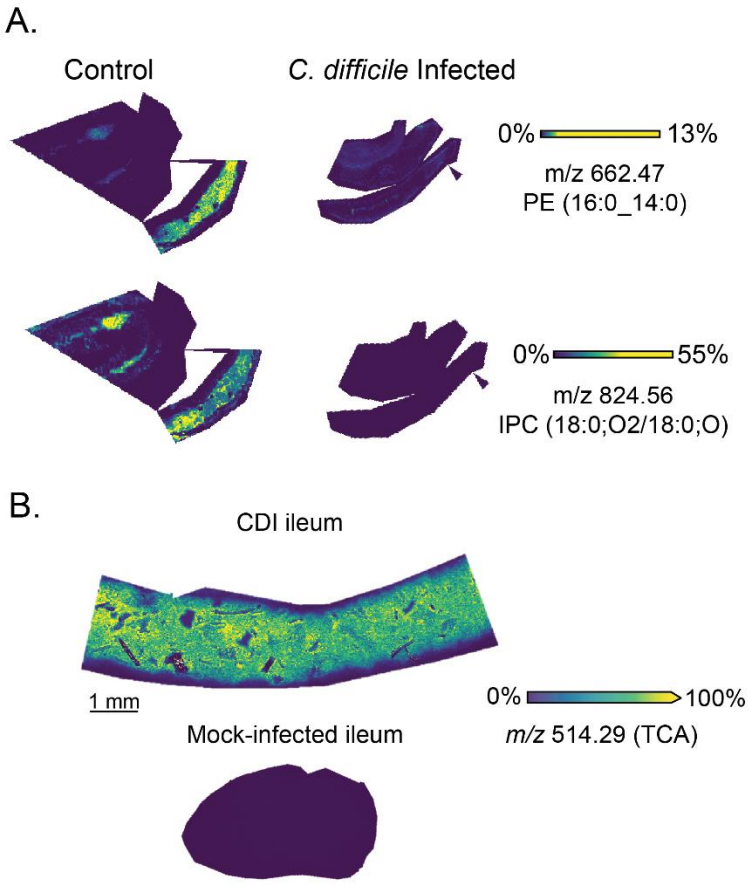

Figure 2.5. Lumen lipid profiles change during *C. difficile* infection. (**A**) MALDI IMS of control proximal intestinal samples with clear lumen localization of lipids (top) and the same lipids in infected tissue (bottom). (**B**) MALDI IMS analysis of the ileal region and lumen of CDI or mock-infected animals at 3 dpi reveals elevated levels of *m/z* 514.3 in CDI mice relative to mock-infected controls.

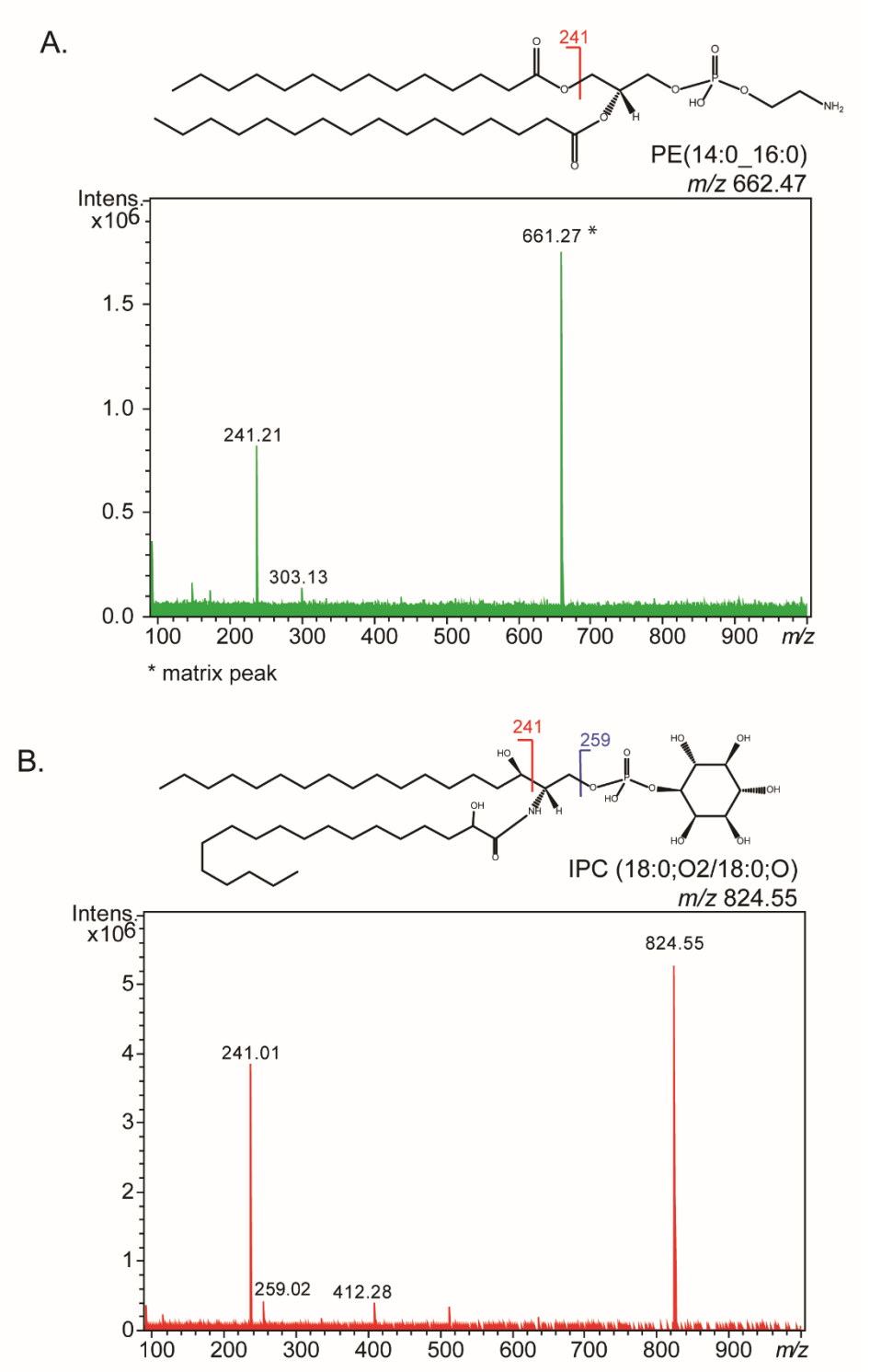

Figure 2.6. Collision induced dissociation (CID) and SORI-CID data were acquired on a 15T FT-ICR to confirm the identity of A) PE (14:0_16:0) and B) IPC (18:0/18:0).

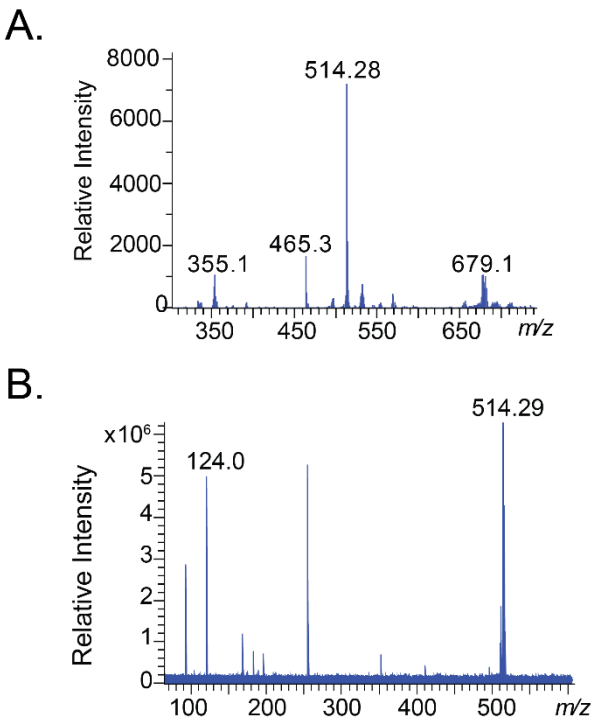

Figure 2.7. The analyte at *m/z* 514.29 was identified as taurocholate (TCA). (**A**) Mass spectrum from MALDI IMS analysis of the ileal region and lumen of a CDI mouse at 3 dpi with *m/z* 514.3 being the most abundance analyte detected. (**B**) LC-MS/MS analysis of CDI distal small intestine tissue and lumen homogenate show peaks at *m/z* 514.3 and *m/z* 124.0 (taurine), supporting the identification of *m/z* 514.3 as TCA.

2.3.4 Various matrices successfully ionize a panel of bile acids from tissue.

In light of the differences between control and CDI tissue TCA levels shown using MALDI IMS, and the biological implications of this molecular class, we also investigated the impact of various matrices on bile acid ionization. Figure 2.8a shows the intensity of three bile acid signals (TCA, GCA, DCA) as detected using a variety of matrices sprayed onto brain homogenate tissue spiked with bile acid standards. These bile acids were chosen to represent both primary (TCA, GCA) and secondary (DCA) bile acids. Only three matrices (DHA, norharmane, 9-AA) were able to reliably ionize all three bile acids. 9-AA, norharmane and DAN were then applied to a mock-infected distal intestine section and analyzed using a continuous accumulation of selected ions (CASI) method. DAN was included in place of DHA, as the ions ionized by DAN showed

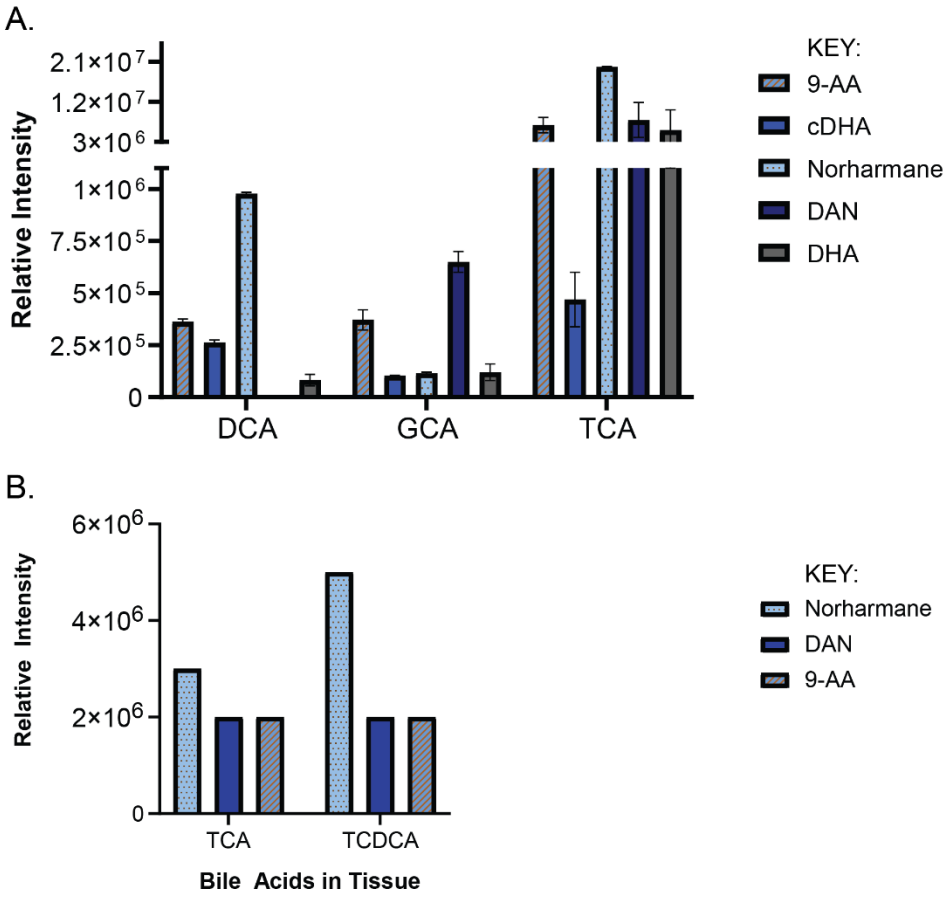

Figure 2.8. Various MALDI matrices (9-AA, norharmane, DHA) can effectively ionize various bile acids (CDA, GCA, TCA) with norharmane best ionizing from tissue. A) Average intensities of brain homogenates with added bile acids ionized using MALDI IMS with different matrices. **B)** Average intensity values for TCA and TCDCA ionized using various matrices (norharmane, DAN, 9-AA) from murine intestine tissue whole image spectra.

reproducibly higher intensity despite the inability to ionize DCA. Figure 2.8b shows the relative intensities of the detected bile acids in tissue (TCA and TCDCA) with these three matrices, although no matrix detected the unconjugated versions of these bile acids. Overall, these two experiments indicate that while all matrices were sufficient for ionizing conjugated primary bile acids, norharmane was the optimal matrix for ionization efficiency and diversity, with the added benefit of ionization in both positive and negative mode.

2.4 CONCLUSIONS

Overall, this novel sample preparation approach with the utilization of poly-l-lysine for improved sample retention offers unique molecular insight into the gastrointestinal tract at a larger scale. Harnessing this approach to investigate differences in infected and control tissue showed multiple lipids and bile acids with differential abundance in the luminal content. A deeper understanding of the GI tract molecularly can further our comprehension of various digestive diseases, and how the complex dynamic of the GI tract may change through all the external factors that act upon it. Application of this method to tissue infected with *C. difficile* opens potential avenues for the discovery of biomarkers and small molecule therapeutics by identifying host molecular changes during CDI. Further investigation into the molecular class of bile acids in the context of CDI, as done below in Chapter Three, can elucidate differences in biologically relevant molecules and expand our understanding of how the host environment changes in response to a gut pathogen.

2.5 METHODS

Materials. Acetic acid, 1,5-diaminonapthalene (DAN), trifluoroacetic acid (TFA), ammonium formate, 2′,6′-Dihydroxyacetophenone (DHA), hematoxylin, and eosin were purchased from Sigma-Aldrich Chemical Co. (St. Louis, MO, USA). HPLC-grade acetonitrile, methanol, ethanol, and chloroform were purchased from Fisher Scientific (Pittsburgh, PA, USA).

Animal Protocols. All animal experiments were performed using protocols approved by the Vanderbilt University Medical Center Institutional Animal Care and Use Committee. Animal studies were conducted using 8- to 12-week old male C57Bl/6 (Jackson Laboratories) mice. Mice infected with *C. difficile* were given cefoperazone in their drinking water (0.5 mg/ml) for 5 days. Following a 2-day recovery period, mice were gavaged orally with 10^5 *C. difficile* spores or PBS to an endpoint of three days.

Sample Preparation. Intestines were rolled into a spiral shape and embedded in 2.6% carboxymethylcellulose (CMC). Tissue and CMC were snap frozen over liquid nitrogen at -80°C, cryosectioned at 10 µm thickness using a CM3050 S cryostat (Leica Biosystems, Wetzlar, Germany) and thaw-mounted onto 1% poly-l-lysine coated ITO slides (Delta Technologies, Loveland, CO) for lipid and protein imaging, or vinyl slides for elemental imaging (VWR, Radnor, PA). Autofluorescence microscopy images were acquired using EGFP, DAPI and DsRed filters on a Zeiss AxioScan Z1 slide scanner (Carl Zeiss Microscopy GmbH, Oberkochen, Germany) prior to matrix application.

Homogenate Preparation. Fresh frozen murine brains were allowed to come to room temperature in a biosafety cabinet. Solutions of TCA, DCA and GCA standards (Sigma Aldrich, St. Louis, MO) in methanol were made at a concentration of 5 mg/mL. 10 µL of each solution was added to the brains, and the resulting mixture was homogenized using a Bullet Blender Storm. The resulting mixtures were spun down for 1 minute at 14,000 rpm, and then extracted and allowed to freeze in a mold. The resulting homogenate was then sectioned at 20 µm thickness and thaw mounted onto an ITO-coated slide (Delta Technologies, Loveland, CO).

MALDI FT-ICR Imaging of Proteins. Samples for protein analysis were washed using graded ethanol washes and Carnoy's Fluid (6 ethanol: 3 chloroform: 1 acetic acid) to remove salts and lipids (70% EtOH, 100% EtOH, Carnoy's Fluid, 100% EtOH, H_2O, 100% EtOH). Samples were sprayed using a robotic aerosol sprayer (HTX Technologies, Chapel Hill, NC) with 90 mg/mL of

2′,6′-dihydroxyacetophenone (DHA) in 70% ACN with 100 uL TFA and 50 uL of 30% ammonium hydroxide. Following matrix application, high-mass-resolution IMS of intact intestinal samples was performed using a Solarix 15T MALDI FT-ICR mass spectrometer (Bruker Daltonics, Billerica, MA). Data were visualized using SCiLS Lab 2020 (Bruker Daltonics, Billerica, MA).

LA-ICP MS Imaging of Elements. Trace element imaging was performed as previously described. Samples were ablated using an LSX-213 laser ablation system (Teledyne CETAC, Omaha, NE, USA) and analyzed using a coupled Element 2 high-resolution sector field ICP-MS (Thermo Fisher Scientific, Waltham, MA) operated in medium-resolution mode. Helium gas was used to assist in transport of ablated sample particles from the ablation chamber to the ICP-MS. The resulting data were converted into vender-neutral imzML format and visualized using SCiLS Lab 2020.

MALDI timsTOF Imaging of Lipids. All samples for lipid analysis were washed with ammonium formate and distilled H_2O prior to matrix applicated. 1,5-diaminonapthalene (DAN) matrix was sublimated onto the tissue. IMS was performed using a prototype timsTOF Pro equipped with a dual ESI/MALDI and operated in qTOF mode with TIMS deactivated.[114] All preliminary lipid identifications were made based on mass accuracy using the LIPIDMAPS lipidomics gateway (lipidmaps.org) with a 5 ppm mass tolerance, and visualized using SCiLS 2020.

MALDI FT-ICR Imaging of Lipids. Samples were sprayed with 1,5-diaminonapthalene (DAN). Following matrix application, high-mass-resolution IMS of intestinal samples was performed using a Solarix 15T MALDI FTICR mass spectrometer. A continuous accumulation of selected ions (CASI) method was used with a Q1 mass of *m/z* 790.00 and an isolation window of 325 Da to reduce abundant taurocholate peak at *m/z* 514.29.

MALDI FT-ICR Tandem Mass Spectrometry. Lipid identifications for the lipids shown in Figure 2.5 were made using either CID or SORI-CID[115] on a 15T FT-ICR. IPC (18:0/18:0) at *m/z* 824.56 was identified using CID with an isolation window of 5 *m/z* and a collision energy of 25 V. PE (14:0_16:0) at *m/z* 662.47 was identified using SORI-CID using 1.1% SORI power, 0.25 sec pulse length, -500 Hz frequency offset, and an isolation window of 5 *m/z*.

MALDI FT-ICR Imaging of Bile Acids. Brain homogenate and liver tissues were sprayed or sublimated with matrix according to the methods detailed in Table 2.3. prior to analysis. Data was collected on a 15T FT-ICR at a 75 µm spatial resolution from *m/z* 251 – 800 with 650 laser shots at 60% laser energy.

Histology. Following MALDI IMS experiments, matrix was removed from samples using 100% ethanol and rehydrated with graded ethanol and double distilled H_2O. Tissue samples were stained using a hematoxylin and eosin stain, and brightfield microscopy of stained tissues was obtained using a Leica SCN400 Brightfield Slide Scanner at 20x magnification (Leica Microsystems, Buffalo Grove, IL).

Table 2.1: Instrumental parameters used for lipid, protein and trace element imaging on a 15T FTICR, LA-ICP MS and timsTOF Pro.

Laser	**MALDI FTICR Imaging of Proteins** Apollo II dual MALDI/ESI ion source and a Smartbeam II 2 kHz frequency tripled Nd:YAG laser 355 nm[116]	**LA-ICP IMS Imaging of Trace Elements** Nd:YAG 213 nm	**MALDI timsTOF Imaging of Lipids** Nd:YAG 355 nm	**MALDI FTICR Imaging of Lipids** Nd:YAG 355 nm
Laser Setting	small (50 um)	100 um	small (50 um)	large (~150 um)
Spatial Resolution	100 um	60 um	25 um	75 um
Laser Shots	1000	-	400	300
Laser Power	70%	35%	40%	35%
***m/z* range**	1000-30,000	-	200-2000	300-2000
Resolving Power	36,507 at *m/z* 8529.91899	-	-	71,928 at *m/z* 885.5498
Transient length	2.3069s	-	-	1.251s
Ionization mode	positive	-	positive	negative

Table 2.2: Sample preparation methods used for lipid, protein and trace element imaging using a TM Sprayer and sublimation apparatus.

	MALDI FTICR Imaging of Proteins	MALDI timsTOF Imaging of Lipids	MALDI FTICR Imaging of Lipids
Matrix	2′,6′-Dihydroxyacetophenone (DHA)	1,5-diaminonapthalene (DAN)[117]	1,5-diaminonapthalene (DAN)
Matrix Solution	90 mg/mL DHA in 70% ACN with 100 µL TFA and 50 µL of 30% ammonium hydroxide	300 mg DAN (~1.0 mg/cm^2)	20 mg/mL DAN in THF
Application Method	Sprayed with automatic robotic aerosol sprayer (TM Sprayer, HTX Technologies, Chapel Hill, NC, USA)	Sublimated using a simple sublimation apparatus at 130°C and 24 mTorr for 3 min[118]	Sprayed with automatic robotic aerosol sprayer (TM Sprayer, HTX Technologies, Chapel Hill, NC, USA)
TM Sprayer Method	45°C, 1050 mm/min, 0.075 mL/min, 1.5 mm track spacing, 8 passes	--	40°C, 1100 mm/min, 0.05 mL/min, 1.5 mm track spacing, 5 passes, 75°C heated stage

Table 2.3: Sample preparation methods used for bile acid detection matrix application experiments using a TM Sprayer and sublimation apparatus.

Matrix	Matrix Solution	Application Method	TM Sprayer Method
cDHA	12 mg/mL in THF	Sprayed with automatic robotic aerosol sprayer	70°C, 0.05 mL/min, 1350 mm/min, 1.5 mm track spacing, 22 passes
DAN	20 mg/mL in 70% ACN	Sprayed with automatic robotic aerosol sprayer	80°C, 0.05 mL/min, 1250 mm/min, 1.5 mm track spacing, 5 passes
DHB	15 mg/mL in 90% ACN	Sprayed with automatic robotic aerosol sprayer	80°C, 0.1 mL/min, 1100 mm/min, 1.5 mm track spacing, 6 passes
9-AA	5 mg/mL in 70% ACN	Sprayed with automatic robotic aerosol sprayer	30°C, 0.04 mL/min, 400 mm/min, 1.5 mm track spacing, 8 passes
Norharmane	45 mg/mL in 100% MeOH	Sublimated using a simple sublimation apparatus at 140°C and 24 mTorr for 3 min	----------
DHA	9 mg/mL in 70% ACN	Sprayed with automatic robotic aerosol sprayer	45°C, 0.075 mL/min, 1050 mm/min, 1.5 mm track spacing, 8 passes

CHAPTER 3

Primary bile acid abundances increase dramatically and rapidly during *C. difficile* infection

A version of the following chapter was previously published and has been adapted from Wexler and Guiberson et al., *Cell Reports,* Copyright 2021 by Cell Press[60]

3.1 OVERVIEW

The enteric pathogen *Clostridioides difficile* is the leading cause of nosocomial intestinal infections in the United States.[119] The high transmission rate of *C. difficile* infection (CDI) is largely due to the formation of metabolically dormant spores, which can remain viable outside of a host for months.[120] When ingested by a susceptible host, *C. difficile* spores encounter environmental cues such as host bile acids, which are necessary to initiate a germination program that leads to the outgrowth of toxin-producing vegetative cells.[15] While disruption to the gut microbiota, often from broad-spectrum antibiotics, is a prerequisite to CDI, the mechanisms *C. difficile* employs to colonize the host remain unclear.[120] Here, we applied imaging mass spectrometry using methods developed in Chapter Two to study how enteric infection changes gut metabolites. We find that CDI rapidly alters host physiology to induce a massive influx of primary bile acids into the gastrointestinal tract within 24 hours of the host ingesting spores. These bile acids, which include the germination factor taurocholate, facilitate *C. difficile* colonization and outgrowth, as mice placed on a diet containing the bile acid-sequestering drug cholestyramine display delayed colonization and reduced spore germination. These findings reveal that *C. difficile* facilitates spore germination upon infection and suggest that altering flux can modulate *C. difficile* outgrowth in patients that are prone to contracting CDI. Investigations into human bile acid levels in pediatric patients also suggest a potential role for bile acids in differentiating between asymptomatic and symptomatic colonization, where asymptomatic patients show higher levels of bile acids with known toxin-binding activity. These data highlight that in addition to aiding in *C. difficile* germination, bile acid levels change dramatically in response to CDI, offering a new avenue for potential therapeutics to investigate in treating this infection.

3.2 INTRODUCTION

In healthy humans, the complex ecological networks of the gut microbiota contribute to a phenomenon termed colonization resistance, whereby the microbiota collectively occupy all available niches.[60,121] This phenomenon effectively blocks invaders – pathogenic or benign – from

gaining a foothold within this ecosystem.[122] However, changes to the microbiota, most commonly by antibiotics, disrupt these networks and provide an opportunity for pathogens such as *Clostridioides difficile* to colonize and cause wide-ranging gastrointestinal disorders.[121,123] These disorders vary in severity from diarrhea to fulminant colitis and death.[17,119,122] Our understanding of the factors that underlie *C. difficile* colonization is limited by a lack of *in situ* information about how *C. difficile* and other pathogens restructure the intestinal environments they invade. The development of powerful molecular imaging technologies allows for the visualization of host-pathogen interactions within tissue microenvironments.[40,41,55] In particular, recent advances in imaging mass spectrometry provide improved sensitivity, specificity, and spatial resolution, presenting a unique opportunity to illuminate these processes *in situ* and improve our understanding of enteric disease progression along the entire length of the gastrointestinal tract.[114,124–127]

One way in which *C. difficile* infection alters the intestinal environment is through inflammation.[128] However, this inflammation is primarily limited to the large intestine, and therefore is unlikely to impact conditions within the small intestine, where the colonization process first begins.[17] The primary mediators of CDI pathology are the toxins TcdA and TcdB, which disrupt host signaling and cause cell death.[3] The epidemic *C. difficile* R20291 strain is considered hypervirulent, as it expresses toxins at higher levels and causes more severe disease than the laboratory-adapted strain 630.[128,129] While CDI is the leading cause of nosocomial enteric infections, cases of community spread are on the rise, as is the emergence of additional hypervirulent strains.[33,120,130]

Patients that develop CDI do so after ingesting spores. While these spores are tolerant of harsh conditions, both outside and inside the host, they are metabolically dormant, and cannot replicate or cause disease. However, once spores enter the small intestine, they sense chemical markers of this location, including the host bile acid taurocholate (TCA).[2,57] These factors are required to initiate spore germination, resulting in vegetative cells capable of replication and pathogenesis.[15] Despite our growing understanding of the processes governing *C. difficile* germination and sporulation *in vitro*, less is known about the conditions that are necessary for these processes to occur during host colonization.

Bile acids are produced by the host in the liver, secreted by the gallbladder into the proximal small intestine, then aid in lipid and vitamin absorption.[68] Approximately 95% of bile acids are reabsorbed by the host in the ileum, while the remainder pass into the large intestine, in which reabsorption is minimal.[68] Although bile acids must undergo a conjugation step to add either a

glycine or taurine moiety to move into the gallbladder from the liver, members of the gut microbiota deconjugate these bile acids using bile salt hydrolases.[62] In mice, 95% of bile acids are taurine-conjugated (as compared to ~35% in humans), and all cholate derivatives stimulate spore germination.[59,72,131]

In this study, we pioneered the application of IMS to study how enteric infection changes gut metabolites. We found that CDI rapidly alters host physiology to increase the availability of germination factors by orders of magnitude within the gut, thereby supporting the colonization and outgrowth of *C. difficile.* Moreover, *C. difficile* toxins determine host bile acid levels in a manner that is independent of inflammation and pathology. Blocking *C. difficile* from accessing this augmented pool of germination factors using the bile acid sequestering drug cholestyramine delays colonization and reduces spore germination. Together, these findings define major biochemical changes occurring within the host during enteric infection that underpin pathogen colonization and disease progression.

3.3 RESULTS

3.3.1 MALDI IMS reveals that CDI increases the abundance of ileal TCA.

The enteric pathogen *C. difficile* colonizes the gastrointestinal tract of patients that have reduced microbiota complexity following, for instance, antibiotic treatment.[57,120] How the intestinal environment changes during CDI is unclear. To determine these changes, we infected wild-type C57BL/6J mice by oral gavage with 10^5 *C. difficile* R20291 spores (or PBS for mock-infections) following cefoperazone treatment. We monitored mice for 3 days post infection (DPI), and subjected cryosections of intestinal tissue and luminal content to MALDI IMS analysis, followed by hematoxylin and eosin (H&E) staining for histopathology. MALDI IMS is a label-free technology that allows for the molecular mapping of hundreds of endogenous analytes from a tissue.[124] Indeed, we detect over 170 differentially abundant analytes between intestinal sections from CDI and mock-infected mice, representing a rich source of molecular information, presented in a visual format, about how CDI changes the intestinal environment. The most prevalent analyte we detected in Chapter Two in CDI mice has a mass-to-charge ratio (*m/z*) of 514.29 in negative ionization mode and was identified as taurocholate (Figure 2.9). This analyte is present at high intensity throughout the lumen of the distal small intestine region of CDI mice, but is largely absent from the same region in mock-infected control and non-antibiotic treated control mice (Figure 3.1). Together, these data suggest that CDI includes a substantial increase in intestinal TCA abundance.

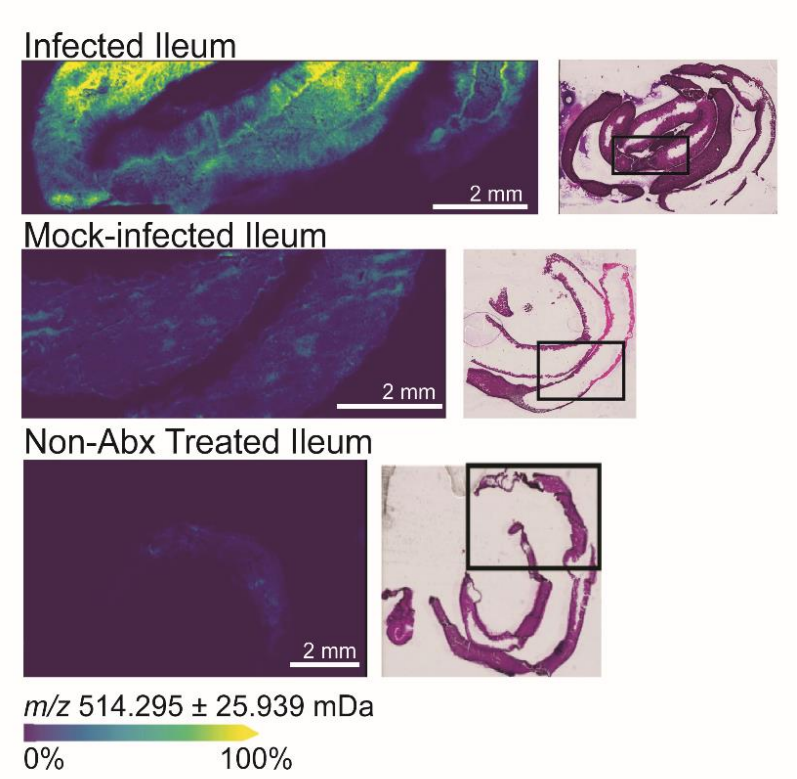

Figure 3.1. MALDI IMS reveals elevated levels of TCA in the ileal lumen of mice infected with *C. difficile*. MALDI IMS analysis of the ileal region and lumen of CDI or mock-infected animals at 2 dpi reveals elevated levels of *m/z* 514.3 in CDI mice relative to mock-infected controls normalized by total ion current. Inset: H&E stain of MALDI-imaged cryosections.

3.3.2 Levels of primary bile acids rapidly rise in the gut following *C. difficile* colonization.

To better understand the degree to which CDI increases intestinal bile acid levels, we measured the abundance of other primary bile acids, including the unconjugated primary bile acids cholate (CA) and β-muricholate (bMCA), as well as their taurine-conjugates TCA and tauro-β-muricholate (TbMCA). These bile acids were measured in CDI and mock-infected mice. The primary bile acid chenodeoxycholate (CDCA), and its taurine-conjugated form, were below the limit of detection in both groups of mice, as CDCA is rapidly converted to bMCA in mice. We extracted bile acids from liver, ileal lumen, and cecal lumen samples to capture key points within the host bile acid cycle. *De novo* production occurs in the liver, the ileum represents pre-absorption, and the cecum shows post-absorption levels. Bile acids were then quantified using LC-MS/MS.

The abundance of unconjugated bile acids CA (Figure 3.2.A) and bMCA (Figure 3.2.C) decrease markedly in the liver of CDI mice relative to mock-infected controls over time, and are undetected in CDI mice by 3 dpi. This is despite the liver being the site of *de novo* bile acid biosynthesis, as well as the organ to which reabsorbed intestinal bile acids recirculate.[73] By contrast, the abundance of CA (Figure 3.2.A) and bMCA (Figure 3.2.C) increase more than 10-fold on average by 3 dpi in the ileum, and by approximately 10-fold on average by 2 dpi in the cecum of CDI mice relative to mock-infected controls.

The abundance of taurine-conjugated bile acids TCA (Figure 3.2.B) and TbMCA (Figure 3.2.D) remain detectable in the livers of both groups of mice throughout the 3-day infection. Surprisingly, concentrations of TCA (Figure 3.2.B) and TbMCA (Figure 3.2.D) also remain higher in the ilea of CDI mice relative to mock-infected controls by ~100-fold or more on average from as early as 1 DPI. TCA (Figure 3.2.B) and TbMCA (Figure 3.2.D) concentrations are also elevated by 10-fold or more on average in the ceca of CDI mice relative to mock-infected controls.

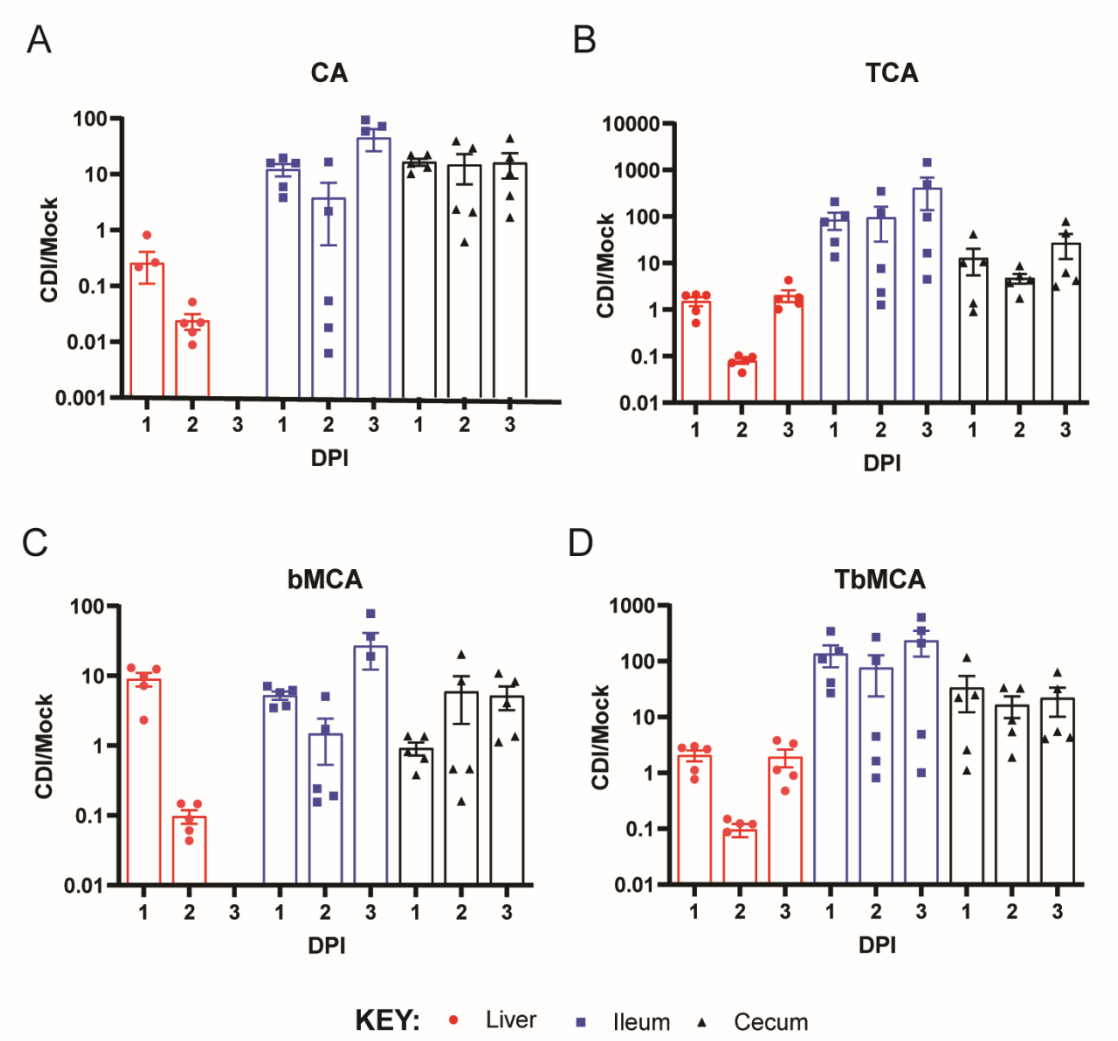

Figure 3.2. CDI induces a rapid influx of primary bile acids into the gut. Ratios of unconjugated (**A**, **C**) and taurine-conjugated (**B**, **D**) in the liver, ileum, and cecum of CDI vs. mock-infected animals, as determined by LC-MS/MS. Sample concentrations are adjusted based on sample weight (μM/g) prior to calculating the CDI/mock ratio for each bile acid. Data are represented as mean ± standard error of the mean (s.e.m); dpi, days post infection; n.d., not detected in CDI mice. N = 5 mice/group.

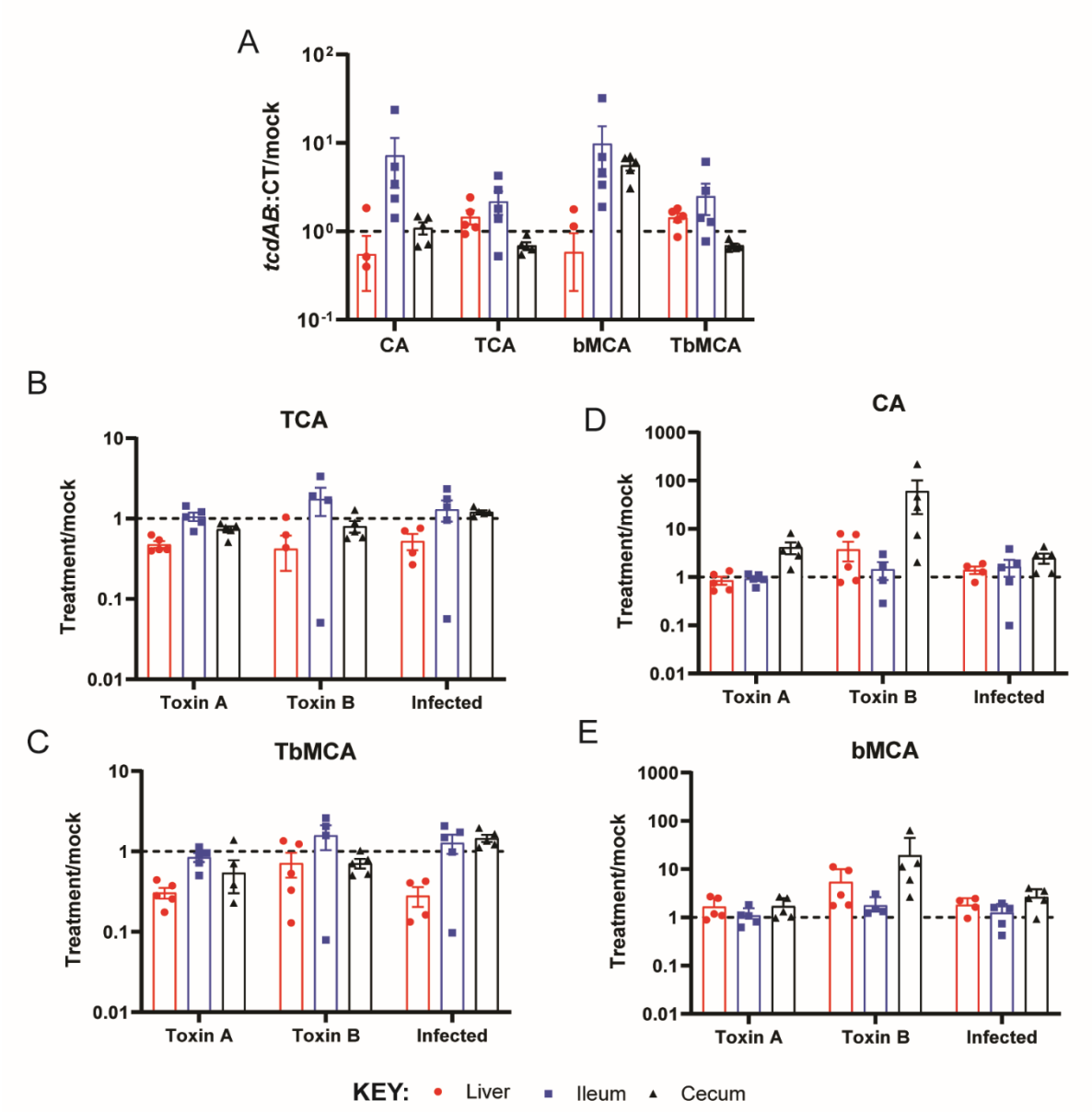

Figure 3.3. *C. difficile* toxins partly contribute to increased bile acid levels, but alone are insufficient to induce a spike in bile acid levels. (**A**) Ratios of primary bile acids in the liver, ileum, and cecum of toxin-deficient (*tcdAB*::CT) versus mock-infected mice at 3 dpi. Ratios of unconjugated (**D**, **E**) and taurine-conjugated (**B**,**C**) bile acids in the liver, ileum, and cecum of mice 8-hours after rectal infusion with 50 µg TcdA or TcdB, or oral gavage with 10^5 wild-type *C. difficile* R20291 spores, relative to mice rectally infused with PBS. N = 5 mice/group.

Together, these data suggest that levels of both unconjugated and conjugated primary bile acids rapidly rise in the gut following the onset of CDI. These data not only support our initial observations from MALDI IMS regarding elevated TCA abundance during CDI (Figure 3.1), but also reveal that CDI increases TCA levels by orders of magnitude within 24 hours of infection, and renders unconjugated primary bile acids undetected in the liver by 3 dpi.

3.3.3 *C. difficile* toxins determine host bile acid levels in a manner that is independent of inflammation and pathology.

C. difficile pathogenesis is primarily mediated by the activity of two cytotoxins, TcdA and TcdB, that disrupt host cell signaling.[128] Without these toxins, *C. difficile* pathogenicity is largely attenuated. To determine the contribution of these toxins to elevated bile acid levels during CDI, we infected mice by oral gavage with 10^5 toxin-deficient *C. difficile* R20291 spores (*tcdAB::*CT) or PBS for mock-infections following cefoperazone treatment, and measured bile acid abundance in tissues at 3 dpi. Contrary to wild-type CDI mice (Figure 3.2), the *tcdAB*::CT-infected mice display a negligible deviation from the mock-infected control group in terms of TCA and TbMCA abundance in all three tissue types, despite colonizing to a similar degree as wild-type *C. difficile.* Moreover, the *tcdAB*::CT-infected mice display on average less than a 10-fold increase in CA and bMCA concentrations in the ileum relative to mock-infected controls (Figure 3.3.A), while CA and bMCA concentrations differ negligibly from the mock-infected control group in the liver and cecum samples (Figure 3.3.A). Additionally, TcdA and TcdB individually are insufficient to significantly augment bile acid levels, as mice receiving a rectal infusion of 50 µg of either toxin largely did not deviate significantly from bile acid levels of PBS-infused mice after 8 hours (Figure 3.3.B-E). While the exposure time was limited to 8 hours because of the toxicity of TcdA and TcdB, it may have been an insufficient duration, as mice gavaged with 10^5 *C. difficile* R20291 spores also did not exhibit a significant increase in bile acid levels after 8 hours.

Dextran sulfate sodium (DSS) is a chemical inducer of intestinal inflammation that impacts the colonic epithelium of mice within 1 day of exposure, and causes severe inflammation within 3-4 days of treatment.[132] To determine the contribution of pathogen-independent intestinal inflammation on host bile acid pool size, we treated mice with 3% DSS in their drinking water (or no DSS for control mice) for 2 days following cefoperazone treatment. We then measured bile acid levels in liver, ileal lumen, and cecal lumen samples by LC-MS/MS. Contrary to mice infected with wild-type *C. difficile* (Figure 3.2), the abundances of CA, TCA, bMCA, and TbMCA are similar or lower in DSS-treated mice than controls (Figure 3.4). These data suggest that intestinal inflammation alone does not account for modulations to host bile acid physiology observed during

CDI. Indeed, histological analysis of H&E stained cryosections of the distal small intestine of CDI and mock-infected mice reveals no signs of inflammation or pathology at 3 dpi (Figure 3.5), despite clear CDI symptomology. Together, these data suggest that CDI induces changes to host bile acid physiology in a manner that is dependent on *C. difficile* toxins, but independent of intestinal inflammation and pathology.

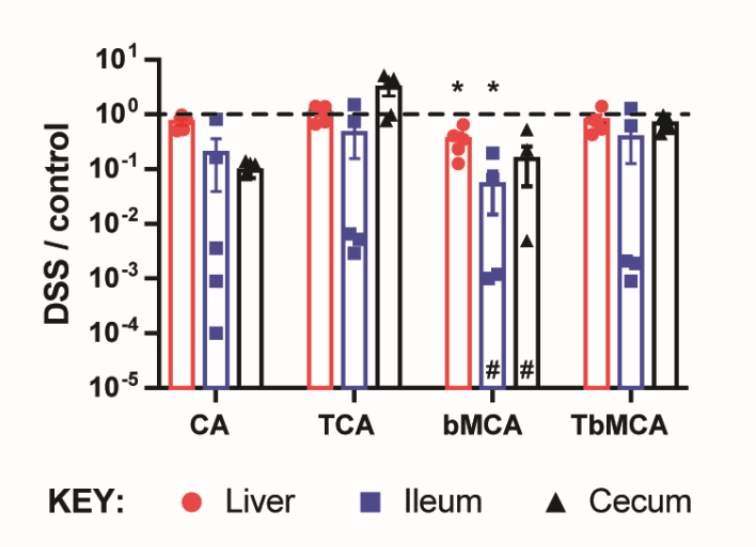

Figure 3.4. Inflammation alone is not sufficient to cause an influx of primary bile acids during *C. difficile* infection. Ratios of primary bile acids in the liver, ileum, and cecum of DSS-treated versus untreated control mice after 2 days of treatment. N = 5 mice/group.

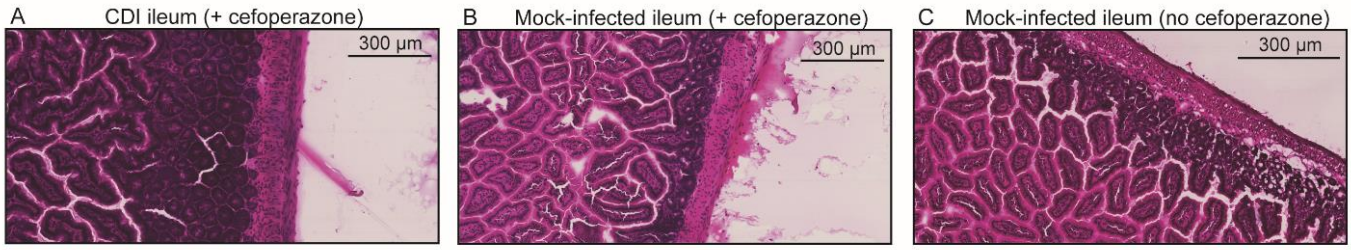

Figure 3.5. Histology reveals no signs of ileal inflammation in CDI mice. Histological analysis of H&E-stained intestinal tissues shows no significant inflammation or damage in either CDI (**A**) or mock-infected (**B**) mouse tissue at 3 dpi, and no signs of inflammation or tissue damage in non-antibiotic treated, mock-infected mouse tissue (**C**).

3.3.4 *C. difficile* access to augmented bile acid levels is necessary for rapid host colonization and spore germination.

Most cases of CDI in humans likely begin following ingestion of *C. difficile* spores, rather than vegetative cells, as spores are far more tolerant of harsh environmental conditions, such as those found outside the host and in the stomach. Upon being ingested, *C. difficile* spores receive environmental cues in the proximal small intestine, such as TCA, which are necessary to begin a germination program that leads to the outgrowth of toxin-producing vegetative cells.[15,59] Without the ability to germinate, *C. difficile* spores are innocuous and incapable of sustaining their presence within the gut ecosystem.

Cholestyramine is an orally administered bile acid-sequestering drug that is often used for lowering a patient's cholesterol, the molecule from which all host bile acids are derived.[58] It functions by reducing bile acid reabsorption in the gut through sequestration, which causes the host to compensate by producing more bile acids, and thus reducing the body's cholesterol supply.[58] To determine the contribution of elevated intestinal bile acid levels to *C. difficile* colonization and spore germination, we placed mice on a diet containing cholestyramine (20 g/kg), or a control diet without cholestyramine, for 7 days prior to infection by oral gavage with 10^5 *C. difficile* R20291 spores, and maintained them on their respective diets throughout the infection. *C. difficile* vegetative cell and spore colony forming units (CFU) were enumerated daily from fecal samples, and liver, ileal lumen, and cecal lumen samples were collected at 3 dpi for bile acid profiling.

While both vegetative cells (avg. ~10^9 CFU/g) and spores (avg. ~ 10^7 CFU/g) are detected in fecal samples of mice on the control diet at 1 dpi, they are undetected in mice on the cholestyramine diet at 1 dpi. By 2 dpi, only 60% of cholestyramine-treated mice have detectable levels of vegetative cells (avg. ~10^9 CFU/g), and 30% have detectable levels of spores (avg. ~10^8 CFU/g). Interestingly, we find the vegetative cell/spore ratio (an indicator of germination frequency) in these 3 mice to be ~10-fold lower on average that the vegetative cell/spore ratio in the control diet mice at 2 dpi (Figure 3.6). This ~10-fold ratio is maintained at 3 dpi, and correlates with lower average burden of vegetative cells in cholestyramine-treated mice. Importantly, intestinal TCA abundance is similarly elevated in CDI mice on both the cholestyramine and control diets at 3 dpi relative to mock-infected mice on the control diet (Figure 3.6). Our extraction method is designed to capture both cholestyramine-bound and unbound bile acids in samples from mice on the cholestyramine diet.

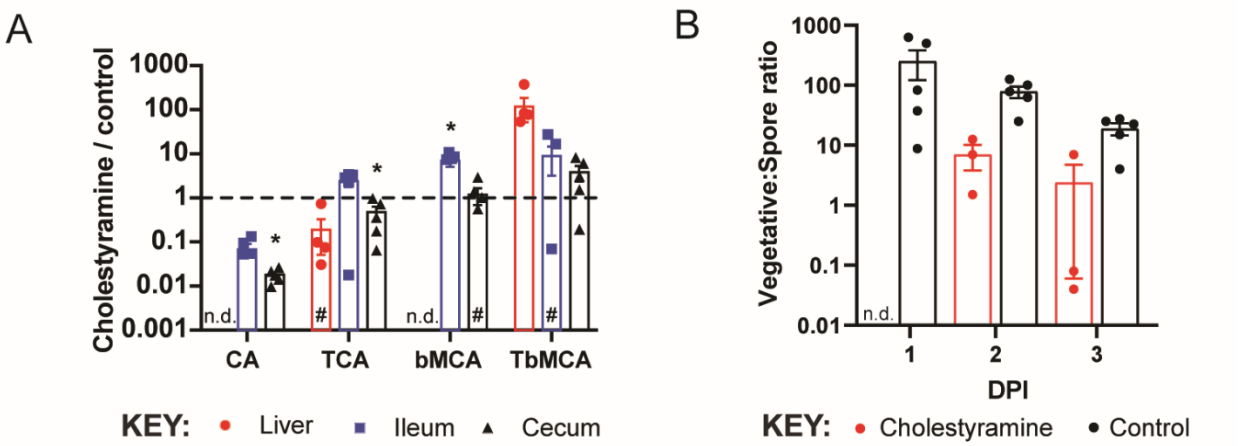

Figure 3.6. Elevated bile acid pool size during CDI is necessary for rapid host colonization and spore germination. (**A**) Spore counts and vegetative cell counts from fecal samples collected over time were used to determine the ratio of vegetative cells to spores in cholestyramine-treated and control mice. (**B**) CDI mice on a cholestyramine-containing diet carry similar levels of primary bile acids in their ilea and ceca compared with CDI mice on a control diet at 3 dpi. Data represented as mean ± s.e.m.

These data show that blocking access to abundance intestinal bile acid levels using cholestyramine limits *C. difficile* colonization efficiency and spore germination during CDI. Collectively, our findings suggest that the massive influx of primary bile acids into the gastrointestinal tract following host consumption of *C. difficile* spores drives spore germination, pathogen outgrowth, and CDI progression.

3.3.5. Toxin-binding bile acid levels are increased in uncolonized and asymptomatic pediatric patient samples.

Secondary bile acids, including deoxycholic acid (DCA), have been shown to inhibit vegetative *C. difficile* growth in the gastrointestinal tract. We collected stool samples from a clinical cohort of children with inflammatory bowel disease (IBD, uncolonized n=76), including patients with both IBD and symptomatic (n=11) or non-symptomatic colonization (n=8) with *C. difficile.* Uncolonized patient samples were collected during routine treatment for IBD. While conjugated primary bile acids (GCA, TCA) trend towards increased abundance in symptomatic patients, other primary bile acids did not show significant changes in this population. The secondary bile acid DCA, however, was significantly elevated in uncolonized patient stool compared to colonized samples regardless of symptom status (Figure 3.7). This elevation suggests that bile acid concentrations may be able to effectively predict colonization, or colonization susceptibility, in a non-invasive manner.

Samples were also collected from a clinical cohort of children with other underlying conditions including patients with cancer (n=10), cystic fibrosis (n=26), or inflammatory bowel disease (n=8) that had non-symptomatic colonization (n=52) or symptomatic CDI (n=57) as determined by nucleic-acid amplification-based testing. When comparing a panel of 8 bile acids between asymptomatic and symptomatic pediatric patients, two primary bile acids (CA, CDCA) and one secondary bile acid (DCA) were elevated compared to symptomatic patient samples (Figure 3.8). DCA was also elevated in uncolonized compared to colonized patients (Figure 3.7), suggesting this bile acid may serve as a marker for both colonization susceptibility and symptomology. Additionally, CA and CDCA were both significantly elevated in asymptomatic patients compared to symptomatic patients (Figure 3.8). All three of these bile acids have been previously found to effectively bind a *C. difficile*-produced toxin (TcdB).[133] The elevation of these molecules in colonized patients that do not develop symptomology suggests that a bile acid pool rich in these bile acids may protect against the impact of TcdB on intestinal tissue during infection. Additionally, this correlation offers potentially novel therapeutic targets that act upon bile acid circulation to impact infection outcomes.

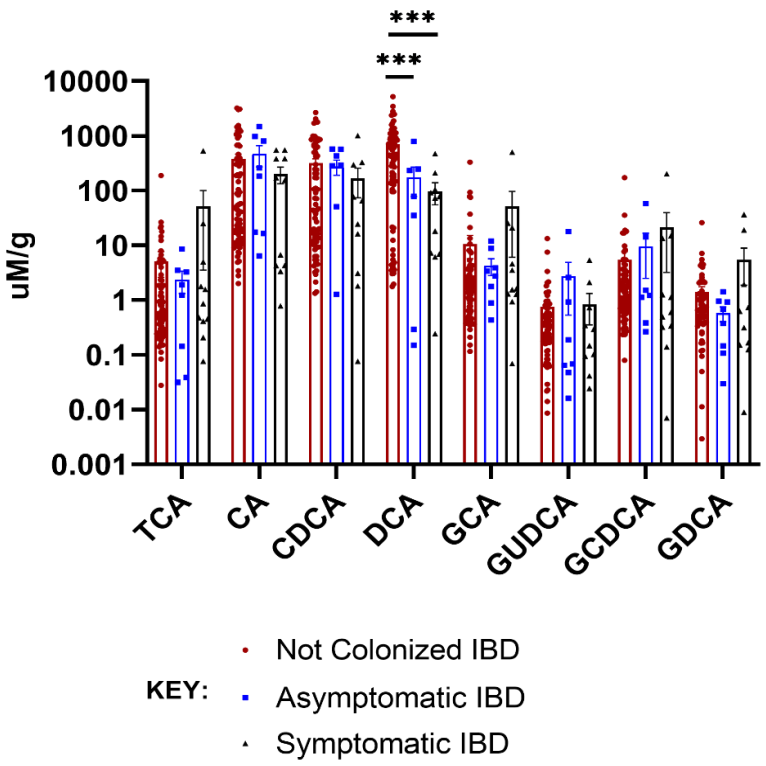

Figure 3.7. Uncolonized pediatric patient samples show higher abundance of secondary bile acid DCA compared to colonized patients. Significance determined using an unpaired two-sided t-test, *** $p < 0.001$.

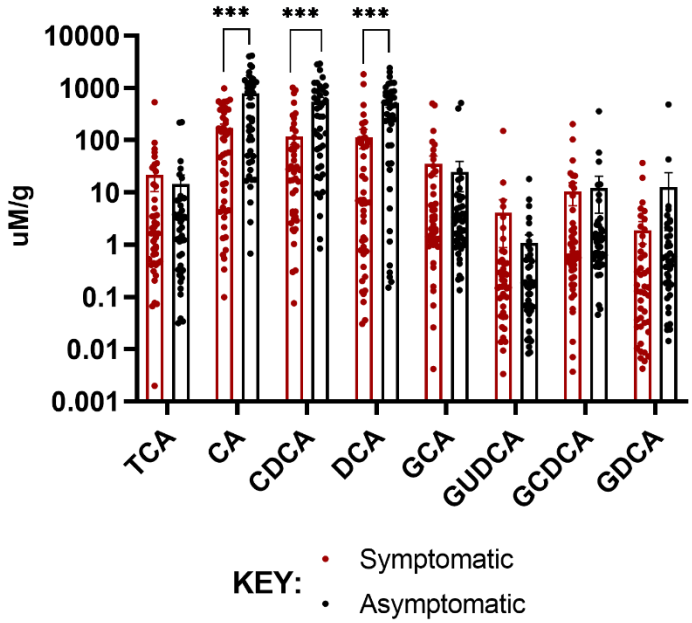

Figure 3.8. Asymptomatic colonized pediatric patient samples show increased abundance of CA, CDCA, and DCA compared to symptomatic colonized patients. Significance determined using an unpaired two-sided t-test, *** $p < 0.001$.

3.4 DISCUSSION

All colonizing microbes – pathogens, commensals, mutualists – affect the biology of their host. They do so in numerous direct and indirect ways, such as through physical interactions with host tissues, or through the production of diffusible compounds and metabolites.[121,123] CDI is mediated through the secretion of diffusible toxins, TcdA and TcdB, that destroy epithelial cells.[58] While CDI can be a life-threatening disease, pathologies associated with CDI are largely limited to the gastrointestinal tract, and do not commonly affect other body sites.

Here, we provide evidence that although *C. difficile* is physically restricted to the intestinal lumen, its influence on host physiology within the first 24 hours of infection extends beyond this site. Our findings stem from the use of cutting-edge IMS technology that allows for untargeted discovery-based visualization of molecular species, revealing spatial localization and intensity patterns that would be impossible to detect with traditional LC-MS/MS alone. This type of approach has been useful in a variety of host-pathogen interaction studies, such as *Staphylococcus aureus* infections, where a bacterial nidus results in an abscess containing both host and pathogen cells.[134] The incorporation of MALDI IMS to study soft tissue abscesses allows for molecular profiling of this bacterial nidus, as well as the surrounding tissue, offering deeper insight into the molecular changes that occur in this region during infection.[40] IMS has also been applied to the intestines in a variety of studies outside the context of host-pathogen interactions.[53] Most imaging experiments have probed discrete regions of the intestine for analysis, due to the difficulty in preparing large sections of intestine for sectioning.[48] Our study, however, emphasizes the importance of including luminal content in MALDI IMS analysis for a fully representative analysis of the intestinal tract using the workflow described in Chapter Two, as seen by the bile acid localization patterns previously not shown with traditional sample preparation approaches.[6]

Bile acid physiology is governed by complex networks of both redundant and counteracting regulatory pathways spanning multiple body sites, including the liver, gallbladder, intestine, and circulatory system.[73,135] Non-pathogen-driven disorders of bile acid physiology can also result in altered bile acid biosynthesis, and include bile acid diarrhea (stemming from disruptions to intestinal bile acid reabsorption in the ileum), cholestasis (stemming from the obstruction of bile acid movement out of the liver), and metabolic disorders like diabetes mellitus (resulting in altered bile acid homeostasis).[73] The gut microbiota also significantly affects bile acid composition and host physiology, as germ-free mice exhibit impaired lipid absorption and many commensal species can modify primary bile acids (host-derived) into secondary bile acids (microbe-derived) that include deoxycholate and lithocholate.[131,136] In addition, some

commensals, including certain strains of *C. difficile,* possess bile salt hydrolases that remove the taurine or glycine moieties from bile acids, thus creating a pool of unconjugated intestinal bile acids that can be reabsorbed by the host or further modified by other microbes.[137,138] Secondary bile acids possess antimicrobial properties, including against *C. difficile.*[17] Use of oral antibiotics such as cefoperazone disrupts the bile acid-modifying activity of the gut microbiota, and reduces the abundance of secondary bile acids. Because the vast majority of gut microbes reside in the large intestine, downstream of ileal receptors for reabsorption, secondary bile acids predominantly exert their effects in the large intestine, and have been linked to the development of colon cancer.[62,136]

While the mechanism by which CDI initially disrupts bile acid regulatory networks is unclear, the consequences are significant. The bile acid sequestrant cholestyramine is not currently used to treat CDI, and in the few studies that have investigated its potential in limiting CDI incidences, the rationale for its use has primarily centered on its ability to inactivate TcdA and TcdB through sequestration. One such pilot-level study investigated whether cholestyramine could reduce CDI incidences in patients with Lyme disease that were receiving long-term intravenous ceftriaxone.[139] The authors reported a ~3.5-fold reduction in the incidence of CDI in their patient cohort, relative to another published report monitoring CDI in a similar patient population that did not receive cholestyramine.[140] The delayed colonization of *C. difficile* in mice on the cholestyramine diet observed is more likely due to bile acid sequestration than toxin sequestration. This is because the toxins are necessary for increasing bile acid abundance during CDI (toxin deficiency through sequestration would likely prevent an increase in bile acid abundance similarly to the *tcdAB*::CT mutant), but dispensable for colonization (*tcdAB*::CT mutant colonizes similarly to wild-type *C. difficile*).[141] Buffie *et. al.* (2015) reported that the addition of the commensal species *Clostridium scindens* and vegetative *C. difficile* to *ex vivo* intestinal content resulted in fewer recoverable *C. difficile* over time, compared with the use of *ex vivo* intestinal content pre-treated with cholestyramine.[142] The authors attributed these results to the ability of *C. scindens* to convert primary bile acids into secondary bile acids that exert an antimicrobial effect against *C. difficile.* Our findings suggest that *C. difficile*'s access to bile acids can be modulated not only by the activity of commensal bacteria, but also through the activity of therapeutic drugs.

Bile acids have been previously shown to bind TcdB, one of the main toxins produced by *C. difficile.* In particular, secondary bile acid DCA and primary bile acids CDCA and CA have high binding efficiency for this toxin. As secondary bile acids were not investigated in the murine models, and CDCA is not present in mice, these bile acids show a particularly interesting trend in

human patient samples. The increased abundance of all three bile acids in patients that are asymptomatically colonized, as compared to symptomatically colonized patients, suggests that bile acid pools may protect patients in some capacity. As these bile acids increase, more of the *C. difficile* toxins are bound, preventing activity against the epithelium. This could potentially explain why some patients, such as those who suffer from cystic fibrosis, rarely develop symptoms despite colonization to a comparable level. Harnessing this trend could give further insight into why symptomology differs between patients, as well as aiding in the prediction of whether a patient will develop symptomology based on the bile acid profile.

A deeper understanding of how pathogen colonization and outgrowth occurs in the human gut, as well as how bile acid levels change within the human gut compared to translational models, is necessary for designing more targeted therapeutics to disrupt these processes in patients. While increasing bile acid levels can be harnessed for diagnostic analysis, it is crucial to dive into why and how the host is causing these increases during infection at a transcriptomic and proteomic level, which we investigate further in Chapter Four.

3.5 METHODS

Bacterial strains. Wild-type *C. difficile* R20291 and *C. difficile* R20291 *tcdAB*::CT were grown at 37°C in an anaerobic chamber (90% nitrogen, 5% hydrogen, 5% carbon dioxide, Coy Lab Products) in brain-heart-infusion broth (BD Life Sciences) supplemented with 0.5% yeast extract (BD Life Sciences) and 0.1% cysteine (Sigma-Aldrich).

Animal models. All animal experiments were performed using protocol M2000027-00 approved by the Vanderbilt University Medical Center Institutional Animal Care and Use Committee and in compliance with NIH guidelines, the Animal Welfare Act, and US Federal law. Animal studies were conducted using 8- to 12-week old male C57Bl/6 (Jackson Laboratories) mice housed in groups of up to five at the Vanderbilt University Medical Center Animal Facilities. Briefly, C57BL/6 mice received cefoperazone in their drinking water (0.5 mg/ml) for 5 days. Following a 2-day recovery period, mice were gavaged orally with PBS or infected with 10^5 *C. difficile* spores to an endpoint of three days. CDI symptomology was monitored daily by weight loss. Mice were humanely euthanized using compressed CO_2. Intestinal segments were dissected, embedded in 2.6% carboxymethylcellulose (CMC), and frozen in liquid nitrogen. Samples were stored at -80°C prior to sectioning. Mice provided a cholestyramine or control diet (Dyets, Inc., Bethlehem, PA) were placed on these diets at the same time they were given cefoperazone, and remained on

their respective modified diets for the duration of the experiment. Mice provided 3% DSS in their drinking water for 2 days were first treated with cefoperazone for 5 days, followed by a 2-day recovery period. Mice receiving rectal infusion of purified, recombinant TcdA or TcdB (or PBS) were placed on 0.5 mg/ml cefoperazone in their drinking water for 5 days, followed by a 2-day recovery period, before receiving 50 µg of either toxin.[143] Mice were euthanized after 8 hours.

Determining bacterial burdens. *C. difficile* CFUs were quantified daily from fecal samples. Fresh samples were weighed, homogenized in PBS, serially diluted, and plated onto taurocholate cycloserine cefoxitin fructose agar (TCCFA) for enumeration as colony forming units per gram of feces (CFU/g). Vegetative cells were enumerated by plating fecal suspensions on cycloserine cefoxitin fructose agar without taurocholate, while spores were enumerated by heating fecal suspensions at 65 °C for 20 minutes aerobically prior to plating onto TCCFA.

MALDI imaging mass spectrometry. Tissue and CMC were cryosectioned at 10 µm thickness using a Cryostar NX70 Cryostat (Thermo Scientific, Waltham, MA, USA) and thaw mounted onto 1% poly-l-lysine coated indium tin oxide coated glass slides (Delta Technologies, Loveland, CO, USA). All slides were kept at room temperature prior to mounting to ensure full thaw-mounting. Sectioned samples were brought to room temperature in a desiccator 30 minutes prior to matrix application. Samples were sprayed with 9-aminoacridine (9-AA) for bile acid analysis using an automated sprayer (TM Sprayer, HTX Technologies, Chapel Hill, NC, USA). 9-AA was prepared at a concentration of 5 mg/mL in 70% acetonitrile, and sprayed at 30°C, 400 mm/min, 0.04 mL/min for 8 passes. Following matrix application, imaging mass spectrometry of intestinal samples was performed using either a Solarix 15T MALDI FT-ICR mass spectrometer (Bruker Daltonik, Billerica, MA, USA; Figure S1B, Figure S4) or a rapifleX MALDI Tissuetyper (Bruker Daltonics, Billerica, MA, USA; Figure 1B). The rapifleX MALDI Tissuetyper was equipped with a Smartbeam 3D 10 kHz Nd:YAG (355 nm) laser. The FT-ICR was equipped with an Apollo II dual MALDI/ESI ion source and a Smartbeam II 2 kHz frequency tripled Nd:YAG laser (355 nm). Images collected on the rapifleX MALDI Tissuetyper were generated using the single spot laser setting with a pixel scan size of 20 µm in both x and y dimensions. Data were collected in negative ion mode from *m/z* 361-801 with 250 laser shots per pixel. Images collected on the 15T MALDI FT-ICR were generated using the small laser setting (~50 µm) with a pixel spacing of 50 µm. Data were collected with 650 laser shots per pixel at 60% power from *m/z* 250-800 with a transient length of 1.1534 s and a resolving power of 260,000 at *m/z* 512.2723. Data were visualized using SCiLS Lab 2020 (Bruker Daltonik, Dillerica, MA, USA).

Histological analysis. Following MALDI IMS, matrix was removed from samples using 100% ethanol, and the samples were rehydrated with graded ethanol washes and double distilled water. Tissue samples were then stained using a hematoxylin and eosin (H&E) stain and coverslipped. After drying, brightfield microscopy images were collected using a Leica SCN400 Brightfield Slide Scanner at 20x magnification (Leica Microsystems, Buffalo Grove, IL, USA) and visually analyzed in a blinded fashion for signs of inflammation and tissue damage.

Bile acid extractions. Liver, ileal lumen, and cecal lumen samples were harvested from mice, fecal samples were collected from human patients, and all samples were flash frozen in liquid nitrogen. Samples were weighed prior to extraction, and homogenized in Lysing Matrix D tubes (MP Biomedicals) containing 2:1:1 mixture of ethanol:chloroform:methanol using a FastPrep-24 (MP Biomedicals) bead beater for 45 seconds at 6.5 m/s (repeated 3 times, incubating on ice for 1 minute in between rounds). Homogenates were centrifuged at 20,000 x g at 4°C for 15 minutes to pellet debris. Supernatant was transferred to a clean glass vial and evaporated under nitrogen gas flow until dry. Samples were reconstituted in methanol prior to LC-MS/MS analysis.

Liquid chromatography tandem mass spectrometry. Bile acids from tissue and fecal extracts were injected in volumes of 5 µL and gradient eluted onto a SecurityGuard C18 guard column (3.2 x 8 mm, Phenomenex, Torrance, CA, USA) Ascentis Express HPLC C_{18} column (25 cm x 2.1 mm, 5 µm particle size, Supelco Analytical, Bellefonte, PA, USA). Mobile phase A consisted of H_2O with 0.1% formic acid, and mobile phase B consisted of acetonitrile with 0.1% formic acid. Bile acids were eluted on a linear gradient of 20-60% B for 15 minutes, followed by 60-100% B for 15 minutes, and 100-20% B for 30 minutes at a flow rate of 0.4 mL/min. All analytes were measured on a TSQ Quantum Triple Quadrupole mass spectrometer (Thermo Fisher Scientific, Waltham, MA, USA) with an identity transition. Optimal collision energies were determined empirically before each experiment. Quantification was determined using a calibration curve from 5 µL injections of 0, 0.1, 0.3, 1, 3, 10, and 30 µM bile acid standards using Xcaliber Quant Browser (Thermo Fisher Scientific, Waltham, MA, USA).

Quantification and statistical analysis. Statistical analyses were performed using GraphPad Prism 8 and Microsoft Excel. Statistical significance was assessed using an unpaired two-sided *t*-tests. Significance was defined as $p < 0.05$, and the data were only excluded on the basis of technical errors associated with the experiment.

CHAPTER 4

Enterohepatic circulation is altered at the transcriptomic, but not proteomic, level during *C. difficile* infection to increase bile acid abundances

4.1 OVERVIEW

Bile acid levels have been shown in the previous chapter to dramatically increase during *C. difficile* infection in a way that benefits colonization by the pathogen, despite ordinarily being strictly controlled by the host through enterohepatic circulation.[6] Primary bile acids are produced in the liver, shuttled to the small intestine, and reabsorbed by enterocytes in the ileum.[61] This chapter aims to understand how the process of enterohepatic circulation is altered during CDI, and whether *C. difficile* contributes to these changes at both the transcriptomic and proteomic level. These data show that biosynthesis transcripts were more abundant initially during CDI at the 1 day post infection (dpi) time point but were less abundant at 3 dpi. *Slc10a2*, which encodes for the protein responsible for bringing bile acids from the lumen into enterocytes, showed a 10x decrease in transcript abundance in infected tissues compared to control at 1 dpi, which returned to mock-infected levels at 3 dpi. Together, these data suggest that the host is attempting to increase bile acid levels within the ileal lumen during infection and then suppress this effect by 3 dpi. These changes are shown to be somewhat impacted by CDI, as Caco2 cells exposed to vegetative *C. difficile* showed significant changes in transcript abundance for absorption genes such as *Slc10a2* after 24 hours. Additionally, colonic transcript levels (*Slc10a2*, *Fabp6*, *Slc51a/b*) were investigated which showed that as ileal absorption transcripts decrease (*Slc10a2*), the colonic absorption transcripts increase. Notably, in both the colon and the liver the gene encoding for FXR (*Nr1h4*) was significantly upregulated during infection, suggesting a potential mechanism for these transcriptional changes. These changes, however, were not translated to the protein level as measured using quantitative immunohistochemistry and bottom-up proteomic analysis, which showed unchanging protein levels during infection. Rather, SLC10A2, BAAT and CYP7A1 were not differentially abundant in infected compared to mock infected tissue. Altogether, these data suggest a complex dynamic in the regulation of bile acid synthesis and absorption at the transcriptomic and proteomic levels in the context of CDI. Future work can investigate the nuanced spatial and temporal changes that impact bile acid levels.

4.2 INTRODUCTION

Bile acids play an important role in the germination of *C. difficile* within the gastrointestinal tract. Recent data show that bile acid levels respond to CDI as well, and increase 10- to 100-fold during infection within the small intestine.[60] This has interesting ramifications for *C. difficile*, which relies on this early increase in abundance for successful colonization and germination.[60] What is surprising about this trend is that these molecules are produced by the host. Ordinarily, bile acid levels are strictly controlled to prevent the negative effects that result from an overabundance of bile acids. Although they play an important role in lipid digestion, bile acids can become toxic to cells at high concentrations. An overabundance of bile acids can lead to liver inflammation and injury, as well as damage to the bile duct epithelium.[92] For this reason, bile acid abundances are tightly regulated through a process known as enterohepatic circulation. This circulatory pathway consists primarily of the biosynthesis of bile acids within the liver, and the reabsorption of bile acids in the intestines.[82]

The synthesis of bile acids from cholesterol occurs in the liver via one of two pathways. Ninety-percent of bile acids are produced through the classic or neutral pathway.[81] This process is initiated by Cytochrome P450 7A1 (CYP7A1), which converts cholesterol to 7a-hydroxycholesterol, and serves as the rate-limiting enzyme in synthesis.[96] The full synthesis of bile acids from cholesterol consists of 18 enzymes for the classic pathway, including CYP8B1 which is responsible for bile acid pool makeup and BAAT which is responsible for the conjugation of bile acids with taurine or glycine. The less common pathway is the alternative or acidic pathway. This pathway is initiated by CYP27A1, which is also utilized in later steps of the classic pathway.[81] Between the two pathways, approximately 0.5g of bile acids are produced by the liver daily in humans, which accounts for the end products of half the cholesterol produced.[144] These bile acids will be recycled between 4 and 12 times a day, with 95% of bile acids being recycled through the ileum. The remaining 5% of bile acids continue to the large intestine, where they interact with the gut microbiome and become secondary, or microbiota-produced, bile acids. These secondary bile acids also enter circulation through passive absorption in the colon. The absorption of bile acids is a highly conserved process, relying on 5 main enzymes. First, SLC10A2 brings bile acids from the lumen into the enterocyte. FABP6 then carries the bile acids to the basolateral membrane, where the heterodimer OSTA/B pumps the bile acids across the membrane back to the portal vein. Upon return to the liver, the bile acids are then imported by SLC10A1 and the cycle continues.

Enterohepatic circulation is heavily controlled by nuclear receptor proteins, in particular the Farnesoid X Receptor (FXR). Commonly referred to as the bile acid receptor, FXR directly

impacts *Cyp7a1, Fabp6,* and *Slc51a/b* expression to control bile acid levels (Figure 1.6). Bile acids serve as ligands for FXR and bind directly to the receptor in a negative feedback loop. When bile acid levels rise, more bind to FXR within the enterocytes and hepatocytes, causing FXR to activate. Once activated, FXR initiates a signaling cascade that represses *Cyp7a1* expression in the liver and increases expression of *Slc51a/b* and *Fabp6* in the intestines. This coordinated approach leads to decreased biosynthesis and increased removal of bile acids from enterocytes. Ordinarily, this process is highly effective in healthy individuals, but can become dysregulated and cause metabolic disorders.[61]

While enterohepatic circulation has been well studied in the context of diseases such as diabetes and liver inflammation, little work has been done looking at this process specifically through the lens of CDI. Research has focused primarily on the role that bile acids play in the life cycle of *C. difficile*, yet new data have shown that bile acids change dramatically in a way that benefits *C. difficile*.[60] Therefore, it is important to investigate how CDI, and potentially *C. difficile* itself, impacts the enterohepatic circulation of bile acids. As bile acid levels are changing, it follows that their regulation may be manipulated by infection to cause this break in homeostasis. Therefore, targeting key genes involved in biosynthesis and absorption of bile acids in the context of CDI could elucidate the signaling relationship between the host and *C. difficile* in this pathway. This approach, utilizing both gene expression analysis and proteomics, shows that enterohepatic circulation is in fact altered at the transcriptional level during CDI at 1 dpi, although these changes do not occur at the proteomic level. These data suggest that *C. difficile* may cause increased abundance of bile acids to facilitate germination.

4.3 RESULTS

4.3.1 The host responds to CDI-induced elevations in bile acid levels by reducing flux through its *de novo* biosynthesis pathway.

The increased abundance of bile acids during CDI raises interesting questions about the mechanism of this accumulation. As bile acid levels are highly conserved via enterohepatic circulation, further investigation into both the production and absorption of bile acids during infection could elucidate how the host regulatory system is manipulated. As all primary bile acids are produced in the liver, a transcriptomic analysis of liver gene expression was conducted to understand how the host responds to these elevations.

Primary bile acids are synthesized in the liver from cholesterol via the classic pathway, involving 18 steps to yield conjugated bile acid products such as TCA.[73] The first step in this

pathway involves the conversion of cholesterol to 7α-hydroxycholesterol by the enzyme CYP7A1, and thus determines the overall bile acid pool size in the host (Figure 4.1a). Two steps later, the pathway splits to yield either chenodeoxycholate (CDCA) or muricholate (MCA) in mice, or cholate (CA) in a manner that depends on the presence and activity of CYP8B1, which leads to production of CA over CDCA/MCA (Figure 4.1a). Prior to entering the gallbladder, primary bile acids must be conjugated with either taurine or glycine, a step mediated by the enzyme bile acid-CoA:amino acid *N*-acyltransferase (BAAT) in the liver (Figure 4.1a).[73]

Given that the levels of CA and bMCA in the liver of CDI mice decline over time and are undetected at 3 dpi (Figure 3.3), and that the levels of conjugated bile acids TCA and TbMCA increase rapidly in the ileum upon *C. difficile* colonization, we suspected that CDI affects transcriptional flux through the bile acid biosynthesis pathway in the liver. To test this, we extracted RNA from the livers of CDI and mock-infected control mice at 1 and 3 dpi, and measured transcript abundance of genes encoding for key enzymes within the *de novo* bile acid biosynthesis pathway using qRT-PCR. *Cyp7a1* expression was approximately 3-fold higher on average in CDI mice relative to mock-infected controls at 1 dpi, but showed comparable expression levels to mock-infected controls by 3 dpi (Figure 4.1). *Cyp8b1* expression in CDI mice was approximately 2-fold higher than mock-infected mice at 1 and 3 dpi (Figure 4.1). *Baat* expression was significantly elevated in CDI mice relative to mock-infected controls at 1 (7x increase) and 3 dpi (5x increase, Figure 4.1). Additionally, *Nr1h4* (FXR) expression was significantly elevated at the 3 dpi time point by about 3-fold in infected mice tissue.

These data suggest that the host may repress transcriptional flux through the bile acid biosynthesis pathway over the course of infection, and potentially does so through FXR. Moreover, the high expression levels of *Baat* in CDI-infected mice suggests that reabsorbed bile acids from the intestinal tract may still be conjugated in the liver during initial colonization and therefore can be recycled back into the intestine.

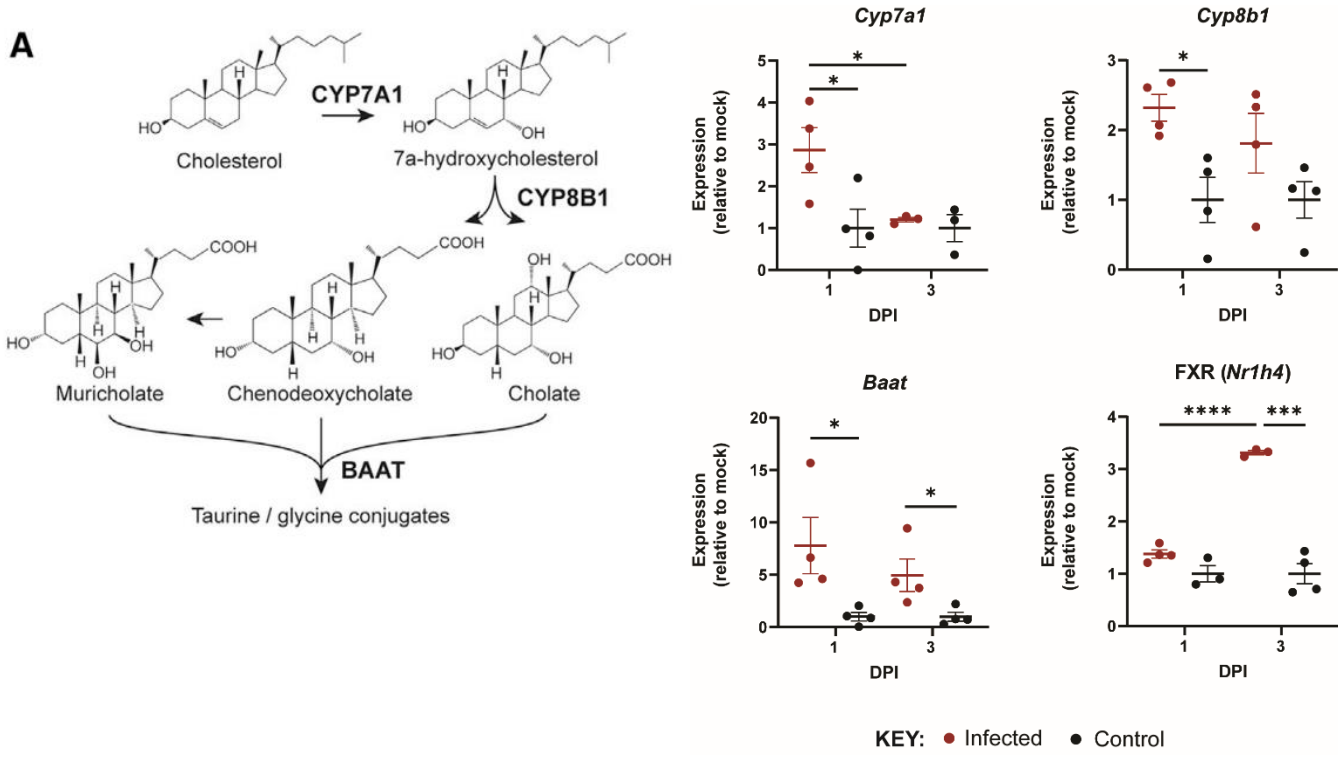

Figure 4.1. The host responds to CDI-induced elevations in bile acid pools by reducing bile acid biosynthesis gene expression. A) Bile acid biosynthesis pathway diagram. B) Bile acid biosynthesis gene expression showing upregulation of *Cyp7a1* and *Cyp8b1* at 1 dpi, *Baat* at 1 and 3 dpi, and *Nr1h4* at 3 dpi. N=4, significance determined using unpaired two-sided t-test. * p<0.05, *** p<0.001, **** p<0.0001. Outliers determined using Grubbs test with an alpha of 0.05.

4.2.1. Absorption of bile acids from the lumen into enterocytes is transcriptionally downregulated during early infection in the ileum.

In addition to the increased transcript levels for biosynthesis genes during infection, we investigated how absorption may be impacted in the ileum. 95% of bile acids are reabsorbed in the ileum and returned to the liver via the hepatic portal vein.[68] Elevated levels of bile acids have been shown previously to impact the expression of *Slc10a2*, which encodes for the protein responsible for reabsorption of these bile acids.[89] Decreased absorption would allow for buildup of bile acids in the ileal lumen, enabling their availability for germination of *C. difficile.*[59]

To test this, we extracted RNA from ileal tissue from CDI-infected and mock-infected mice at 1 and 3 dpi to determine changes in transcript levels using qPCR. We targeted the 4 genes involved in the reabsorption of bile acids in the ileum including *Slc10a2*, which absorbs bile acids from the lumen into enterocytes,[144] *Fabp6*, *Slc51a* and *Slc51b*. I-BABP (encoded by *Fabp6*) is responsible for transporting bile acids to the basolateral membrane, where they are then secreted by the heterodimer OSTαβ (encoded by *Slc51a/b)* into portal blood vessels.[68]

We saw minimal significant changes in the genes that encode for transport proteins (*Fabp6, Slc51ab*), although all three are trending towards downregulation during infection (Figure 4.2). The slight downregulation of *Slc51a* is recovered by 3 dpi, and is significantly increased in comparison to the infection 1 dpi time point. *Slc10a2* transcript abundance, however, is significantly downregulated 10x in infected tissue at the 1 dpi time point compared to mock-infected samples (Figure 4.2). This downregulation is then recovered by 3 dpi. These data suggest differential changes at the transcriptional level, to decrease absorption of bile acids in the lumen at 1 dpi without altering transport within the enterocyte.

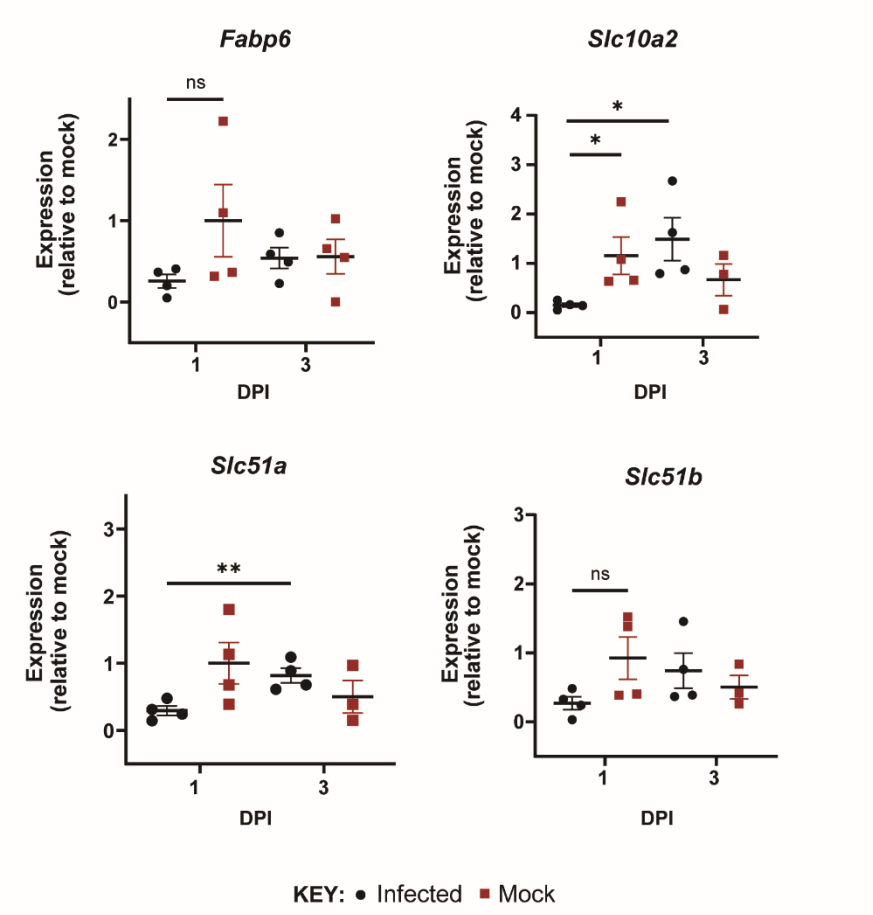

Figure 4.2. Bile acid absorption gene expression in the ileum is moderately downregulated during CDI. Bile acid absorption gene *Slc10a2 i*s significantly downregulated at 1 dpi compared to mock-infected samples, which is restored by 3 dpi. Transportation genes trend downwards insignificantly during CDI. N=4, significance determined using unpaired two-sided t-test. * $p<0.05$, ** $p<0.01$. Outliers determined using Grubbs test with an alpha of 0.05.

4.3.3. A decrease in absorption protein-encoding gene transcripts during CDI is specific to *C. difficile*.

Due to the complex nature of enterohepatic circulation in mice during CDI, it can be difficult to differentiate between bile acid-driven changes and CDI-driven changes. In light of the changes in biosynthesis and bile acid levels that seems specific to CDI, we hypothesized that *C. difficile* could cause changes in absorption protein-encoding gene transcript abundance in the absence of bile acids, initiating the influx of bile acids during infection. We utilized a cell culture model with a *Caco2* cell line (colonic tissue), where cells were exposed to stimuli for 24 hours. Cells were exposed to either vegetative *C. difficile*, *C. difficile* spores, physiological concentrations of CDCA, or media alone. After exposure, cells were collected and RNA was extracted for analysis.

Overall, cells treated with spores behaved erratically making it difficult to draw many meaningful conclusions. Of note, *Slc51a* transcript abundance was significantly elevated (10x, Figure 4.3) in cells treated with *C. difficile* spores alone. The other genes of interest show increased expression after exposure to spores as well, although these data are not significant due to highly variable results. Interestingly, only *Fabp6* expression was elevated in the presence of the bile acid CDCA (Figure 4.3). There are a variety of potential reasons for this, including an insufficient exposure timeframe, but it offers compelling evidence for a more direct role of *C. difficile* spores in the changes shown above in enterohepatic circulation.

Vegetative *C. difficile* showed the most obvious changes in the transcript abundances of these genes. This is especially intriguing because *C. difficile* is an obligate anaerobe and is most likely dead, or has sporulated, under cell culture conditions, and yet it is able to impact these expression levels. In both *Fabp6* and *Slc10a2* transcripts, the abundances increased significantly in cells exposed to vegetative *C. difficile.* This increase was more moderate in *Fabp6* (4x increase, Figure 4.3), and more prevalent in *Slc10a2* (15x increase, Figure 4.3), but both suggest an active contribution of *C. difficile* to enterohepatic circulation gene expression. It is important to note that none of these cells (with the exception of the CDCA condition) were exposed to any bile acids, indicating that these changes may occur as a direct result of CDI rather than the influx of bile acids alone.

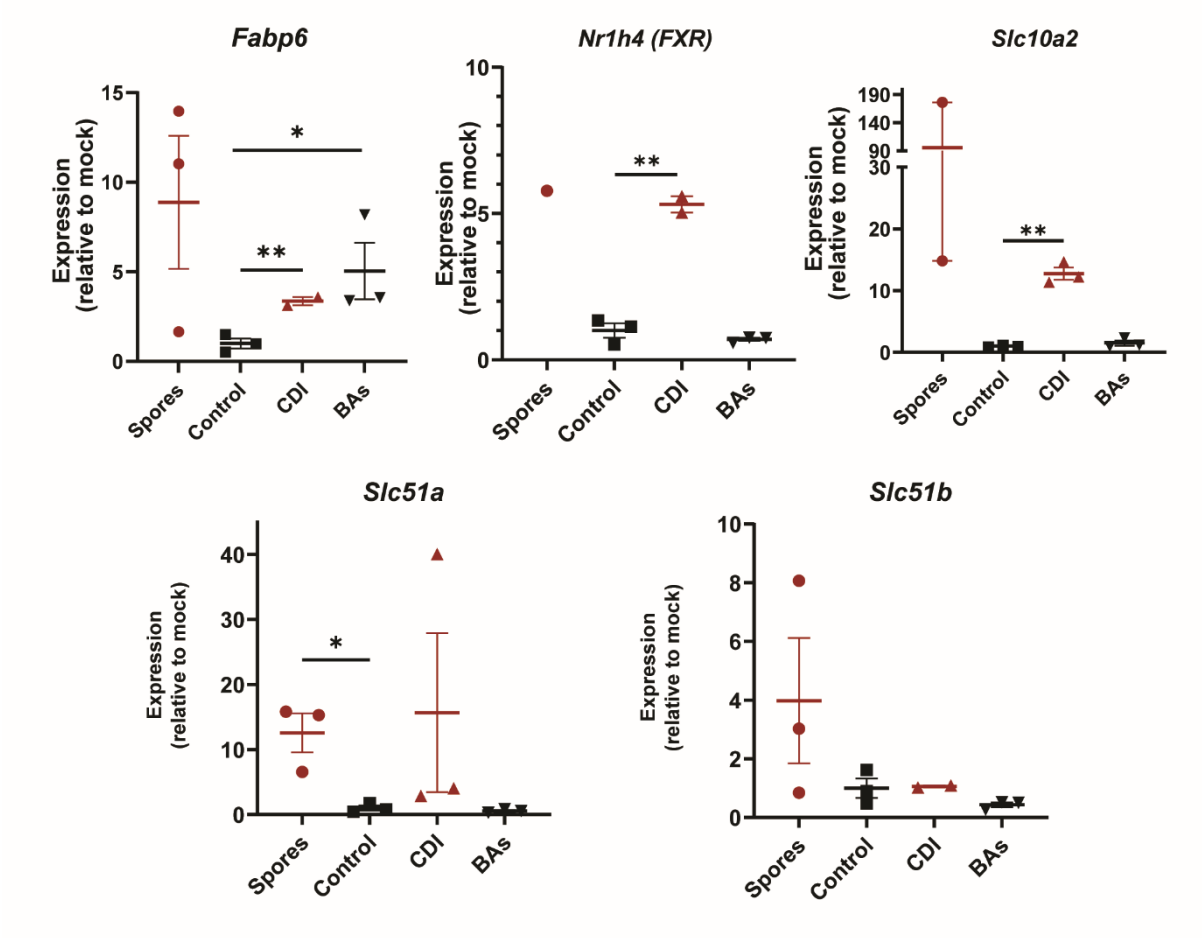

Figure 4.3. Bile acid absorption gene expression increases in cell culture models without the presence of bile acids. Caco2 cell cultures exposed to either *C. difficile* R20291 spores, vegetative cells, chenodeoxycholic acid, or media only for 24 hours and resulting gene expression. Bile acid absorption (*Slc10a2*) and transport (*Slc51a, Fabp6*) genes are upregulated in cells exposed to vegetative cells or spores without the presence of bile acids. Bile acid receptor gene (*Nr1h4*) is upregulated in cells exposed to vegetative *C. difficile*. N=3 wells, significance determined using unpaired two-sided t-test. * p<0.05, ** p<0.01. Outliers determined using Grubbs test with an alpha of 0.05.

4.3.4. Bile acid absorption gene expression levels increase in the colon during early infection.

In light of the cell culture model showing elevated expression of absorption gene transcripts for *Slc10a2*, in direct contrast to the decreased abundance seen in ileal tissue, we hypothesized that a colonic tissue model would be a more suitable comparison for the cell culture model, and may show differential absorption between the small and large intestine. We collected proximal colonic tissue from CDI-infected and mock-infected mice at 1 and 3 dpi and extracted RNA for transcriptional analysis. As ileal absorption seems to be transcriptionally stunted during infection, yet bile acid levels remain elevated at 3 dpi, we hypothesized that the colon could increase absorption during infection to recover the bile acids reaching the large intestine.

These data show similar trends to the cell culture experiment at the 1 dpi time point. *Slc10a2, Fabp6,* and *Slc51b* all show increased transcript abundance at 1 dpi in infected tissue compared to mock infected tissue (Figure 4.4). *Fabp6* and *Slc51b* showed the most dramatic increases (10x and 12x, respectively, Figure 4.4), while *Slc10a2* showed a 3x increase in transcript abundance at this time point. All three of these genes, however, showed no changes in expression compared to mock-infection at the later time point, similar to the trends seen in liver and ileal tissue, suggesting that changes to enterohepatic circulation occur rapidly and then are dampened by the host. Additionally, *Nr1h4* (FXR) showed a significant 5x increase in transcript abundance in infected tissue at this 1 dpi time point, once against suggesting potential FXR-mediation in these transcriptional changes (Figure 4.4). Overall, these data in concert with that from ileal tissue suggest that the host response leads to decreased ileal bile acid absorption during CDI, but this process may be shifted to the large intestine in place of the ileum.

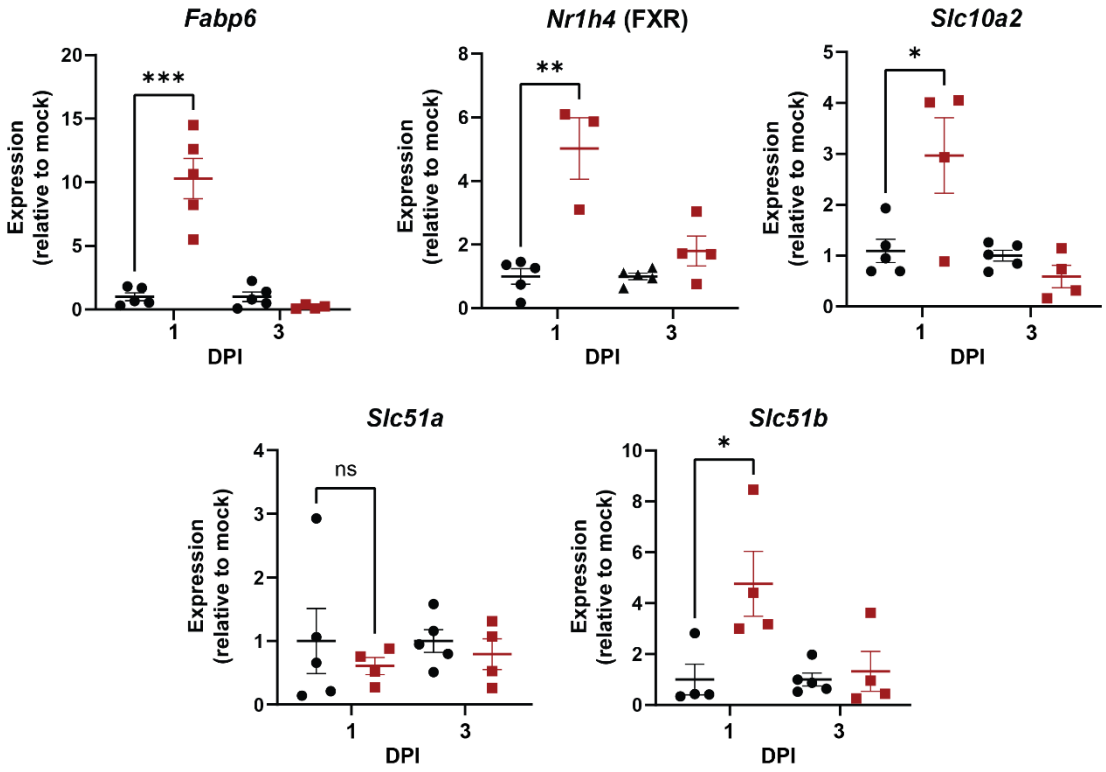

Figure 4.4. Expression of genes involved in absorption and transport of bile acids are moderately increased in the colon during early CDI. Absorption (*Slc10a2*) and transportation (*Fabp6, Slc51b*) genes are significantly upregulated at 1 dpi compared to mock-infected controls, as well as bile acid receptor gene expression (*Nr1h4*). None of these genes are upregulated at 3 dpi post-infection. N=5, significance determined using unpaired two-sided t-test.* p<0.05, ** p<0.01, *** p<0.001. Outliers determined using Grubbs test with an alpha of 0.05.

4.3.5. Protein levels involved in enterohepatic circulation do not change during infection despite increased transcript abundances.

The qRT-PCR data suggest that the host is in battle during CDI to maintain regulation of bile acid levels and circulation. At the 1 dpi time point, the host seems to be increasing biosynthesis in the liver, while decreasing absorption in the ileum, based on transcript abundances. These trends are then lost by 3 dpi, returning to comparable levels with mock-infected tissue in most cases. While these data seem consistent with the bile acid abundances described in Chapter Three, transcriptional changes are not always representative of the true proteomic landscape at the time, but rather the desired protein levels by the host. To ascertain whether this was the case for enterohepatic circulation, we utilized both quantitative immunohistochemistry and targeted bottom-up proteomics to visualize protein expression levels for key proteins in this process.

Formalin-fixed paraffin-embedded (FFPE) ileum and colon tissues from infected and mock-infected samples at 2 dpi were sectioned onto glass slides and then stained including additional biological replicates. FFPE tissue underwent paraffin-removal and an acidic antigen retrieval prior to staining with antibodies. An anti-SLC10A2 antibody and GFP secondary antibody was utilized to mark absorption of bile acids from the lumen. A secondary antibody-only tissue was also stained on the same slide to determine the auto fluorescent background. Liver tissues were collected at 3 dpi and fresh frozen over liquid nitrogen prior to sectioning onto glass slides in triplicate. Liver tissues were fixed with paraformaldehyde for 10 minutes prior to staining. Tissues were stained with either an anti-BAAT or anti-CYP7A1 antibody, and then conjugated with a GFP-tagged secondary antibody for visualization. Three biological replicates of each tissue type and antibody were conducted and analyzed.

Immunofluorescence quantitation was conducted on 5 functional tissue units in each ileal and colon replicate, or full liver sections, and normalized against the DAPI signal for each cell. GFP and DAPI intensities for each annotated region was determined using QuPath 0.32. Intensity values were plotted as ratios of GFP to DAPI signal as a method of normalization. The DAPI channel was utilized for normalization to account for differences in the number of FTUs selected as well as inter-sample variation during imaging. For ileal and colonic tissue, the GFP:DAPI ratios from each FTUs were averaged and plotted as averaged ratios per biological replicate. For liver tissue, the entire liver sections were quantitated and the resulting GFP/DAPI ratio is the average across the tissue sections.

For proteomics, fresh frozen infected and mock-infected tissues were homogenized and underwent a membrane extraction utilizing detergent and urea washes. Membrane extracts were then quantified with a BCA assay and approximately 100 µg of protein was aliquoted for each sample. Samples were then digested with trypsin at 57 °C for two hours. Resulting tryptic peptides were then loaded onto evosep tips and analyzed using a Thermo Orbitrap Fusion Tribrid. A targeted PRM approach using existing literature and a Skyline library was utilized for targeting specific tryptic peptides for proteins of interest and data were quantified using MaxQuant and MSSstats.

Both the quantitative IHC approach and targeted proteomics showed no significant differences in SLC10A2 abundances between control and infected samples, in contrast to what the qPCR data suggested. In the ileum, SLC10A2 protein abundance was comparable in infected tissue to mock-infected tissue at the 2 dpi time point (Figure 4.5A). In the colon, mock-infected data slightly decreased in expression, but this trend is not statistically significant (Figure 4.5B). None of the ileal membrane absorption proteins showed a statistically significant change in protein expression during infection at either 1 or 3 dpi, although soluble protein I-BABP/FABP6 seems to be trending towards downregulation during infection at 3 dpi. This lack of significant changes suggest that alterations to protein expression are not reflective of changes at the transcriptional level, or are at least not occurring at the same magnitude.

For liver tissue IHC, either an anti-CYP7A1 or anti-BAAT antibody was used to mark bile acid production or conjugation. Full tissue sections were analyzed for average GFP/DAPI ratios for 3 biological replicates per condition. These data also show no significant differences in protein expression between mock and infected tissues for either BAAT or CYP7A1, and neither does targeted proteomic analysis, suggesting that the biosynthesis changes seen at the transcriptional level have also not been converted to changes in protein levels within this time frame. While measuring protein abundance cannot identify whether these proteins are functional, or activated, the lack of protein abundance changes suggests that these protein levels are not driving the changes in bile acid levels.

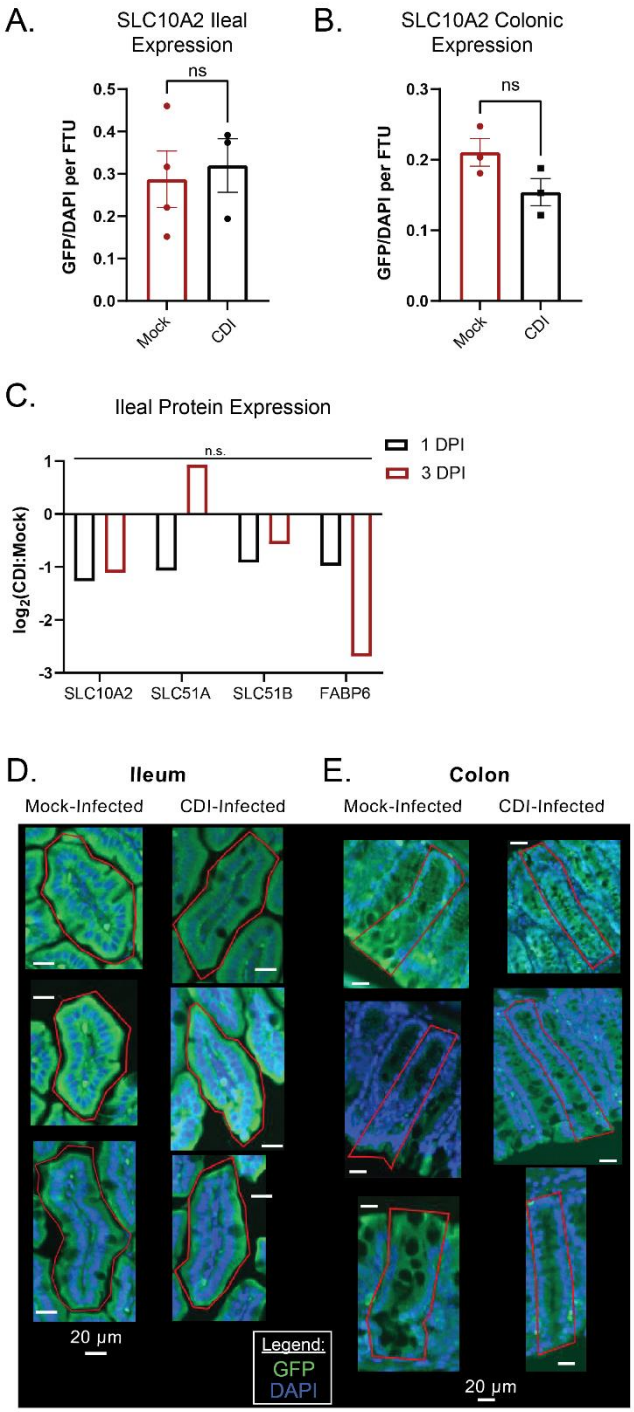

Figure 4.5. SLC10A2 protein expression does not significantly change in the ileum or colon during CDI. A) SLC10A2 average ileal expression values measured in green after IHC analysis. Each data point represents the average cellular fluorescence of functional tissue units (cypts) per tissue. **B)** SLC10A2 average colonic expression values measured in green after IHC analysis. Each data point represents the average cellular fluorescence of 5 cells per tissue. **C)** $\log_2$ fold change of protein expression quantified with LC-MS/MS comparing mock and CDI tissue at 1 and 3 dpi. **D)** Representative ileal villi imaged using IHC for quantitation. **E)** Representative colonic crypts imaged using IHC for quantitation. SLC10A2 was tagged with an anti-SLC10A2 antibody and conjugated with GFP, shown in green, and quantified as a ratio against DAPI, shown in blue. Each data point represents the cellular average of one biological replicate, where 5 FTUs per biological replicate were analyzed. Error bars show S.E.M. Significance determined using an unpaired t-test.

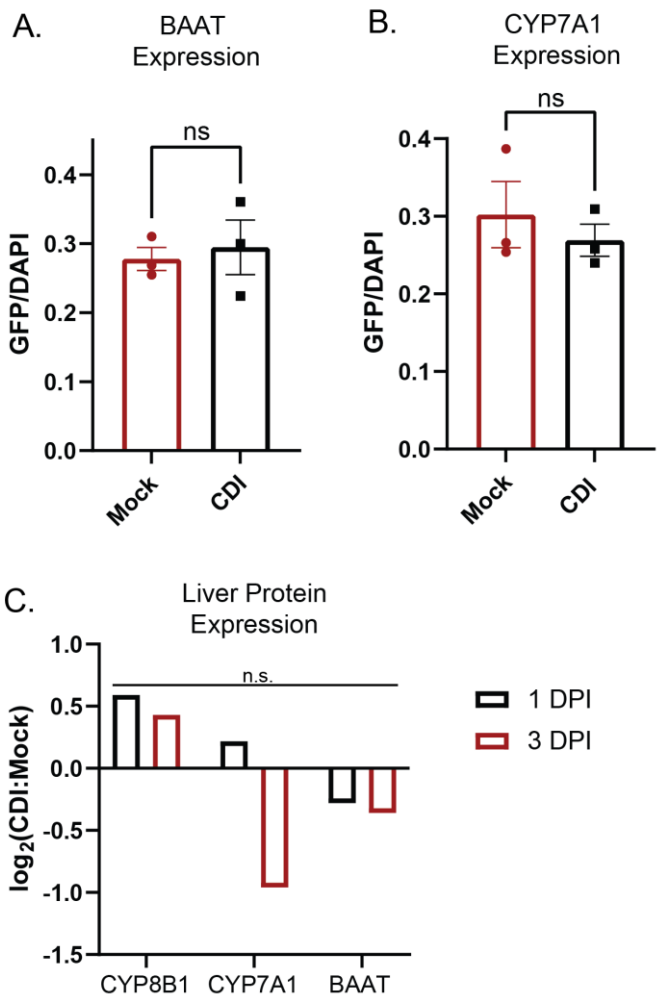

Figure 4.6. BAAT and CYP7A1 protein expression do not significantly change in the liver during CDI. Representative ratios of GFP to DAPI in full liver sections for tissues stained for either anti-BAAT or anti-CYP7A1 antibodies. **A)** GFP/DAPI ratios for three full liver sections from three different biological replicates after IHC analysis targeting BAAT expression. **B)** GFP/DAPI ratios for three full liver sections from three biological replicates after IHC analysis targeting CYP7A1 expression. **C)** $\log_2$ fold change of protein expression quantified with LC-MS/MS comparing mock and CDI tissue at 1 and 3 dpi. Error bars show S.E.M. Significance determined using an unpaired t-test.

4.4 DISCUSSION

Due to dramatic changes in bile acid abundances during CDI, this study proposed to further investigate the enterohepatic circulation of bile acids in this infection context. The overall goal was to determine if this circulatory pathway was altered by infection, and if these changes could result in the increased accumulation of bile acids in the lumen during infection. This approach was two-fold, first investigating the transcriptional changes to this pathway, and then the resulting proteomic changes. This particular pathway has been well studied, yet the impact of infection, specifically with *C. difficile,* has been understudied. The end products of enterohepatic circulation, namely bile acids, have been shown to have major implications in other gastrointestinal disorders and diseases as well,[68,92] further adding incentive to study this pathway in the context of disease.

Enterohepatic circulation has been implicated in both disorders of the host, and other pathogenic invaders.[68,87,145,146] While bile acids are primarily thought of as germination factors in their relationship to pathogens, they can also have implications for other pathogenic bacteria such as *Salmonella.* This relationship is especially interesting in the context of this investigation, because bile acids can cause repression of certain *Salmonella* genes.[146,147] Bile acids have been shown to repress activity of SPI-1 genes, which are responsible for the invasion and pathogenicity of *Salmonella*.[146] This interaction suggests that bile acids may play an even larger role as signaling molecules than previously thought, and once again highlights the importance of studying the relationship between pathogens, hosts, and bile acids.

Perturbations in bile acids have been shown in patients with inflammatory bowel disease. In particular, patients with IBD have increased primary bile acids and decreased secondary bile acids, similar to the trends seen in patients with CDI in Chapter Three.[148] There is also evidence that suggests that these bile acids may directly interact with intestinal and immune cells in a way that causes inflammation. Indeed, some studies have shown that bile acids may play an active role in shaping immune responses, such as decreasing expression of proinflammatory cytokines[99] or regulating colonic T regulatory cells.[149] Considering the implications this host-produced molecule can have on inflammatory pathways in the host, it is especially important to understand how the production of bile acids may be altered in similar inflammatory conditions such as CDI.

Theriot *et. al.* showed that inflammation mediated by *C. difficile* does in fact cause differential expression of transcripts of host genes within 2 and 4 dpi.[150] In particular, they utilized a *tcdR*$^{-/-}$ mouse model compared to a wild type CDI model, to see what genetic implications CDI

has on the host with or without toxin-mediated inflammation.[150] Although we have seen previously that toxins and inflammation alone cannot cause the same level of changes to bile acids as seen with a wild type CDI infection,[60] a combination of the two may drive many of the phenotypes shown in Chapter Three. While this particular experiment focused on genes that encode for metalloproteinases, as part of an immune response by the host, the idea that *C. difficile* inflammation can cause changes in gene expression within the host is encouraging for studying enterohepatic circulation genes in the context of infection.

Thus, transcriptional changes in the host during CDI were first investigated to see how the host responds to infection in this pathway. Enterohepatic circulation consists of both the biosynthesis of bile acids from cholesterol in the liver, as well as reabsorption in the ileum, both aspects of which were probed with qPCR at 1 and 3 dpi. The biosynthesis genes, specifically *Cyp7a1, Cyp8b1* and *Baat*, were all significantly upregulated at the earlier time point, which was no longer the case at 3 dpi. These data are indicative of the attempted changes by the host at the time, suggesting the host tries to increase synthesis of these bile acids during the first 24 hours of infection. This trend seems to coincide with the initial increase of bile acids at 1 dpi within the liver and the ileum (Figure 3.2). Increased production of bile acids within the liver would partially explain the increase in bile acids, yet these changes are modest for the 100x increase in bile acid abundance.

As this circulatory pathway also involves the ileum, genes involved in the absorption and transport of bile acids were investigated at the same time points in both the ileum and the colon. These data show a cohesive trend, with decreased ileal absorption via *Slc10a2* at 1 dpi, although there were minimal changes in transport genes. While the ileum is thought to be a major site of bile acid absorption, absorption seems to also be impacted in the colon at the transcriptional level, with increased colonic absorption at the earlier time point. One potential interpretation of these data is that absorption in the ileum decreases, potentially due to inflammation or active host interference. However, to maintain increased bile acid levels bile acids still need to be recirculated. This causes an increase in colonic absorption of bile acids, allowing them to recirculate while simultaneously causing an accumulation in the ileal lumen to aid in germination of *C. difficile.* These data together suggest the host transcript signals manipulate enterohepatic circulation in a way that benefits *C. difficile* germination and survival at 1 dpi, with a rapid dampening of these changes by 3 dpi. These changes also seem to be related to the pathogen *C. difficile* based on cell culture models, where colonic cells show increased absorption gene expression after exposure to vegetative *C. difficile* in a comparable way to the trends seen in

colonic tissue at the same time point. This raises a variety of interesting questions about the mechanism by which CDI impacts host enterohepatic circulation, with one potential explanation being through FXR.

FXR has been directly linked to bile acid homeostasis though bile acids binding the receptor as ligands. FXR is present in both the ileum and the liver, allowing it to contribute to enterohepatic circulation as a whole. When bile acids bind to FXR, activating it, *Cyp7a1* and *Cyp8b1* are downregulated in the liver, while *Fabp6* and *Slc51a/b* are upregulated in enterocytes. The relationship between bile acids, FXR and *Slc10a2* expression is a bit more complex, but also suggests that FXR can downregulate *Slc10a2* in the presence of high bile acid levels. These contributions of FXR are especially interesting in light of the gene expression data in both the liver and the colon. Unfortunately, the primers utilized for FXR (*Nr1h4*) showed no transcript for FXR in either control or infected tissues. In the liver, we see increased bile acids at 1 dpi (Figure 3.2) as well as increased transcript abundance of *Cyp7a1* and *Cyp8b1*, but *Cyp7a1* transcript abundance greatly decreases by day 3. In parallel, *Nr1h4* transcript abundance increases dramatically at 3 dpi. This correlation potentially suggests that FXR is somehow activated in response to increased bile acid levels, resulting in decreased expression of biosynthesis genes such as *Cyp7a1* to try and reduce bile acid accumulation. This potential trend is also supported in the colon, where *Nr1h4* has higher transcript abundance at 1 dpi during infection, and not at 3 dpi. When FXR is upregulated, both *Fabp6* and *Slc51b* show significantly higher transcript abundance at this same time point. When FXR expression returns to comparable levels at 3 dpi during infection, so do the transport genes. While it is unlikely that FXR alone is causing, or regulating, these bile acid phenotypes, these data suggest that FXR may be one avenue through which the host and pathogen regulate bile acid levels. This is especially interesting in the cell culture data, which show increased transcript abundance of *Nr1h4* after 24 hour exposure to vegetative *C. difficile*. Since there are no bile acids available in the media at this time point, these data hint at a potential mechanism for *C. difficile* to interact with FXR through something like bacterial-produced ligands.

While the transcriptional data are interesting and suggest altered regulation of enterohepatic circulation during CDI, it has been shown that protein and transcript levels are not frequently related.[151] It is estimated that up to 53% of protein expression is determined by transcript abundance,[152] yet “transcript levels alone are not sufficient to predict protein levels in many scenarios.”[153] While transcript levels give a unique insight into the goals of the host in that moment in time, proteins are necessary to initiate these changes. As we saw dramatic changes

in the byproduct of this pathway, bile acids, we anticipated seeing changes in protein levels as well. Therefore, both quantitative immunohistochemistry and targeted bottom-up proteomics methods were utilized to measure protein expression levels in both liver and ileal tissue. As many of these proteins are hydrophobic membrane proteins, making both extraction and digestion difficult, IHC was also utilized for confirmation as well as the addition of spatial information.

This investigation is a prime example of the disconnect between transcript levels and protein levels. While there could be arguably some modest changes in protein expression in some proteins, such as FABP6 and CYP7A1, these changes are not statistically significant. The IHC analysis also visualizes the comparable expression of BAAT, CYP7A1 and SLC10A2 in tissue, absent of any notable changes. Potential explanations for this disconnect, include the fact that transcriptional changes may not lead to protein changes in the time frames investigated, that protein regulation may occur at a post-translational level via modifications, or the possibility that protein activity or activation was altered in place of protein expression which is discussed further in the Future Directions section. Ultimately, regardless of the reason, these data seem to imply that changes to bile acid levels within the first 3 days of infection are not driven in a major way by changes to enterohepatic circulation. Some individual elements of enterohepatic circulation may be altered, such as damage to the ileum impacting SLC10A2 activity, some metabolite of *C. difficile* binding antagonistically to proteins to prevent their absorption of bile acids, or even changes to cholesterol levels further upstream that trickle down to bile acid levels. However, based on these data, it is clear that although the host may try to change enterohepatic circulation at the transcriptional level, these changes are not translated to changes in protein levels that would cause increased bile acid levels. The cause of these bile acid levels remains incomplete, and some potential future investigations to further probe and understand what is causing these changes are discussed in the next chapter.

4.5 METHODS

Bacterial strains. Wild-type *C. difficile* R20291 was grown at 37°C in an anaerobic chamber (90% nitrogen, 5% hydrogen, 5% carbon dioxide, Coy Lab Products) in brain-heart-infusion broth (BC Life Sciences) supplemented with 0.5% yeast extract (BD Life Sciences) and 0.1% cysteine (Sigma-Aldrich).

Animal models. All animal experiments were performed using protocol M2000027-00 approved by the Vanderbilt University Medical Center Institutional Animal Care and Use Committee and in compliance with NIH guidelines, the Animal Welfare Act, and US Federal law. Animal studies were conducted using 8- to 12-week old male C57BL/6 (Jackson Laboratories) mice housed in groups of up to five at the Vanderbilt University Medical Center Animal Facilities. Briefly, C57BL/6 mice received cefoperazone in their drinking water (0.5 mg/ml) for 5 days. Following a 2-day recovery period, mice were gavaged orally with PBS or infected with 10^5 *C. difficile* spores to an endpoint of one or three days. CDI symptomology was monitored daily by weight loss. Mice were humanely euthanized using compressed CO_2. Intestinal segments and liver were dissected and frozen over dry ice. Samples were stored at -80°C prior to protein extraction.

Tissue RNA extraction. Liver and ileal samples from mice were flash frozen over dry ice and stored at -80 °C prior to RNA extraction. Tissues were homogenized in Lysing Matrix D tubes (MP Biomedicals) containing 700 µl RLT buffer with 1% (v/v) β-mercaptoethanol (Qiagen) using a FastPrep-24 (MP Biomedicals) bead beater for 40 seconds at 6.0 m/s (repeated 6 times, incubating on ice for 1 minute in between rounds). Homogenates were centrifuged at 20,000 x g at 4 °C for 5 minutes to pellet debris, RNA was extracted using phenol:chloroform:IAA, pH 6.7 (Sigma), and samples were mixed with 50% or 100% ethanol prior to being transferred to Qiagen RNeasy columns, according to the manufacturer's instructions.

Cell Assays. Caco2 cells acquired from the Byndloss Lab at Vanderbilt were grown in tissue flasks according to manufacturer specifications. Prior to assays, toxicity assays were completed on cells to determine optimal conditions of vegetative *C. difficile* (R20291)*, C. difficile* spores, and chenodeoxycholic acid in multiple conditions of 10x dilutions. Cells were then grown in a 12-well culture dish and exposed to each condition in triplicate for 24 hours before collection.

Cell RNA extraction. Caco2 cells were lysed directly in a culture dish by adding TRIzol® Reagent to the dish and passaging the cell lysate several times through an RNase-free pipette tip. Lysed cells were stored at -80°C until RNA extraction. RNA was extracted using 4-Bromoanisole, and samples were mixed with 70% ethanol prior to being transferred to a PureLink RNA mini kit

column, according to manufacturer's instructions. An on-column PureLink DNase treatment was conducted on RNA bound to the spin column prior to elution. RNA samples were then stored at -80°C prior to qRT-PCR preparation.

qRT-PCR. RNA samples were aliquoted to 800 ng samples using a nanodrop 8000 (Thermo Scientific) prior to DNase treatment. Aliquoted RNA samples post-DNase treatment were subjected to DNase treatment (Invitrogen) prior to cDNA synthesis using an iScript cDNA synthesis kit (Bio-Rad). qRT-PCR was conducted using iQ SYBR Green mix (Bio-Rad), gene-specific primers (Tables 5.1 and 5.2), and a CFX96 qPCR cycler (Bio-Rad). Transcript abundance was calculated using the ΔΔCq method and data were normalized to 18S gene expression.

Immunohistochemistry. Formalin-fixed paraffin embedded colon and ileal tissues were sectioned using a microtome at a thickness of 8 µm. Prior to staining, sections were deparaffinized in xylenes for 3 min twice, then fixed with 100% EtOH for 20 dips, 95% EtOH for 20 dips, 70% EtOH for 20 dips, then ddH_2O. Following deparaffinization, samples underwent antigen retrieval in acidic conditions (ImmunoRetriever with Citrate, Bio SB, Santa Barbara, CA) for 20 minutes at 95 °C, allowed to come to room temperature, and then underwent a buffer exchange. Fresh frozen liver sections were fixed with 4% paraformaldehyde for 10 minutes, then washed 2x with PBS prior to blocking. All sections were then blocked for 1 hour at room temperature with blocking solution (PBS, 0.5% Tween, 0.1% BSA) followed by overnight primary antibody incubation with either the SLC10A2 (1:100), CYP7A1 (1:100) or BAAT (1:100) antibody at 4°C. Primary antibodies were diluted in blocking buffer, and secondary antibodies were diluted in PBS. An anti-SLC10A2 (1:100 ratio, Abcam, Cambridge U.K.) primary antibody was used for ileal and colonic tissue. Anti-CYP7A1 (1:100 ratio, Bioss Antibodies, Woburn, MA) and anti-BAAT (1:100 ratio, Thermo Fisher Scientific, Waltham, MA) primary antibodies were used for liver tissue. Anti-rabbit IgG conjugated to Alexa Fluor 488 (Thermo Fisher Scientific) was used for as a secondary antibody for visualization. The following morning sections were washed 2x with PBST and 1x with PBS, then stained with GFP-tagged fluorescent secondary antibodies for 1 hour at room temperature (1:500 ratio). Finally, tissues were washed 2x with PBST and 1x with PBS then mounted with DAPI Fluoromount-G (SouthernBiotech, Birmingham, AL) and coverslipped. Sections incubated with blocking buffer without primary antibodies prior to adding the secondary antibody were used as negative controls. Imaging was performed using a Zeiss AxioScan microscope slide scanner (Zeiss, Jena, Germany) with DAPI, Cy5 and EGFP channels.

Quantitation was determined using QuPath version 0.23. Fluorescent levels were normalized to serial sections stained with only secondary antibodies to determine background

fluorescence for each biological replicate. Three replicates per condition were analyzed, and 5 FTUs were selected per section of colon or ileal tissue. Full tissue sections were analyzed for liver tissue. FTUs were selected using QuPath and both DAPI and GFP channel intensities were quantified for each FTU or tissue. GFP signal was normalized as a ratio against DAPI signal on a section-to-section basis and plotted as GFP/DAPI ratio.

Membrane protein extraction sample preparation. Intestinal and liver tissue samples were manually homogenized in buffer containing 25 mM Tris, 5 mM EDTA, 150 mM NaCl, 1mM DTT and 1% protease and phosphatase inhibitors. Homogenized samples were centrifuged at 100,000 x g for 30 minutes at 4°C then supernatant was collected for soluble protein analysis. Centrifugation was repeated twice. Pellets were then washed with buffer containing 8 M urea and centrifuged for 20 minutes at 100,000 x g and supernatant was discarded. Resulting pellets were reduced in buffer containing 8 M urea and 10 mM DTT then incubated at 57°C for 45 minutes. IAA was then added to 50 mM for alkylation and resulting mixture was incubated at room temperature for 45 minutes. Samples were then centrifuged at 100,000 x g for 20 minutes and supernatant was discarded. Remaining pellet was washed twice with MilliQ water for 20 minutes at 100,000 x g and supernatant was discarded. The pellet was then solubilized in 100 mM Tris and centrifuged at 500 rpm. A BCA assay was conducted on resulting samples, with 10 µL of sample mixed with 2.5% SDS before addition to the assay. 100 µg aliquots of sample were digested using trypsin gold in 50 mM Tris at a 1:25 ratio for 2 hours at 57°C. After digestion trypsin activity was stopped with dry ice and samples were stored at -80°C in solution. Prior to mass spectrometry analysis, samples were loaded onto EvoSep One Evotips containing C_{18} material.

Soluble proteins sample preparation. Supernatant from the membrane protein extraction preparation was analyzed using a BCA assay to determine protein concentration. 100 µg aliquots and buffer were added to equal 100 µL prior to acetone precipitation. 300 µL of ice cold 75 ACN: 25 MeOH was added to samples and briefly vortexed. Samples were then incubated at -80°C overnight then centrifuged in a cold centrifuge for 15 minutes at 10,000 x g and supernatant was discarded. 300 µL of cold ACN was added to each tube, and sample mixtures were centrifuged for 10 minutes at 10,000 x g. Supernatant was discarded and acetone was allowed to evaporate for 15 minutes. Aliquots were resuspended in 10 µL TFE and 10 µL of 100 mM Tris then reduced with 1 µL of 0.5M TCEP at room temperature for 30 minutes. Samples were then alkylated with 2 µL of 0.5M IAA in the dark at room temperature for 30 minutes. Ammonium bicarbonate was added to samples to a final volume of 100 µL then 2 µg trypsin gold was added and samples were digested overnight at 57°C.

Liquid chromatography tandem mass spectrometry. Tryptic peptides from both preparation methods were loaded onto EvoSep One Evotips using manufacturer's protocols (EvoSep Biosystems, Odense, Denmark). Briefly, tips were washed with ACN with 0.1% formic acid, soaked in 1-propanol for 1 minutes, equilibrated with H2O containing 0.1% formic acid then 0.5 µg of sample were loaded, washed, then preserved with H_2O containing 0.1% formic acid. Liquid chromatograph was perfomed using an EvoSep One coupled to an Orbitrap Fusion Tribrid mass spectrometer (Thermo Scientific, San Jose, CA). A Reprosil C18 reverse phase column was utilized (1.9 µm particle size, 75 µm id x 15 cm) with a fused silica emitter tip (EvoSep Biosystems, Odense, Denmark). Mobile phase A consisted of H_2O with 0.1% formic acid, and mobile phase B consisted of acetonitrile with 0.1% formic acid. Fourier transform mass spectra (FTMS) were collected using 60,000 resolving power, an automated gain control target of 1e6, and a maximum injection time of 50 ms over the mass range of 375-1500 *m/z*. For targeted membrane protein analysis, peptide *m/z* lists were generated using Skyline 20.2 for 2-5 peptides per protein of interest (Table 4.3). 5 biological replicates were run per condition.

MS-Proteomics Data analysis. For protein and peptide identification, tandem mass spectra were searched using MaxQuant version 1.6.7. against a database containing the mouse proteome from the UniProt KB. These were supplemented with the reversed sequences and common contaminants automatically (decoy database) used for quality control and estimation of FDR by MaxQuant. Carbamidomethylation was set as a fixed modification. Minimal peptide length was 7 amino acids. Peptide and protein FDRs were both set to 1%. Proteins identified as "reverse', "only identified by site", or "potential contaminants" were removed. Proteins identified by MaxQuant were filtered based on 2 unique peptides contributing to the protein identification. Fold changes were determined using 5 combined biological replicates per condition compared using MSStats. Proteins with few measurements or only 1 peptide were removed prior to processing. Log2 fold changes were determined with the following conditions: normalization by equalize medians method, minimum feature count of 2, a Tukey's median polish summary method, and a 0.999 max quantile for censored data. Data were compared by both infection status and time point.

Quantification and statistical analysis. Statistical analyses were performed using GraphPad Prism 8 and Microsoft Excel. Statistical significance was assessed using an unpaired two-sided t-test. Significance was defined as $p<0.05$, and the data were only excluded on the basis of technical errors associated with the experiment or by outlier identification using a Grubbs test with an alpha of 0.05.

Table 4.1: Primers used for murine qRT-PCR experiments.

Primer for qRT-PCR		***Source DOI***
18S_qPCR_murine_F	CTCAACACGGGAAACCTCAC	*Andy Weiss*
18S_qPCR_murine_R	CGCTCCACCAACTAAGAACG	*Andy Weiss*
Slc10a2_qPCR_murine_F	TGGGTTTCTTCCTGGCTAGACT	10.1126/scitranslmed.aaf4823
Slc10a2_qPCR_murine_R	TGTTCTGCATTCCAGTTTCCAA	10.1126/scitranslmed.aaf4823
Slc51a_qPCR_murine_F	GTTCCAGGTGCTTGTCATCC	10.1016/j.jhep.2016.01.016
Slc51a_qPCR_murine_R	CCACTGTTAGCCAAGATGGAGAA	10.1016/j.jhep.2016.01.016
Slc51b_qPCR_murine_F	AGATGCGGCTCCTTGGAATTA	10.1016/j.jhep.2016.01.016
Slc51b_qPCR_murine_R	TGGCTGCTTCTTTCGATTTCTG	10.1016/j.jhep.2016.01.016
Fabp6_qPCR_murine_F	GGTCTTCCAGGAGACGTGAT	10.1194/jlr.M500417-JLR200
Fabp6_qPCR_murine_R	ACATTCTTTGCCAATGGTGA	10.1194/jlr.M500417-JLR200
Baat_qPCR_murine_F	CACCTGATTGAGCCTCCCTA	10.1016/j.celrep.2021.109683
Baat_qPCR_murine_R	GGAAGGAGATGCTGCTTGAG	10.1016/j.celrep.2021.109683
Cyp7a1_qPCR_murine_F	TTCTTTGATCTGGGGGATTG	10.1096/fj.12-223008
Cyp7a1_qPCR_murine_R	ATTTCCCCATCAGTTTGCAG	10.1096/fj.12-223008
Cyp8b1_qPCR_murine_F	ACAAGCAGCAAGACCTGGAT	10.1038/nm1785
Cyp8b1_qPCR_murine_R	ATGGAAGAGACGCTGCAACT	10.1038/nm1785

Table 4.2: Primers used for cell culture qRT-PCR experiments.

Primer for qRT-PCR		***Source DOI***
18S_qPCR_human_F	CTACCACATCCAAGGAAGCA	10.4049/jimmunol.1401075
18S_qPCR_human_R	TTTTTCGTCACTACCTCCCCG	10.4049/jimmunol.1401075
Slc10a2_qPCR_human_F	TGGCCTTGGTGATGTTCTCC	10.1038/srep05251
Slc10a2_qPCR_human_R	TGTCGCCATCGACCCAATAG	10.1038/srep05251
Slc51a_qPCR_human_F	TTCCTCTAAAACCAGGTCTCAAGT	10.1016/j.jhep.2016.01.016
Slc51a_qPCR_human_R	GCACAGTCATTAGAAAAGTCTCCA	10.1016/j.jhep.2016.01.016
Slc51b_qPCR_human_F	GCAGCTGTGGTGGTCATTAT	10.1194/jlr.M500417-JLR200
Slc51b_qPCR_human_R	TAGGCTGTTGTGATCCTTGG	10.1194/jlr.M500417-JLR200
Fabp6_qPCR_human_F	CTCCAGCGATGTAATCGAAA	10.1194/jlr.M500417-JLR200
Fabp6_qPCR_human_R	CCCCCATTGTCTGTATGTTG	10.1194/jlr.M500417-JLR200
FXR_qPCR_human_F	ACCAGCCTGAAAATCCTCAACAC	10.1038/s41598-017-12629-4
FXR_qPCR_human_R	CTCTCCATGACATCAGCATCTCAG	10.1038/s41598-017-12629-4

Table 4.3. Tryptic peptide sequences used for PRM analysis of enterohepatic circulation membrane proteins.

Encoding Gene	Peptide Sequences	*m/z*	Charge
Slc51a	K.ITLSIVGLFLIPDGIYDPGEISEK.S	1295.2067	2+
	K.MHLGEQNMGSK.F	616.2815	2+
Slc51b	K.AAANAEVPQELLEEMLWYFR.A	1190.5857	2+
	K.ENNSQVFLR.E	553.7831	2+
Slc10a2	K.LWIIGTIFPIAGYSLGFFLAR.L	1178.1668	2+
	K.NDAEFLEK.T	483.2324	2+
	K.TDNEMDSRPSFDETNK.G	943.3971	2+
Fabp6	K.NYDEFMK.R	473.7024	2+
	R.LGLPGDVIER.G	534.8060	2+
	K.ECEMQTMGGK.K	585.7330	2+
	K.VVAEFPNYHQTSEVVGDK.L	1009.9945	2+
	K.LVEISTIGDVTYER.V	797.9198	2+
Cyp7a1	K.FGSNPLEFLR.A	590.3115	2+
	R.SIDPSDGNTTENINK.T	802.8736	2+
Baat	K.VDLEYFEEGVEFLLR.H	929.4671	2+
	K.AHGHFLFVVGEDDK.N	785.8861	2+
	K.VHANQAIAQLMK.N	662.3637	2+
Cyp8b1	R.EWVEVSQLQR.L	637.3304	2+
	K.VALFPYLSVHMDPDIHPEPTAFK.Y	875.4454	3+

CHAPTER 5

Biological Outcomes and Future Directions

5.1. OVERVIEW

Bile acids contribute greatly to *C. difficile* infection, and also change in abundance as a result of infection.[5,60] In order to study these changes, and their impact on the host and pathogen, mass spectrometry and transcriptional approaches were utilized. First, a sample preparation workflow was developed, optimized, and implemented in Chapter Two to study the murine gastrointestinal tract via MALDI IMS with intact luminal content.[100] In Chapter Three, bile acid levels were shown to increase dramatically in the context of infection in a way that benefits the fitness of the pathogen.[60] This increase was most notable in conjugated primary bile acids and is somewhat reliant on the toxins produced by the pathogen. Additionally, human bile acid levels varied based on colonization and symptom status, where bile acids known to bind *C. difficile* toxins were increased in uncolonized and asymptomatic patients. The underlying enterohepatic circulation of bile acids was investigated at the transcriptional level in Chapter Four, which showed that during early infection biosynthesis-related gene expression increased, while absorption-related gene expression decreased. These trends were no longer detected at 3 dpi. Protein abundances, as measured with IHC and mass spectrometry, were unchanged during infection, however, suggesting that host transcriptional changes were not translated into protein abundance changes within this time frame. In this chapter I will discuss the potential implications on human health for the research detailed in this thesis, as well as future directions for this investigation.

5.2. IMS ANALYSIS OF GASTROINTESTINAL TRACT WITH LUMINAL CONTENT

The gastrointestinal tract is a complex, dynamic interface between the host, the environment, and the gut microbiome.[154,155] This region is the site of digestion, drug absorption, as well as microbial activity.[107] Current approaches to study this region, however, miss out on this rich interplay by eliminating regions of sample. In particular, the luminal content is commonly flushed out of samples, often taking the mucus layer with it, which eliminates a large portion of dietary contributions to the gut.[108,109] Additionally, the gastrointestinal tract is one of the largest organs making it difficult to study it in its entirety. While many studies have focused on small regions of tissue for their studies, these cannot be properly correlated to the GI tract as a whole. Each region of the small intestine (duodenum, jejunum, ileum) and the large intestine has a unique

function and differing bacterial burdens that greatly shape their activity.[107] Microbes present in the colon are likely absent in the jejunum, and vice versa, thereby changing the chemical landscape of each region. Since microbe-host interactions contribute greatly to the gut microenvironment, each region needs to be analyzed for a representative view of the gastrointestinal tract.

As these host-microbe interactions frequently occur through chemical signaling, detecting these molecular markers is key for understanding this dynamic region. Additionally, these chemical markers need to be studied in context through spatially-driven methods to understand where these signals are being sent. These two needs in parallel are best accomplished through the application of imaging mass spectrometry, which allows for robust untargeted molecular analysis in a spatially-resolved manner.[4] Unfortunately, IMS (especially MALDI IMS) requires involved sample preparation methods including washing and matrix application that can cause delocalization for certain tissue types. Additionally, samples are limited in size to a standard glass slide. The GI tract compounds these difficulties through problems with tissue retention and the large amount of tissue. In particular, the luminal content that houses dietary contributions and some bacteria is easily delocalized or removed entirely during sample preparation.[100]

In order to more fully study and visualize this unique region, a sample preparation method for the GI tract prior to MALDI IMS analysis was required. As detailed in Chapter Two, this method included two alterations to the sample preparation protocol. First, tissues were prepared in a "Swiss roll" morphology that allows for much larger swaths of the intestine to colocalize on the same slide.[110] These modified Swiss rolls also include the luminal content as it is located within the mouse. Second, tissues were mounted onto slides coated with polylysine, which improves tissue retention.[112] Together, these alterations allowed for multimodal IMS analysis of the small intestine, which highlighted the unique molecular makeup of the luminal content compared to the tissue. Additionally, this approach allowed us to compare samples from mice infected with CDI and mock-infected mice, which highlighted unique changes in bile acid abundances that had previously gone undetected.

While this study emphasized the applicability of an adapted sample preparation method to study changes to the GI tract during infection with *C. difficile*, a wide variety of applications would benefit from the use of this approach. For instance, the gastrointestinal tract can house a variety of other potential pathogens and diseases such as *Salmonella enterica* or inflammatory bowel disease.[147,148] In the case of other pathogenic bacteria, this approach could elucidate signaling molecules harnessed by either the host or pathogen in the competitive infection environment. For chronic conditions such as ulcerative colitis, this approach could help us better understand what is changing at the molecular level during inflammation, as well as understanding

what specific regions of the GI tract are impacted. The more we characterize the molecular changes that contribute to these diseases, the more options for potential pharmaceutical interventions open.

Pharmaceuticals often rely on the absorptive nature of the gut to introduce drugs into the host system.[54] Tracking where these drugs end up, and in what form, however, can be extremely difficult. The ability to visualize drugs, and their potential derivatives, is a powerful potential application for this method. As the microbiome often interacts with pharmaceuticals, this offers the ability to see where these interactions may occur by tracking where derivatives begin to appear within the GI tract. This is also powerful for studying the microbiome in a unique light. The microbiome is a huge area of study, and a major component of the gastrointestinal tract that was not addressed in this study. Microbiota produce unique metabolites that interact with the microenvironment, and the ability to visualize these metabolites could potentially be harnessed as a way to fingerprint the localization of specific microbial classes.[156] Altogether, the development of this reproducible sample preparation strategy for MALDI IMS of the gastrointestinal tract further opens the possibilities for IMS in investigating the gut.

5.3. BILE ACID LEVELS IN THE CONTEXT OF *C. DIFFICILE*

One of the main molecular classes that change in abundance during CDI, as visualized using the sample preparation method in Chapter Two, is bile acids.[60] Bile acids have long been studied in the context of lipid digestion as well as in CDI due to their role as germination factors.[59] Most of this work, however, emphasized which bile acids are best able to induce germination based on conjugation status. For instance, conjugated versions of cholic acid are the most potent germination factors for *C. difficile* spores.[59] Recent studies have also heavily focused on novel bile acids produced by the microbiota, and the rich diversity of secondary bile acids.[73] Secondary bile acids have been shown to play an interesting role in CDI by serving as antimicrobials against vegetative *C. difficile*.[99] What has not been investigated in any major way, however, is the inverse relationship. It is clear how bile acids function during germination, and their impact on *C. difficile*. How *C. difficile* and CDI impacts bile acids, however, has not been thoroughly addressed. Understanding how the host responds to CDI, especially in a manner that has major implications for *C. difficile* survival and success, is crucial to furthering our understanding of *C. difficile* pathogenesis in the gastrointestinal tract.

In Chapter Three, we quantified the levels of primary bile acids within the GI tract luminal content and liver tissue using LC-MS/MS in the context of CDI. These data showed that primary bile acid abundances increase dramatically in the ileum during infection. Specifically,

unconjugated bile acids increase around 10x and conjugated bile acids increase almost 100x. These changes occur rapidly, as elevations are detected within 1 day of infection. In contrast, liver levels of unconjugated bile acids steadily decrease during infection and are below the limit of detection by day 3, while conjugated species remain elevated. Although bile acid levels in the cecum were not as dramatic as in the ileum, large fold changes in primary bile acid abundances in the cecum still occurred within the same time frame. As bile acids are ordinarily reabsorbed in the ileum, the presence of so many in the cecum suggests that ileal absorption is either not occurring, or is unable to maintain sufficient absorption in response to rising bile acid levels.

CDI is a complex disease, and a variety of secondary effects could potentially contribute to the rise in bile acid levels. We investigated a variety of potential contributions and monitored the resulting bile acid concentrations. To determine the potential impact of inflammation, mice were treated with dextran sulfate sodium to cause general GI inflammation. Bile acid levels in these mice compared to mock-infected mice showed minimal changes, suggesting that inflammation is not driving these changes, and the dramatic increase may be *C. difficile* specific. We also investigated whether CDI could damage the epithelium in a way that would prevent absorption, which was confirmed to not be the case by histological analysis. With these data, it seems that the bile acid changes are in fact specific to CDI, which is intriguing as *C. difficile* is one of the few pathogens that benefits from these rising levels. Next, we interrogated the potential impact of the toxins produced by *C. difficile* (TcdA and TcdB), which showed that bile acid levels are somewhat reliant on toxins, yet this phenotype cannot be induced by toxins alone. Summed together, these data suggest that something unique to the pathogen itself is driving this increase in bile acid abundances.

Having established that *C. difficile* somehow impacts bile acid levels during infection, it followed that potentially *C. difficile* may benefit in some way from this influx. We treated mice with cholestyramine to reduce the levels of available bile acids in the intestine, and this experiment showed that germination and colonization were negatively impacted. This suggests that the influx of bile acids shown in the gut is beneficial for *C. difficile* survival, and although colonization can occur in these bile acid sparse conditions, there is a notable delay. This raises a lot of questions about why bile acid levels are rising in response to CDI, when this accumulation better prepares *C. difficile* for colonization of the host.

These data are highly encouraging for better understanding a mechanism of CDI in mice, but as humans have slightly different bile acid pools it was important to see if changes in bile acids also occurred in human infection models. We measured bile acid levels in over 100 pediatric patient stool samples from patients with or without CDI. The colonized patients included those

with and without common CDI symptomology. This was an important clinical distinction, as asymptomatic patients can be difficult to diagnose. These data show that bile acid pools do differ between colonized and uncolonized patients, most notably in the secondary bile acid DCA. In addition, there were significant changes in bile acid levels between asymptomatic and symptomatic patients for CDCA, DCA and CA. All of these bile acids have known toxin-binding activity, suggesting that the reduction of free *C. difficile* toxins in the system may alleviate many of the symptoms associated with *C. difficile*.[58] Altogether, this study suggests that bile acid changes do play a role in disease and symptomology, and these changes are in some way manipulated by the pathogen itself.

CDI is a persistent disease that currently relies heavily on a small panel of antibiotics for treatment, a treatment that causes recurrent infection in 20% of cases.[25] These results suggest that bile acids may be a marker for diagnosis, as well as a potential target for treatment, and offer novel avenues for CDI management in a clinical setting. For instance, if primary bile acid levels can be artificially reduced early in infection, *C. difficile* colonization may be weakened enough to improve treatment of infection with vancomycin. If the toxin-binding power of bile acids, especially DCA which is already lowered in colonized patients, shows to be reproducible in human models then treatment of patients with DCA to reduce toxin levels in the gut could help alleviate symptomology. Should bile acid levels be reliably altered in asymptomatic patients compared to uninfected patient samples, then this offers alternative diagnostic tests for CDI from noninvasive samples. This study has focused primarily on ileal bile acid levels in mice but excreted fecal bile acid levels in humans. New investigations and tools have been developed to sample luminal content along the GI tract in pH-specific balloons that are expelled naturally with feces, which could be harnessed to better map bile acid levels within the small intestine of humans without invasive surgery, giving further insight into changes in these levels at the human level. Overall, the more we understand about changing bile acid levels, and their impact on CDI, the better chance of developing novel diagnostic and therapeutic approaches for helping patients impacted by CDI.

5.4. TRANSCRIPTIONAL CHANGES TO ENTEROHEPATIC CIRCULATION DURING CDI

The dramatic increase in bile acids in the ileum and cecum during the first day post-infection with CDI, as shown in Chapter Three, raised many additional questions. First and foremost: what is causing the increased levels of bile acids during infection? Ordinarily, bile acid levels are strictly controlled, as increased abundance can lead to a variety of metabolic disorders

as well as liver injury or damage.[61] These levels are controlled primarily through enterohepatic circulation, or the synthesis and recycling of bile acids.[83] Enterohepatic circulation includes the biosynthesis of bile acids from cholesterol in the liver, the release into the small intestine, and the reabsorption of bile acids in the ileum where they are then returned to the liver.[6] When bile acid levels get too high, the synthesis of bile acids is dampened, and bile acids are pushed out of enterocytes without absorbing any more from the lumen into the cell.[144] As this pathway is controlled by FXR through the binding of bile acids as ligands, we strove to understand how this pathway is altered in the context of *C. difficile.* Previous work on FXR and bile acids focused on how various bile acids interacted with FXR, especially as agonists, and the FXR-regulated control of the microbiota.[88] While these factors contribute to FXR activation, it is unclear why these transcriptional changes would occur so dramatically during infection.

In order to better understand how *C. difficile* interacts with its host, it is important to study how the host responds to infection. In particular, how the host attempts to change the environment at the transcriptional level could give insight into which of these changes may be host-mediated, and which the host may try to repress, giving insight into how *C. difficile* may be manipulating host activities. In light of the changes in bile acid levels, it follows that interrogating the enterohepatic circulatory pathway in the context of CDI could be deeply informative for how the increased bile acid levels occur. As enterohepatic circulation at the transcriptional level has been understudied in the context of CDI, and the end products of this pathway are changing, it made sense to probe changes to gene expression during infection to better understand how the host initiates, and responds to, elevated bile acid levels.

In order to target particular genes of interest that encode for proteins involved in either biosynthesis in the liver (*Cyp7a1, Cyp8b1, Baat*) or absorption in the ileum and colon (*Slc10a2, Fabp6, Slc51a/b*), a quantitative PCR method was employed in Chapter Four to analyze RNA extracted from murine tissue. These data allowed us to see changes in transcript abundance for each of these genes in both control and infected mouse models, at both 1 and 3 dpi. As we have seen changes in bile acid levels at both of these time points in Chapter Three, it was interesting to see if the host was responding the same way throughout the first 3 days of infection. In the liver, we saw that all three genes of interest had significantly higher transcript abundances in infected samples compared to mock-infected tissues at the 1 dpi time point. By day 3, however, *Cyp7a1* transcripts had returned to the mock-infected levels, while *Baat* remained significantly elevated. This suggests that biosynthesis may be initially upregulated, but the buildup of bile acids leads the host to eventually dampen this signal. In the ileum, absorption into the enterocyte via *Slc10a2* showed significantly lower transcript abundances at 1 dpi, with recovery to mock-infected

levels by 3 dpi. The pairing of this ileal and liver data suggests that enterohepatic circulation results in increased bile acid levels at 1 dpi, but is regulated by 3 dpi. Potentially in response to decreased encoding for *Slc10a2* in the ileum, transcript abundances increase in the colon for this same gene, suggesting that absorption shifts from the ileum to the large intestine to retain the bile acids leaving the ileum in high amounts.

Interestingly, in a cell culture model utilizing a colonic cell line (Caco2), we saw changes in transcript abundance for *Slc10a2* and *Fabp6* in cells exposed to vegetative *C. difficile*, even in the absence of bile acids. This suggests that some of the initial changes detected may be driven by *C. difficile* in order to increase bile acids available for germination. All of these changes at the transcriptional level are absent at the proteomics level as measured by IHC and mass spectrometry, however, suggesting a more complex dynamic to bile acid regulation during CDI. While it is most likely that *C. difficile* would make changes at the transcriptional level, without the same changes to protein abundances it is difficult to fully comprehend where these additional bile acids come from. Still, changes to enterohepatic circulation resulting from CDI offers interesting insight into the environment *C. difficile* responds to when colonizing a host, and how the host in turn responds.

C. difficile is a difficult pathogen to treat, and current treatment methods are lacking due to high rates of recurrent infections. While manipulating *C. difficile* genetics is less feasible as a treatment for CDI, a better understanding of its impact on the host could elucidate vulnerabilities that can be targeted for treatment. The data summarized in Chapter Four suggest that the enterohepatic circulatory pathway may be such a target. It seems that CDI causes alterations of this pathway by increasing the abundance of bile acids during early infection, and the implications of this increase are improved germination and colonization of the pathogen in the gut. Targeting a host pathway, especially with a specific gene target, widens the potential therapeutic options. If these transcriptional changes are FXR-mediated, as these data seem to suggest, then targeting FXR could be a potential early-stage intervention. Artificial FXR agonists have already been developed, such as GW4065, and could potentially be deployed to combat this increase in enterohepatic circulation transcripts. Of course, it is crucial to recognize that while these transcript abundance changes are encouraging, they are not seen in the protein expression data. There are a few potential explanations for this seemingly incongruous data. The first is that the timepoints studied at the proteomics level are not the correct timepoints to see changes in protein abundance, and additional time points throughout infection could be studied to remedy this. The second is that while the protein expression levels do not change, there is differential activity or activation during infection, which is explored in the future directions section. To truly understand

what is causing these increased bile acids requires additional studies, including some focused on the proteins involved in enterohepatic circulation.

5.5. LIMITATIONS

As with any scientific investigation, there are limitations that should be addressed. Potential avenues to address and remedy these limitations are discussed below in Future Directions. In regards to the sample preparation work, and a recurrent theme throughout this thesis, is the lack of optimization for secondary bile acid analysis. The matrices selected and tested were evaluated mostly on their ionization efficiency for primary bile acids, reducing further studies into secondary bile acids within the GI tract. Additionally, most images were collected at low spatial resolution. To truly get the most information out of these regions, a higher resolution imaging method would greatly benefit these investigations, especially when trying to study regions such as the mucus layer.

In regards to the LC-MS/MS work aiming to quantify bile acid levels, additional quantification of secondary bile acids would also greatly benefit this study. In light of the gene expression data in the colon during CDI, additional samples collected from the colon lumen and tissue would be interesting to further understand where these bile acids are and their changing abundances. For the human work, due to sample limitations resulting from human patients and sample access, many of the “control” samples are from patients that have some underlying health condition with an unknown effect on bile acid levels. While the large sample sizes hopefully remedied the majority of this impact, a future investigation would benefit from additional samples from healthy human donors.

Finally, the investigation into enterohepatic circulation raises quite a few questions into the proteomics involved in this process. The existing IHC and MS data suggests that protein levels are not changing in abundance during CDI in the time frames investigated, and the Future Directions section addresses additional difficulties and suggestions for improving the understanding of the proteomic landscape. Another aspect of this project that could be improved in the future is the limited time frames. In many instances, these time frames are limited by the health of the mice, as mice infected with CDI usually experience high levels of weight loss within these 3 days. The ability to study bile acids, genes, and protein levels at later and earlier time points in infection, however, would be interesting to understand the long-term effects of these changes.

Finally, this entire investigation was conducted without consideration for the impact of the larger microbiome. This is a rich area of study, and a major contributor to the gut that is deeply perturbed by the antibiotic treatment administered prior to CDI. While this was a necessary approach for the scope of this investigation, future work would benefit greatly from reintroducing this region into CDI studies, especially in the microbiota-rich regions of the large intestine and the cecum.

5.6. FUTURE DIRECTIONS

Clearly the relationship between bile acids and CDI is an important, yet complex, dynamic. While this thesis has begun to answer some initial questions about how and why primary bile acids rise during CDI, there are a few limitations addressed previously that could be improved with additional research to better understand this relationship and how to harness it to improve human health. Much more work could be done on this topic, but there are a few key experiments and investigations that would answer some of the unresolved questions resulting from this thesis.

From a methodological standpoint, more work can be done to fully understand changes at the proteomic level. It is well known in the field that transcriptomic and proteomic expression do not always correlate. The host may signal via transcripts to increase production of a protein, but there is no guarantee this signaling will reach the end goal, making it difficult to reconcile what the host is attempting to impart and what in fact occurs within the cell. Additionally, there may be a time delay between gene upregulation and increased protein abundance which can be difficult to effectively predict or monitor with minimal information. This thesis primarily focused on the transcriptional level of enterohepatic circulation and the end products of the pathways, namely the bile acids present. Although this approach is still highly beneficial in understanding how *C. difficile* attempts to manipulate the host, it is lacking a rich interrogation of what is causing the increased bile acids at the protein level. While Chapter Four addresses the protein abundance of a few key proteins using IHC and targeted MS, a robust profiling of proteomic changes within the bile acid landscape would be greatly beneficial. Due to the difficulty with working with membrane proteins, of which the majority of the proteins of interest are, technological advances in this field and additional training would benefit this endeavor. A highly efficient membrane protein extraction and digestion protocol, as well as a targeted analysis method, would allow for the acquisition of untargeted quantitative protein expression data.

In addition to understanding how the levels of proteins change, an added difficulty at the proteomic level is determining whether proteins are functional. While the assays and techniques

involved in validating protein function are outside the scope of this thesis, additional work on determining if the proteins involved in enterohepatic circulation are functional during CDI would be an important addition to understanding the protein impact. For instance, if the proteins involved in absorption are highly abundant, but CDI inactivates them or reduces functionality in some way, then absorption is still effectively inhibited. In a similar concern, measuring whether proteins have been activated would also give interesting insight into this circulatory pathway. As many of the proteins involved are sodium-dependent transporters, a method to determine whether sodium is bound to these proteins would also give additional information about what is truly happening in this process and how they contribute to bile acid levels. Altogether, these types of studies would round out our understanding of enterohepatic circulation, and how CDI changes the process.

This thesis focused almost exclusively on primary bile acids and the circulation between the ileum and the liver. However, as seen in the human samples data, secondary bile acids also show promising changes. Secondary bile acids are already known to have antibacterial effects on vegetative *C. difficile*, yet due to the antibiotic treatments that make mice susceptible to CDI it is difficult to study these bile acids during infection. Recent work has shown, however, that some strains of *C. difficile* are able to produce bile salt hydrolases, a key step in the production of secondary bile acids.[138] This suggests that even after antibiotic treatment *C. difficile* may aid in the production of secondary bile acids through deconjugation of taurine-conjugated bile acids.

Some secondary bile acids have also been shown to bind to FXR antagonistically, which would impact enterohepatic circulation in a way that may clarify some of the confusing phenotypes seen in this study. Additional investigations into secondary bile acid levels throughout the GI tract, including abundances and pool makeup, would further our understanding of this circulatory system and its dynamic with *C. difficile*. As we have investigated these bile acids on a small scale in human data, future directions for this project would also benefit from a longitudinal study of human stool bile acid levels. The ability to monitor bile acid levels and pool makeup pre-, during, and post-CDI in the same patient would offer novel information about whether bile acid levels respond to CDI, or if pre-existing bile acid pools could protect against symptomology or even infection. A control group of patients who were only treated with antibiotics would also be greatly informative to see if antibiotic treatment may lay the groundwork for some of the more dramatic changes seen later during CDI.

Antibiotic treatment in general is an understudied factor in this investigation due to limitations with susceptibility to CDI in mouse models. Further studies into antibiotics and other

CDI risk factors in the context of bile acids would be extremely informative. For instance, studying bile acid levels longitudinally in mice prior to antibiotic treatment, as well as throughout CDI, would potentially give a plethora of new information especially on secondary bile acids. Additional types of controls to compare these data against would also be highly useful. A control mouse without antibiotic treatment was utilized in Chapter Three for imaging of bile acids and showed no difference from the mock-infected mice, however an analysis at the transcriptional level of these mice could be informative. In mice, antibiotics are the standard treatment to induce CDI susceptibility, however in reality there are a lot of other risk factors such as chemotherapy, chronic kidney disease, and proton pump inhibitors. Various infection models with these differing treatments, and their potential impact on bile acid levels, could give crucial information on how changes in enterohepatic circulation impact *C. difficile* and vice versa.

In addition to bile acids, other metabolites may contribute to some of these changes in enterohepatic circulation. One potential avenue to explore in light of the cell culture data is the impact of secondary metabolites produced by *C. difficile*. As *C. difficile* vegetative cells can cause changes in transcript levels in Caco2 cells, it is possible that a product of *C. difficile* may interact with the circulation of bile acids, or more directly through FXR as a ligand. While the toxins produced by *C. difficile* were shown to impact bile acid levels somewhat in Chapter Three, they were also shown to not be the sole drivers of this phenotype, suggesting other possible products of *C. difficile* that contribute. It would be interesting to repeat the cell culture experiment with *C. difficile* culture supernatant and see if the phenotype repeats itself, and then whether the supernatant can also interact with FXR to manipulate enterohepatic circulation.

Finally, the role of FXR during CDI is a fascinating topic that was not fully explored in this work. FXR is associated most prominently with bile acid circulation, and its' encoding gene expression was shown to change in the context of infection in Chapter Four. Future work on this topic would benefit from a more direct probing of the role of FXR in this infection landscape. An FXR knockout mouse has been developed and utilized efficiently before,[157] and a CDI infection model in these mice would be enlightening to understand how FXR impacts infection in the gut. Other interesting applications would be using an FXR reporter to determine if *C. difficile* in either vegetative or spore form can directly activate FXR, or whether products of vegetative *C. difficile*, such as toxins, can antagonize the receptor. While it is unlikely that FXR alone causes all the bile acid changes seen in Chapter Three, a better understanding of the exact role it does play could give a new avenue for potential treatments for CDI by introducing a new target gene.

5.6. CONCLUSIONS

Deeper understanding of the pathogens that plague the healthcare community can only help to further the ability to treat and diagnose these infections. As a highly dynamic region interfacing with the host, bacteria, and environmental factors, infections of the gastrointestinal tract are especially interesting to understand at the molecular level. With a method to study the GI tract with MALDI IMS, it will be possible to molecularly characterize more and more diseases and disorders. Studying bile acids in these disorders, as well as further investigations into bile acids during CDI, could be a potential new avenue for understanding and treating these diseases. As understanding of the dynamic between bile acids and *C. difficile* grows, so will future diagnostic and therapeutic targets that do not rely on antibiotics.

CHAPTER 6

REFERENCES

1. Dubberke, E. R. & Olsen, M. A. Burden of clostridium difficile on the healthcare system. *Clin. Infect. Dis.* **55**, 88–92 (2012).

2. Paredes-Sabja, D., Shen, A. & Sorg, J. A. Clostridium difficile spore biology: Sporulation, germination, and spore structural proteins. *Trends Microbiol.* **22**, 406–416 (2014).

3. Shen, A. Clostridium difficile toxins: Mediators of inflammation. *J. Innate Immun.* **4**, 149–158 (2012).

4. Cornett, D. S., Reyzer, M. L., Chaurand, P. & Caprioli, R. M. MALDI imaging mass spectrometry: Molecular snapshots of biochemical systems. *Nat. Methods* **4**, 828–833 (2007).

5. Kochan, T. J. *et al.* Intestinal calcium and bile salts facilitate germination of Clostridium difficile spores. *PLoS Pathog.* **13**, 1–21 (2017).

6. Dawson, P. A. & Karpen, S. J. Intestinal transport and metabolism of bile acids. *J. Lipid Res.* **56**, 1085–1099 (2015).

7. Iqbal, J. & Hussain, M. M. Intestinal lipid absorption. (2008) doi:10.1152/ajpendo.90899.2008.

8. Wiegand, P. N. *et al.* Clinical and economic burden of Clostridium difficile infection in Europe: A systematic review of healthcare-facility-acquired infection. *J. Hosp. Infect.* **81**, 1–14 (2012).

9. Rolfe, R. D., Helebian, S. & Finegold, S. M. Bacterial Interference Between Clostridium Difficile and Normal Fecal Flora. *J. Infect. Dis.* **143**, 470–475 (1981).

10. Bien, J., Palagani, V. & Bozko, P. The intestinal microbiota dysbiosis and Clostridium difficile infection: Is there a relationship with inflammatory bowel disease? *Therap. Adv. Gastroenterol.* **6**, 53–68 (2013).

11. Howerton, A., Patra, M. & Abel-santos, E. Fate of Ingested Clostridium difficile Spores in Mice. **8**, (2013).

12. Seretny, M. *et al.* Incidence, prevalence, and predictors of chemotherapy-induced peripheral neuropathy: A systematic review and meta-analysis. *Pain* (2014) doi:10.1016/j.pain.2014.09.020.

13. Johnson, S. *et al.* Prospective, controlled study of Vinyl Glove use to interrupt Clostridium difficile nosocomial transmission. *Am. J. Med.* **88**, 137–140 (1990).

14. Rodriguez-Palacios, A. & LeJeune, J. T. Moist-heat resistance, spore aging, and superdormancy in Clostridium difficile. *Appl. Environ. Microbiol.* **77**, 3085–3091 (2011).

15. Shen, A. A Gut Odyssey: The Impact of the Microbiota on Clostridium difficile Spore Formation and Germination. *PLoS Pathog.* **11**, 1–7 (2015).

16. Saujet, L., Pereira, F. C., Henriques, A. O. & Martin-Verstraete, I. The regulatory network controlling spore formation in Clostridium difficile. *FEMS Microbiol. Lett.* **358**, 1–10 (2014).

17. Abt, M. C., McKenney, P. T. & Pamer, E. G. Clostridium difficile colitis: Pathogenesis and host defence. *Nat. Rev. Microbiol.* **14**, 609–620 (2016).

18. Rineh, A., Kelso, M. J., Vatansever, F., Tegos, G. P. & Hamblin, M. R. Clostridium difficile infection: molecular pathogenesis and novel therapeutics. *Expert Rev Anti Infect Ther* **12**, 131–150 (2015).

19. Lyerly, D. M., Krivan, H. C. & Wilkins, T. D. Clostridium difficile: its disease and toxins. *Clin. Microbiol. Rev.* **1**, 1–18 (1988).

20. Hundsberger, T. *et al.* Transcription Analysis of the Genes tcdA-E of the Pathogenicity locus of Clostridium difficile. *Eur. J. Biochem.* **244**, 735–742 (1997).

21. Dobson, G., Hickey, C. & Trinder, J. Clostridium difficile colitis causing toxic megacolon, severe sepsis and multiple organ dysfunction syndrome [3]. *Intensive Care Med.* **29**, 1030 (2003).

22. Wilson, K. H. & Perini, F. Role of competition for nutrients in suppression of Clostridium difficile by the colonic microflora. *Infect. Immun.* **56**, 2610–2614 (1988).

23. Ramirez, J. *et al.* Antibiotics as Major Disruptors of Gut Microbiota. *Front. Cell. Infect. Microbiol.* **10**, 1–10 (2020).

24. Lessa, F. C. *et al.* Burden of Clostridium difficile Infection in the United States . *N. Engl. J. Med.* **372**, 825–834 (2015).

25. Allegretti, J. R. *et al.* Recurrent Clostridium difficile infection associates with distinct bile acid and microbiome profiles. *Aliment. Pharmacol. Ther.* **43**, 1142–1153 (2016).

26. Zar, F. A., Bakkanagari, S. R., Moorthi, K. M. L. S. T. & Davis, M. B. A comparison of vancomycin and metronidazole for the treatment of Clostridium difficile-associated diarrhea, stratified by disease severity. *Clin. Infect. Dis.* **45**, 302–307 (2007).

27. van Nood, E. *et al.* Duodenal Infusion of Donor Feces for Recurrent Clostridium difficile . *N. Engl. J. Med.* **368**, 407–415 (2013).

28. Spigaglia, P. *et al.* Multidrug resistance in European Clostridium difficile clinical isolates. *J. Antimicrob. Chemother.* **66**, 2227–2234 (2011).

29. Sipponen, T. Diagnostics and Prognostics of Inflammatory Bowel Disease with Fecal Neutrophil-Derived Biomarkers Calprotectin and Lactoferrin. *Dig. Dis.* **31**, 336–344 (2013).

30. Kraft, C. & Mehta, N. Is the Ultrasensitive Toxin Immunoassay the Solution to the Goldilocks Problem of Clostridioides difficile Diagnostics? . *Clin. Infect. Dis.* 1–2 (2021) doi:10.1093/cid/ciab833.

31. Antonara, S. & Leber, A. L. Diagnosis of Clostridium difficile Infections in Children. *J. Clin. Microbiol.* **54**, 1425–1433 (2016).

32. Hourigan, S. K., Sears, C. L. & Oliva-Hemker, M. Clostridium difficile infection in pediatric inflammatory bowel disease. *Inflamm. Bowel Dis.* **22**, 1020–1025 (2016).

33. Furuya-Kanamori, L. *et al.* Asymptomatic Clostridium difficile colonization: Epidemiology and clinical implications. *BMC Infect. Dis.* **15**, 1–11 (2015).

34. Darkoh, C., Plants-Paris, K., Bishoff, D. & DuPont, H. L. Clostridium difficile Modulates

the Gut Microbiota by Inducing the Production of Indole, an Interkingdom Signaling and Antimicrobial Molecule. *mSystems* **4**, (2019).

35. Caprioli, R. M., Farmer, T. B. & Gile, J. Molecular Imaging of Biological Samples: Localization of Peptides and Proteins Using MALDI-TOF MS. *Anal. Chem.* **69**, 4751–4760 (1997).

36. Van De Plas, R., Yang, J., Spraggins, J. & Caprioli, R. M. Image fusion of mass spectrometry and microscopy: A multimodality paradigm for molecular tissue mapping. *Nat. Methods* (2015) doi:10.1038/nmeth.3296.

37. Tanaka, K. *et al.* Protein and polymer analyses up to m/z 100 000 by laser ionization time-of-flight mass spectrometry. *Rapid Commun. Mass Spectrom.* **2**, 151–153 (1988).

38. Hillenkamp, F., Karas, M., Beavis, R. C. & Chait, B. T. Matrix-Assisted Laser Desorption/Ionization Mass Spectrometry of Biopolymers. *Anal. Chem.* **63**, (1991).

39. Wakeman, C. A. *et al.* The innate immune protein calprotectin promotes Pseudomonas aeruginosa and Staphylococcus aureus interaction. *Nat. Commun.* **7**, (2016).

40. Cassat, J. E. *et al.* Integrated molecular imaging reveals tissue heterogeneity driving host-pathogen interactions. *Sci. Transl. Med.* **10**, (2018).

41. Zackular, J. P. *et al.* Dietary zinc alters the microbiota and decreases resistance to Clostridium difficile infection. *Nat. Med.* **22**, 1330–1334 (2016).

42. Chumbley, C. W. *et al.* Absolute Quantitative MALDI Imaging Mass Spectrometry: A Case of Rifampicin in Liver Tissues. *Anal. Chem.* **88**, 2392–2398 (2016).

43. Irie, M., Fujimura, Y., Yamato, M., Miura, D. & Wariishi, H. Integrated MALDI-MS imaging and LC-MS techniques for visualizing spatiotemporal metabolomic dynamics in a rat stroke model. *Metabolomics* **10**, 473–483 (2014).

44. Tal'roze, V. L., Karpov, G. V., Gordetskii, I. G. & Skurat, V. E. Capillary Systems for the Introduction of Liquid Mixtures into an Analytical Mass Spectrometer. *Russ. J. Phys. Chem.* **42**, 1658–1664 (1968).

45. Hong, S. M., Tanaka, M., Yoshii, S., Mine, Y. & Matsui, T. Enhanced visualization of small peptides absorbed in rat small intestine by phytic-acid-aided matrix-assisted laser desorption/ionization-imaging mass spectrometry. *Anal. Chem.* **85**, 10033–10039 (2013).

46. Kaya, I., Jennische, E., Lange, S. & Malmberg, P. Dual polarity MALDI imaging mass spectrometry on the same pixel points reveals spatial lipid localizations at high-spatial resolutions in rat small intestine. *Anal. Methods* **10**, 2428–2435 (2018).

47. Carter, C. L. *et al.* Characterizing the Natural History of Acute Radiation Syndrome of the Gastrointestinal Tract: Combining high mass and spatial resolution using MALDI-FTICR-MSI Claire. *Health Phys.* **116**, 454–472 (2020).

48. Genangeli, M. *et al.* MALDI-Mass Spectrometry Imaging to Investigate Lipid and Bile Acid Modifications Caused by Lentil Extract Used as a Potential Hypocholesterolemic Treatment. *J. Am. Soc. Mass Spectrom.* (2019) doi:10.1007/s13361-019-02265-9.

49. Garate, J. *et al.* Imaging mass spectrometry increased resolution using 2-mercaptobenzothiazole and 2,5-diaminonaphtalene matrices: application to lipid distribution in human colon. *Anal. Bioanal. Chem.* **407**, 4697–4708 (2015).

50. Huizing, L. R. S. *et al.* Quantitative Mass Spectrometry Imaging to Study Drug Distribution in the Intestine following Oral Dosing. *Anal. Chem.* **93**, 2144–2151 (2021).

51. Strindberg, S., Plum, J., Bagger, C., Janfelt, C. & Müllertz, A. Visualizing the Journey of Fenofibrate through the Rat Gastrointestinal Tract by Matrix-Assisted Laser Desorption/Ionization-Mass Spectrometry Imaging. *Mol. Pharm.* **18**, 2189–2197 (2021).

52. Masaoka, Y., Tanaka, Y., Kataoka, M., Sakuma, S. & Yamashita, S. Site of drug absorption after oral administration: Assessment of membrane permeability and luminal concentration of drugs in each segment of gastrointestinal tract. *Eur. J. Pharm. Sci.* **29**, 240–250 (2006).

53. Carter, C. L. *et al.* Characterizing the Natural History of Acute Radiation Syndrome of the Gastrointestinal Tract: Combining High Mass and Spatial Resolution Using MALDI-FTICR-MSI. *Health Phys.* **116**, 454–472 (2019).

54. Nguyen, H. N. *et al.* Novel in situ visualisation of rat intestinal absorption of polyphenols via matrix-assisted laser desorption/ionisation mass spectrometry imaging. *Sci. Rep.* **9**, (2019).

55. Knippel, R. J. *et al.* Heme sensing and detoxification by HatRT contributes to pathogenesis during Clostridium difficile infection. *PLoS Pathog.* **14**, 1–21 (2018).

56. Perry, W. J. *et al.* Staphylococcus aureus exhibits heterogeneous siderophore production within the vertebrate host. *Proc. Natl. Acad. Sci. U. S. A.* **116**, 21980–21982 (2019).

57. Francis, M. B., Allen, C. A., Shrestha, R. & Sorg, J. A. Bile Acid Recognition by the Clostridium difficile Germinant Receptor, CspC, Is Important for Establishing Infection. *PLoS Pathog.* **9**, (2013).

58. Chandrasekaran, R. & Lacy, D. B. The role of toxins in clostridium difficile infection. *FEMS Microbiol. Rev.* **41**, 723–750 (2017).

59. Sorg, J. A. & Sonenshein, A. L. Bile salts and glycine as cogerminants for Clostridium difficile spores. *J. Bacteriol.* **190**, 2505–2512 (2008).

60. Wexler, A. G. *et al.* Clostridioides difficile infection induces a rapid influx of bile acids into the gut during colonization of the host ll Clostridioides difficile infection induces a rapid influx of bile acids into the gut during colonization of the host. *CellReports* **36**, 109683 (2021).

61. Chiang, J. Y. L. & Ferrell, J. M. Bile acid metabolism in liver pathobiology. *Gene Expression* (2018) doi:10.3727/105221618X15156018385515.

62. Ridlon, J. M., Kang, D. J., Hylemon, P. B. & Bajaj, J. S. Bile acids and the gut microbiome. *Current Opinion in Gastroenterology* vol. 30 332–338 (2014).

63. Ibrahim, E. *et al.* Bile acids and their respective conjugates elicit different responses in neonatal cardiomyocytes: Role of Gi protein, muscarinic receptors and TGR5. *Sci. Rep.* **8**, 1–12 (2018).

64. Ding, L., Yang, L., Wang, Z. & Huang, W. Bile acid nuclear receptor FXR and digestive system diseases. *Acta Pharm. Sin. B* **5**, 135–144 (2015).

65. Cha, B. H. *et al.* Administration of tauroursodeoxycholic acid enhances osteogenic differentiation of bone marrow-derived mesenchymal stem cells and bone regeneration.

Bone **83**, 73–81 (2016).

66. Amonyingcharoen, S., Suriyo, T., Thiantanawat, A., Watcharasit, P. & Satayavivad, J. Taurolithocholic acid promotes intrahepatic cholangiocarcinoma cell growth via muscarinic acetylcholine receptor and EGFR/ERK1/2 signaling pathway. *Int. J. Oncol.* **46**, 2317–2326 (2015).

67. Mahmood, H. Intestinal Lipid Absorption and Lipoprotein Formation. *Curr. Opin. Lipidol.* **25**, 200–206 (2014).

68. Ticho, A. L., Malhotra, P., Dudeja, P. K., Gill, R. K. & Alrefai, W. A. Intestinal absorption of bile acids in health and disease. *Compr. Physiol.* **10**, 21–56 (2020).

69. Chiang, J. Y. L. & Ferrell, J. M. Bile Acid Biology, Pathophysiology, and Therapeutics. *Clin. Liver Dis.* **15**, 91–94 (2020).

70. Hillier, K., Valentovic, M. & Rakkar, M. Cholestyramine. *xPharm Compr. Pharmacol. Ref.* **104**, 1–4 (2007).

71. Yunpeng Qi1, 2, Changtao Jiang1, Jie Cheng1, 3, Kristopher W. Krausz1, Tiangang Li3, Jessica M. Ferrell3, Frank J. Gonzalez1, and J. Y. L. C. 1Laboratory. Bile acid signaling in lipid metabolism: Metabolomic and lipidomic analysis of lipid and bile acid markers linked to anti- obesity and anti-diabetes in mice. *Biochim Biophys Acta* **23**, 19–29 (2015).

72. Garbutt, J. T., Heaton, K. W., Lack, L. & Tyor, M. P. Increased Ratio of Glycine- to Taurine-Conjugated Bile Salts in Patients with Ileal Disorders. *Gastroenterology* **56**, 711–720 (1969).

73. Ridlon, J. M., Kang, D. J. & Hylemon, P. B. Bile salt biotransformations by human intestinal bacteria. *J. Lipid Res.* **47**, 241–259 (2006).

74. Vassileva, G. *et al.* Targeted deletion of Gpbar1 protects mice from cholesterol gallstone formation. *Biochem. J.* **398**, 423–430 (2006).

75. Kawamata, Y. *et al.* A G protein-coupled receptor responsive to bile acids. *J. Biol. Chem.* **278**, 9435–9440 (2003).

76. Reich, M. *et al.* TGR5 is essential for bile acid-dependent cholangiocyte proliferation in vivo and in vitro. *Gut* **65**, 487–501 (2016).

77. Zhang, L. *et al.* Promotion of liver regeneration/repair by farnesoid X receptor in both liver and intestine in mice. *Hepatology* **56**, 2336–2343 (2012).

78. Adorini, L., Pruzanski, M. & Shapiro, D. Farnesoid X receptor targeting to treat nonalcoholic steatohepatitis. *Drug Discov. Today* **17**, 988–997 (2012).

79. Yoshida, T., Honda, A., Miyazaki, H. & Matsuzaki, Y. Determination of key intermediates in cholesterol and bile acid biosynthesis by stable isotope dilution mass spectrometry. *Anal. Chem. Methods Appl.* 164–190 (2011) doi:10.4137/aci.s611.

80. Ferdinandusse, S. & Houten, S. M. Peroxisomes and bile acid biosynthesis. *Biochim. Biophys. Acta - Mol. Cell Res.* **1763**, 1427–1440 (2006).

81. Pandak, W. M. & Kakiyama, G. The acidic pathway of bile acid synthesis: Not just an alternative pathway. *Liver Res* **3**, 88–98 (2019).

82. Molinaro, A., Wahlström, A. & Marschall, H. U. Role of Bile Acids in Metabolic Control.

Trends in Endocrinology and Metabolism (2018) doi:10.1016/j.tem.2017.11.002.

83. Hylemon, P. B. *et al.* Bile acids as regulatory molecules. *J. Lipid Res.* **50**, 1509–1520 (2009).

84. Takahashi, S. *et al.* Cyp2c70 is responsible for the species difference in bile acid metabolism between mice and humans. *J. Lipid Res.* **57**, 2130–2137 (2016).

85. Pellicoro, A. *et al.* Human and rat bile acid CoA amino acid N-acyltransferase are liver-specific peroxisomal. *Hepatology* **45**, 340–348 (2007).

86. Staels, B. & Fonseca, V. A. Bile acids and metabolic regulation: mechanisms and clinical responses to bile acid sequestration. *Diabetes Care* **32 Suppl 2**, (2009).

87. Hofmann, A. F. *The Continuing Importance of Bile Acids in Liver and Intestinal Disease*. https://jamanetwork.com/.

88. Ding, L., Yang, L., Wang, Z. & Huang, W. Bile acid nuclear receptor FXR and digestive system diseases. *Acta Pharm. Sin. B* **5**, 135–144 (2015).

89. Chen, F. *et al.* Liver receptor homologue-1 mediates species- and cell line-specific bile acid-dependent negative feedback regulation of the apical sodium-dependent bile acid transporter. *J. Biol. Chem.* **278**, 19909–19916 (2003).

90. Coppola, C. P. *et al.* Molecular analysis of the adaptive response of intestinal bile acid transport after ileal resection in the rat. *Gastroenterology* **115**, 1172–1178 (1998).

91. Grober, J. *et al.* Identification of a Bile Acid-responsive Element in the Human Ileal Bile Acid-binding Protein Gene. *J. Biol. Chem.* **274**, 29749–29754 (1999).

92. Chiang, J. Y. L. Bile acid metabolism and signaling in liver disease and therapy. *Liver Res.* **1**, 3–9 (2017).

93. Inagaki, T. *et al.* Regulation of antibacterial defense in the small intestine by the nuclear bile acid receptor. *Proc. Natl. Acad. Sci. U. S. A.* **103**, 3920–3925 (2006).

94. Wahlström, A., Sayin, S. I., Marschall, H. U. & Bäckhed, F. Intestinal Crosstalk between Bile Acids and Microbiota and Its Impact on Host Metabolism. *Cell Metab.* **24**, 41–50 (2016).

95. Li, T., Chanda, D., Zhang, Y., -SikChoi, H. & Chiang, J. Y. L. Glucose stimulates cholesterol 7 α-hydroxylase gene transcription in human hepatocytes. *J. Lipid Res.* **51**, 832–842 (2010).

96. Ferrell, J. M., Boehme, S., Li, F. & Chiang, J. Y. L. Cholesterol 7α-hydroxylase-deficient mice are protected from high-fat/high-cholesterol diet-induced metabolic disorders. *J. Lipid Res.* **57**, 1144–1154 (2016).

97. Li, T. & Apte, U. Bile acid metabolism and signaling in cholestasis, inflammation and cancer. *Adv Pharmacol* **74**, 263–302 (2015).

98. Schaap, F. G., Trauner, M. & Jansen, P. L. M. Bile acid receptors as targets for drug development. *Nat. Rev. Gastroenterol. Hepatol.* **11**, 55–67 (2014).

99. Sinha, S. R. *et al.* Dysbiosis-Induced Secondary Bile Acid Deficiency Promotes Intestinal Inflammation. *Cell Host Microbe* **27**, 659-670.e5 (2020).

100. Guiberson, E. R. *et al.* Multimodal Imaging Mass Spectrometry of Murine Gastrointestinal Tract with Retained Luminal Content. *J. Am. Soc. Mass Spectrom.* 8–11 (2022) doi:10.1021/jasms.1c00360.

101. Thursby, E. & Juge, N. Introduction to the human gut microbiota. *Biochem. J.* **474**, 1823–1836 (2017).

102. Peery, A. F. *et al.* Burden and Cost of Gastrointestinal, Liver, and Pancreatic Diseases in the United States: Update 2018. *Gastroenterology* **156**, 254-272.e11 (2019).

103. Li, Z. *et al.* Effects of metabolites derived from gut microbiota and hosts on pathogens. *Front. Cell. Infect. Microbiol.* **8**, (2018).

104. Jensen, R., Buffangeix, D. & Covi, G. Measuring water content of feces by the Karl Fischer method. *Clin. Chem.* **22**, 1351–1354 (1976).

105. Rose, C., Parker, A., Jefferson, B. & Cartmell, E. The characterization of feces and urine: A review of the literature to inform advanced treatment technology. *Crit. Rev. Environ. Sci. Technol.* **45**, 1827–1879 (2015).

106. Rzagalinski, I., Hainz, N., Meier, C., Tschernig, T. & Volmer, D. A. MALDI Mass Spectral Imaging of Bile Acids Observed as Deprotonated Molecules and Proton-Bound Dimers from Mouse Liver Sections. *J. Am. Soc. Mass Spectrom.* **29**, 711–722 (2018).

107. Hillman, E. T., Lu, H., Yao, T. & Nakatsu, C. H. Microbial ecology along the gastrointestinal tract. *Microbes Environ.* **32**, 300–313 (2017).

108. Bialkowska, A. B., Ghaleb, A. M., Nandan, M. O. & Yang, V. W. Improved swiss-rolling technique for intestinal tissue preparation for immunohistochemical and immunofluorescent analyses. *J. Vis. Exp.* **2016**, 1–8 (2016).

109. Pereira, A. *et al.* Comparison of two techniques for a comprehensive gut histopathological analysis : Swiss Roll versus Intestine Strips. *Exp. Mol. Pathol.* **111**, 104302 (2019).

110. Veličković, D., Chu, R. K., Myers, G. L., Ahkami, A. H. & Anderton, C. R. An approach for visualizing the spatial metabolome of an entire plant root system inspired by the Swiss-rolling technique. *J. Mass Spectrom.* **55**, (2020).

111. Hugenholtz, F. & Vos, W. M. De. Mouse models for human intestinal microbiota research : a critical evaluation. *Cell. Mol. Life Sci.* **75**, 149–160 (2018).

112. Mazia, D., Schatten, G. & Sale, W. Adhesion of Cells to Surfaces Coated with Polylysine. *J. Cell Biol.* **66**, 198–200 (1975).

113. Peggi A., J., S., S., B. & R., C. Enhanced Sensitivity for High Spatial Resolution Lipid Analysis by Negative Ion Mode MALDI Imaging Mass Spectrometry. *Changes* **29**, 997–1003 (2012).

114. Spraggins, J. M. *et al.* High-Performance Molecular Imaging with MALDI Trapped Ion-Mobility Time-of-Flight (timsTOF) Mass Spectrometry. (2019) doi:10.1021/acs.analchem.9b03612.

115. Gauthier, J. W., Trautman, T. R. & Jacobson, D. B. Sustained off-resonance irradiation for collision-activated dissociation involving Fourier transform mass spectrometry. Collision-activated dissociation technique that emulates infrared multiphoton dissociation. *Anal. Chim. Acta* **246**, 211–225 (1991).

116. Prentice, B. M., Chumbley, C. W. & Caprioli, R. M. High-speed MALDI MS/MS imaging mass spectrometry using continuous raster sampling. *J. Mass Spectrom.* **50**, 703–710 (2015).

117. Thomas, A., Charbonneau, J. L., Fournaise, E. & Chaurand, P. Sublimation of new matrix candidates for high spatial resolution imaging mass spectrometry of lipids: Enhanced information in both positive and negative polarities after 1,5-diaminonapthalene deposition. *Anal. Chem.* **84**, 2048–2054 (2012).

118. Hankin, J. A., Barkley, R. M. & Murphy, R. C. Sublimation as a Method of Matrix Application for Mass Spectrometric Imaging. *J Am Soc Mass Spectrom* **18**, 1646–1652 (2007).

119. Leffler, D. A. & Lamont, J. T. Clostridium difficile Infection. *N. Engl. J. Med.* **372**, 1539–1548 (2015).

120. Ghose, C. Clostridium difficile infection in the twenty-first century. *Emerg. Microbes Infect.* **2**, 0 (2013).

121. Hasegawa, M. *et al.* Protective Role of Commensals against Clostridium difficile Infection via an IL-1β–Mediated Positive-Feedback Loop . *J. Immunol.* **189**, 3085–3091 (2012).

122. Ducarmon, Q. R. *et al.* Gut Microbiota and Colonization Resistance against Bacterial Enteric Infection. *Microbiol. Mol. Biol. Rev.* **83**, (2019).

123. Wexler, A. G. & Goodman, A. L. An insider's perspective: Bacteroides as a window into the microbiome. *Nat. Microbiol.* **2**, (2017).

124. Buchberger, A. R., DeLaney, K., Johnson, J. & Li, L. Mass Spectrometry Imaging: A Review of Emerging Advancements and Future Insights. *Anal. Chem.* **90**, 240–265 (2018).

125. Niehaus, M., Soltwisch, J., Belov, M. E. & Dreisewerd, K. Transmission-mode MALDI-2 mass spectrometry imaging of cells and tissues at subcellular resolution. *Nat. Methods* **16**, 925–931 (2019).

126. Prentice, B. M. *et al.* Dynamic Range Expansion by Gas-Phase Ion Fractionation and Enrichment for Imaging Mass Spectrometry. *Anal. Chem.* **92**, 13092–13100 (2020).

127. Stoeckli, M., Farmer, T. B. & Caprioli, R. M. Automated mass spectrometry imaging with a matrix-assisted laser desorption ionization time-of-flight instrument. *J. Am. Soc. Mass Spectrom.* **10**, 67–71 (1999).

128. Matamouros, S., England, P. & Dupuy, B. Clostridium difficile toxin expression is inhibited by the novel regulator TcdC. *Mol. Microbiol.* **64**, 1274–1288 (2007).

129. Stabler, R. A. *et al.* Comparative genome and phenotypic analysis of Clostridium difficile 027 strains provides insight into the evolution of a hypervirulent bacterium. *Genome Biol.* **10**, 1–15 (2009).

130. McDonald, L. C. *et al.* Clinical Practice Guidelines for Clostridium difficile Infection in Adults and Children: 2017 Update by the Infectious Diseases Society of America (IDSA) and Society for Healthcare Epidemiology of America (SHEA). *Clin. Infect. Dis.* **66**, e1–e48 (2018).

131. Giel, J. L., Sorg, J. A., Sonenshein, A. L. & Zhu, J. Metabolism of bile salts in mice

influences spore germination in clostridium difficile. *PLoS One* **5**, (2010).

132. Scaldaferri, F., Pizzoferrato, M., Ponziani, F. R., Gasbarrini, G. & Gasbarrini, A. Use and indications of cholestyramine and bile acid sequestrants. *Intern. Emerg. Med.* **8**, 205–210 (2013).

133. Tam, J. *et al.* Intestinal bile acids directly modulate the structure and function of C. Difficile TcdB toxin. *Proc. Natl. Acad. Sci. U. S. A.* **117**, 6792–6800 (2020).

134. Guiberson, E. R. *et al.* Spatially Targeted Proteomics of the Host-Pathogen Interface during Staphylococcal Abscess Formation. *ACS Infect. Dis.* **7**, 101–113 (2021).

135. Martinez-Guryn, K. *et al.* Small Intestine Microbiota Regulate Host Digestive and Absorptive Adaptive Responses to Dietary Lipids. *Cell Host Microbe* **23**, 458-469.e5 (2018).

136. Kleinridders, A. *et al.* Regional differences in brain glucose metabolism determined by imaging mass spectrometry. *Mol. Metab.* **12**, 113–121 (2018).

137. Theriot, C. M., Bowman, A. A. & Young, B. Antibiotic-Induced Alterations of the Gut difficile Spore Germination and Outgrowth in the Large Intestine. *mSphere* **1**, 1–16 (2016).

138. Aguirre, A. M. & Sorg, J. A. Clostridioides difficile bile salt hydrolase activity has substrate specificity and affects biofilm formation. *bioRxiv* (2022) doi:10.1007/978-3-030-83217-9_2.

139. Westh, H., Iversen, J. T. & and Gyrtrup, H. . Clostridium difficile in faecal flora after perioperative prophylaxis with ampicillin or ceftriaxone. *J Infect.* **23**, 347–350 (1991).

140. Newman, N. *et al.* Host response to cholestyramine can be mediated by the gut microbiota. *biorxiv*.

141. Gray, W. R. [12] Dansyl chloride procedure. *Methods Enzymol.* **11**, 139–151 (1967).

142. Buffie, C. G. *et al.* Precision microbiome reconstitution restores bile acid mediated resistance to Clostridium difficile. *Nature* **517**, 205–208 (2015).

143. Markham, N. O. *et al.* Murine Intrarectal Instillation of Puri fi ed Recombinant Pathogenesis. *Infect. Immun.* **89**, e00543-20 (2021).

144. Chiang, J. Y. L. Bile acid metabolism and signaling. *Compr. Physiol.* **3**, 1191–1212 (2013).

145. Camilleri, M. Bile Acid Diarrhea : Prevalence , Pathogenesis , and Therapy. **9**, 332–339 (2015).

146. Eade, C. R. *et al.* Bile acids function synergistically to repress invasion gene expression in salmonella by destabilizing the invasion regulator hilD. *Infect. Immun.* **84**, 2198–2208 (2016).

147. Hernández, S. B., Cota, I., Ducret, A., Aussel, L. & Casadesús, J. Adaptation and preadaptation of Salmonella enterica to bile. *PLoS Genet.* **8**, (2012).

148. Thomas, J. P., Modos, D., Rushbrook, S. M., Powell, N. & Korcsmaros, T. The Emerging Role of Bile Acids in the Pathogenesis of Inflammatory Bowel Disease. *Front. Immunol.* **13**, 1–14 (2022).

149. Song, X. *et al.* Microbial bile acid metabolites modulate gut RORγ+ regulatory T cell homeostasis. *Nature* **577**, 410–415 (2020).

150. Fletcher, J. R. *et al.* Clostridioides difficile exploits toxin-mediated inflammation to alter the host nutritional landscape and exclude competitors from the gut microbiota. *Nat. Commun.* **12**, 1–14 (2021).

151. Rocca, J. D. *et al.* Relationships between protein-encoding gene abundance and corresponding process are commonly assumed yet rarely observed. *ISME J.* **9**, 1693–1699 (2015).

152. Avallone, G., Pellegrino, V., Muscatello, L. V., Sarli, G. & Roccabianca, P. Spindle Cell Lipoma in Dogs. *Vet. Pathol.* **54**, 792–794 (2017).

153. Liu, Y., Beyer, A. & Aebersold, R. On the Dependency of Cellular Protein Levels on mRNA Abundance. *Cell* **165**, 535–550 (2016).

154. Ley, R. E., Peterson, D. A. & Gordon, J. I. Ecological and evolutionary forces shaping microbial diversity in the human intestine. *Cell* vol. 124 837–848 (2006).

155. Rooks, M. G. & Garrett, W. S. Gut microbiota, metabolites and host immunity. *Nature Reviews Immunology* vol. 16 341–352 (2016).

156. He, X., Marco, M. L. & Slupsky, C. M. Emerging aspects of food and nutrition on gut microbiota. *Journal of Agricultural and Food Chemistry* (2013) doi:10.1021/jf4029046.

157. Huang, F. *et al.* Deletion of mouse FXR gene disturbs multiple neurotransmitter systems and alters neurobehavior. *Front. Behav. Neurosci.* **9**, 1–10 (2015).

CURRICULUM VITAE

Emma R. Guiberson

EDUCATION

Ph.D. in Chemistry Fall 2022
Vanderbilt University, Nashville, TN
Advisor: Dr. Richard Caprioli
Dissertation: *Discovery of Bile Acid-Associated Molecular Changes in the Murine Gastrointestinal Tract During Clostridioides difficile Infection*
Committee Members: Dr. Eric Skaar, Dr. Jeff Spraggins, Dr. Kevin Schey, Dr. Renã Robinson

B.S. in Chemistry and Philosophy May 2018
University of Notre Dame, Notre Dame, IN

RESEARCH EXPERIENCE

Mass Spectrometry Research Center Fall 2018 – Present
Dr. Richard Caprioli, Vanderbilt University
Graduate Research Assistant

- Developed multi-omic research workflows for analysis of infected intestinal tissue
- Investigated host molecular changes resulting from *S. aureus* and *C. difficile* infections
- Utilized spatially-targeted mass spectrometry approaches in lipidomics, proteomics and transcriptomics

Naval Nuclear Laboratory- Radiochemistry Summer 2017 and 2018
Jeff Wetzler, Bechtel Marine Propulsion Corporation
Research Intern

- Independent project on portable liquid scintillation counter
- Developed and optimized procedure for use in the field
- Focused on analysis of beta-counts resulting for Tritium in water sources

Warren Family Drug Development and Discovery Facility Fall 2015 – Fall 2016
Dr. Bruce Melancon, University of Notre Dame
Undergraduate Research Assistant

- Recrystallization, purification and spectral analysis procedures
- Run procedural research on optimum conditions for synthesis reactions
- Contribute to cataloguing project and independent synthesis reaction AR-42
- Synthetic chemistry laboratory with highly independent projects

PUBLICATIONS

Guiberson ER, Good CJ, Wexler AG, Skaar EP, Spraggins JM, Caprioli RM. "Multimodal Imaging Mass Spectrometry of Murine Gastrointestinal Tract with Retained Luminal Content" *JASMS.* **2022***.* DOI: 10.1021/jasms.1c00360

Guiberson ER*, Wexler AG*, Beavers WN, Washington MK, Shupe JA, Lacey DB, Caprioli RM, Spraggins JM, Skaar EP. "*Clostridioides difficile* infection induces a rapid influx of bile acids into the gut during colonization of the host". *Cell Reports.* **2021.** (36) DOI: 10.1016/j.celrep.2021.109683 *Equal Contributions

Guiberson ER*, Weiss A*, Ryan DJ, Monteith AJ, Sharman K, Gutierrez DB, Perry WJ, Caprioli RM, Skaar EP, Spraggins JM. "Spatially-targeted proteomics of the host-pathogen interface during staphylococcal abscess formation." *ACS Infect. Dis.* **2021.** (7) 101-113. DOI: 10.1021/acsinfecdis.0c00647

Sharman K, Patterson NH, Weiss A, Neumann EK, **Guiberson ER**, Gutierrez DB, Spraggins JM, Van de Plas R, Skaar EP, Caprioli RM. "Analyzing High-Dimensional Spatially Targeted Proteomics Data to Investigate *Staphylococcus aureus* Infection.." *J.Proteome Res.* **2022.** DOI: 10.1021/acs.jproteome.2c00206

Rivera, ES, Jones, MA, **Guiberson, ER**, & Norris, JL, (2020). Fundamentals of Mass Spectrometry-Based Metabolomics. In G. Sindona, J. H. Banoub & M. L. Di Gioia (Eds.), Toxic Chemical and Biological Agents: Detection, Diagnosis and Health Concerns (pp. 61-81). Springer. https://doi.org/10.1007/978-94-024-2041-8'

Nicholson MR, Strickland BA, **Guiberson ER,** Spraggins JM, Caprioli RM, Das S, Skaar EP. "The Gut Microbiome and Bile Acids Differentiate *Clostridioides difficile* Infection and Colonization in Children." *In Preparation.*

AWARDS

Richard Armstrong Prize for Research Excellence — Summer 2022
Outstanding Individual Research Proposal — Spring 2022
Outstanding Chemistry Forum Presentation Award — Spring 2021
MSACL Young Investigator Educational Grant — Spring 2020
American Society of Mass Spectrometry Student Stipend — Spring 2019
Communications in Science Conference – Atlanta — Spring 2019

- Selective conference focusing on developing scientific communications skills, accompanying financial award

Vanderbilt Microbiome Venture Fund ($3000 awarded) — Fall 2019

- "Spatially Targeted Proteomics of Bacterial Proteins in the Human Gut Microbiota" Proposal Funded

Department of Chemistry and Biochemistry Leadership Award, University of Notre Dame — Spring 2018

- Awarded to a senior student in the department for outstanding and lasting contributions to the department and student experience

TEACHING EXPERIENCE

Certificate in College Teaching Facilitator — Fall 2021 – Present
Center for Teaching | Vanderbilt University | *Nashville, TN*

- Led 8-week course for Certificate in College Teaching (CiCT) program each semester
- Course focused specifically on STEM teaching

Teaching Affiliate — Fall 2019 – Present
Center for Teaching | Vanderbilt University | *Nashville, TN*

- Led cohort of chemistry graduate students through TA orientation
- Prepared incoming TAs for teaching positions in the department
- Paid position with rigorous application and interview process

Graduate Teaching Assistant — Fall 2018 – Spring 2019
Vanderbilt University | *Nashville, TN*

- Led two General Chemistry Lab sections (CHEM 1601L) and two Physical Chemistry Lab sections (CHEM 3315)
- Prepared for ten different labs each to highlight various chemical concepts
- Efficiently and thoroughly graded weekly assignments and returned student feedback

Laboratory Course Development — Spring 2017
University of Notre Dame | *Notre Dame, IN*

- Laboratory Instrumentation Giving Hope to Students (LIGHTS) program for lab project developments
  for local high schools
- Independently developed two lab projects utilizing a centrifuge and pH meter

Teaching Assistant Summer 2016

Center for Bright Kids Summer Program | *Golden, CO*

- Instructor for philosophy and neurobiology accredited summer courses
- Programs spanned from 4th grade through high school
- Involved in extracurricular and residential aspects of program

PROFESSIONAL MEMBERSHIPS

American Society of Mass Spectrometry 2019 – Present
American Society for Microbiology 2021 – Present
Imaging Mass Spectrometry Society 2021 – Present

PRESENTATIONS

ORAL PRESENTATIONS

Presentation: *Clostridioides difficile Infection Causes a Rapid Influx of Bile Acids in the Murine Gastrointestinal Tract* (March 2022)

- Chemical Biology Association of Students Seminar, Nashville, TN

Presentation: *Clostridioides difficile Infection Causes a Rapid Influx of Bile Acids in the Murine Gastrointestinal Tract* (November 2021)

- American Society for Mass Spectrometry Annual Conference, Philadelphia, PA

Presentation: *Clostridioides difficile Infection Causes a Rapid Influx of Bile Acids in the Murine Gastrointestinal Tract* (September 2021)

- Mass Spectrometry Applied to the Clinical Laboratory EU, Online

Presentation: *Discovery of Bile Acid-Associated Molecular Changes in the Murine Gastrointestinal Tract during Clostridioides difficile Infection* (June 2021)

- Just Another Chemistry Webinar Series

Presentation: *Discovery of Bile Acid-Associated Molecular Changes in the Murine Gastrointestinal Tract during Clostridioides difficile Infection* (January 2021)

- Chemistry Forum Seminar, Vanderbilt University, Nashville, TN
- Awarded “Outstanding Chemistry Forum Presentation” from Chemistry Department

Presentation: *Spatially-Targeted Proteomics for Analysis of Host-Pathogen Interactions in Staphylococcus aureus* (December 2020)

- Lightning talk for Imaging Mass Spectrometry Society International Poster Gala, Virtual

Presentation: *Spatially-targeted Proteomics for Analysis of Staphylococcus aureus Abscess Formation* (July 2020)

- Mass Spectrometry Applied to the Clinical Laboratory 2020, Palm Springs, CA
- Presented later virtually on MSACL Connect due to COVID-19

Presentation: *Spatially-targeted Proteomics for Analysis of Staphylococcus aureus Abscess Formation* (June 2020)

- American Society for Mass Spectrometry Annual Conference, Houston, TX
- Presented virtually due to COVID-19

Invited Presentation: *MALDI IMS and Spatially-Targeted Proteomics for the Visualization of Host-Pathogen Interactions* (April 2020)

- Advanced Imaging Mass Spectrometry Course, Vanderbilt University, Nashville, TN
- Course canceled due to COVID-19

Presentation: *Imaging Mass Spectrometry of the Clostridioides difficile Infected Gastrointestinal Tract* (October 2019)

- NATO Advanced Study Institute G5535, Cetraro, Italy

Workshop Assistant: *Small Volumes: Spatially Targeted Analyses* (April 2019)

- Analytical Imaging Mass Spectrometry Laboratory Course, Nashville, TN

POSTERS

Poster: *Clostridioides difficile Infection Causes a Rapid Influx of Bile Acids in the Murine Gastrointestinal Tract* (July 2022)

- GRS and GRC on Microbial Toxins and Pathogenesis, Southbridge, MA

Poster: *Clostridioides difficile Infection Causes a Rapid Influx of Bile Acids in the Murine Gastrointestinal Tract* (April 2022)

- Vanderbilt Institute for Infection, Immunology and Inflammation Annual Symposium, Nashville, TN

Poster: *Mapping Molecular Interactions in the Clostridium difficile Infected Gastrointestinal Tract Using Multimodal Imaging Mass Spectrometry* (October 2021)

- Imaging Mass Spectrometry Society, Colorado Springs, CO

Poster: *Spatially-targeted Proteomics for Analysis of Staphylococcus aureus Abscess Formation* (December 2020)

- Imaging Mass Spectrometry Society International Poster Gala, Virtual

Poster: *Spatially-targeted Proteomics for Analysis of Staphylococcus aureus Abscess Formation* (August 2020)

- VICB Student Research Symposium, Nashville, TN

Poster: *Spatially-targeted proteomics for the analysis of Staphylococcus aureus Abscess Formation* (June 2020)

- Vanderbilt Institute of Infection, Immunology and Inflammation Annual Symposium (VI4), Nashville, TN

Poster: *Mapping Bile Acids in the Clostridioides difficile Infected Gastrointestinal Tract Using Multimodal Imaging Mass Spectrometry* (March 2020)

- Digestive Disease Research Center Retreat, Nashville, TN

Poster: *Mapping Molecular Interactions in the Clostridium difficile Infected Gastrointestinal Tract Using Multimodal Imaging Mass Spectrometry* (October 2019)

- NATO Advanced Study Institute G5535, Cetraro, Italy

Poster: *Using Multimodal Imaging Mass Spectrometry to Map Molecular Interactions in the Clostridium difficile Infected Gastrointestinal Tract* (August 2019)

- VICB Student Research Symposium, Nashville, TN

Poster: *Mapping Molecular Interactions in the Clostridium difficile Infected Gastrointestinal Tract Using Multimodal Imaging Mass Spectrometry* (June 2019)

- American Society for Mass Spectrometry Annual Conference, Atlanta, GA

Poster: *Mapping Molecular Interactions in the Clostridium difficile Infected Gastrointestinal Tract Using Multimodal Imaging Mass Spectrometry* (April 2019)

- Vanderbilt Institute of Infection, Immunology and Inflammation Annual Symposium, Nashville, TN

LEADERSHIP

Chemistry Forum Committee — Fall 2019 – Spring 2021

- **Chair, 2020-2021**

President, *Graduate School Honor Council* — Summer 2020 – Summer 2021
Vice President, *Graduate School Honor Council* — Summer 2019 – Summer 2020
Departmental Representative, *Graduate Student Council* — Fall 2018 – Spring 2019
Notre Dame Chemistry and Biochemistry Mentoring Program — Fall 2016 – Spring 2018

- **Program Head, 2017-2018**

CERTIFICATIONS

Certificate in College Teaching
Center for Teaching | Vanderbilt University | *Nashville, TN* Spring 2020

- Completed two-semester certification in college teaching